MECHANICAL AND TRANSPORT PHENOMENA IN ADVANCED POLLUTANTS CONTAINMENT SYSTEMS

A THEORETICAL AND EXPERIMENTAL STUDY

GIACOMO BOFFA

PH.D. IN NATURAL AND BUILT ENVIRONMENT ENGINEERING

Advisor: Prof. Mario Manassero
Co-Advisors: Prof. Guido Musso
Dr. Andrea Dominijanni

POLITECNICO DI TORINO
DEPARTMENT OF STRUCTURAL, GEOTECHNICAL AND BUILDING ENGINEERING

MAY 2016

Politecnico di Torino
DISEG – Dipartimento di Ingegneria Strutturale, Edile e Geotecnica

Dottorato di Ricerca in Ingegneria per l'Ambiente Naturale e Costruito
XXVIII ciclo

Coordinatore del Dottorato:
Prof. Claudio Scavia – Politecnico di Torino

Commissione esaminatrice:
Prof.ssa Monica Barbero – Politecnico di Torino
Prof.ssa Sabrina Sorlini – Università degli Studi di Brescia
Prof. Vincenzo Torretta – Università degli Studi dell'Insubria

Esane finale:
16 maggio 2016

A Mamma, Papà e Edo

"Scientists study the world as it is,

Engineers create the world that never has been."

Theodore Von Kármán (1881 – 1963)

CONTENTS

INTRODUCTION

Geotechnical engineers and hydrologists have dedicated most of their efforts devoted to problems concerning environmental protection and human health since the 1970's, by studying the interaction between soils and polluting substances. Such remarkable impetus of studies emerged mainly from the need to manage the disposal of radioactive materials produced by nuclear stations with solutions which would be able to guarantee an adequate level of safety in the long term (Daniel, 1993). Scientific community was soon called on to study industrial waste landfills and pollution of the sub-soil deriving from materials produced by chemical and petro-chemical industries: in particular, the main problem to solve was that of designing adequate pollutant barrier systems in order to limit contaminant discharge to groundwater and related migration in the subsoil (Benson, 2000).

Initially, such barriers were made up by mineral type materials (drainage layers in sand and gravel, compacted clay liners, soil-bentonite and cement-bentonite cutoff-walls), since their properties for long-term use were considered sufficiently durable. Clay liners and clay caps were used respectively in order to provide isolation of waste leachate from the subsoil (in the case of liners), or to guarantee long-term control of percolation into the waste and control leachate generation (in the case of covers).

The design of pollutant barrier systems has been innovatively modified since the mid-1980's with the introduction of the so-called Geosynthetic Clay Liners (GCLs),

which are defined as factory-manufactured hydraulic or gas barriers consisting of a layer of bentonite or other very low permeability material supported by geotextiles and/or geomembranes, mechanically held together by needling, stitching or chemical adhesives (Koerner and Koerner, 2010). The hydraulic resistance of conventional GCLs (i.e. which are not comprised of a geomembrane component) is attributed to the bentonite component of the GCL, which swells in the presence of water to form a tight sealing layer (Shackelford, 2007).

GCLs have been utilized greatly as the lower portion of geomembrane/GCL composites in both landfill liners and final covers (e.g. Bouazza, 2002; Koerner, 2005); they have also been used in other containment applications and by themselves as single barrier systems when modified with a geofilm or polymer coating within the cover geotextiles. In most applications they have served as replacement materials for the more traditional compacted clay liners (CCLs) in cover systems or in bottom lining of waste containment facilities, since they present very low hydraulic conductivity to water and relatively low cost (Bouazza, 2002).

GCLs have undergone great change since the 1990's. Engineers had to explore new theoretical problems, such as the study of solute diffusion phenomena in soils and chemical osmosis in bentonites, since hydraulic performances of GCLs are greatly affected by the chemical composition of the environment surrounding the barrier (e.g. they can be worsen by a simple variation of the chemical and physical boundary conditions), and depend on the swelling and osmotic behaviour which bentonite, characterized by a high content in montmorillonite, may exhibit. Moreover, new specific design methodologies have been developed, whose distinctive features derive from the specific nature of the objective to reach, of the materials employed, of the boundary conditions and of the reference regulations; an important example of such new methodologies is represented by risk analysis.

The research project developed during the PhD has been focused on bentonite barriers which are designed both in urban waste landfill, hazardous or radioactive wastes final disposal. The theoretical and experimental study has had the aim of studying the mechanical and chemico-osmotic behaviour of bentonite in contact

with standard (i.e. de-ionized water, DW) and non standard liquids (i.e. sodium chloride solutions), acting on its state parameters, chemical composition, and boundary conditions at installation. The whole laboratory activity, comprising oedometer and chemico-osmotic tests, was carried out at "Politecnico di Torino", in the Disaster Planning Laboratory (DIPLAB) of the Department of Structural, Geotechnical and Building Engineering (DISEG). The contents of the 3-year PhD research are reported in this thesis and are resumed in the short summary reported below:

Chapter 1 – Bentonite barriers

This chapter is aimed at introducing the main topics concerning the mineralogical, chemical and physical description of sodium bentonite; swelling and osmotic phenomena are also presented. Particular attention is devoted to the engineering properties which can be evaluated in order to characterize bentonite, in particular of Geosynthetic Clay Liners, for geoenvironmental applications: in this regard the most important characteristics of sodium bentonite which was employed for the PhD research activity are resumed. A propaedeutic study on mechanical behaviour of bentonites, referring in particular to the swelling phenomenon, is also described. Finally the main aspects and issues concerning practical application and proper use of Geosynthetic Clay Liners and Clay membrane barriers in general are introduced.

Chapter 2 – Theoretical models for mechanical and osmotic behaviour of sodium bentonites

The electric interaction between montmorillonite particles, which represent the main mineralogical component of bentonite, and the ions in pore solution determines macroscopic phenomena which cannot be modelled on the basis of the classical theories used to describe the movement of water and solutes through porous media. This chapter is focused on the theoretical approaches which can be adopted in order to model transport properties of bentonites and the related aspects of their mechanical behaviour. The phenomenological and physical theoretical approaches

are complementary and represent a very useful tool for experimental data interpretation, in order to reduce the number of tests to be performed and simulate GCLs behaviour in applications, even in the long-term, under boundary conditions different from those adopted in laboratory.

Chapter 3 – Mechanical and swelling behaviour of bentonites

In the Paper included in this chapter, titled "MECHANICAL AND SWELLING BEHAVIOUR OF SODIUM BENTONITES IN EQUILIBRIUM WITH LOW MOLARITY NaCl SOLUTIONS UNDER OEDOMETRIC CONDITIONS", a theoretical and experimental study on mechanical and swelling behaviour of tested sodium bentonite is presented. Several oedometer tests (i.e. with a conventional apparatus and a new testing device) were performed on sodium bentonite specimens in equilibrium with NaCl 0.01 M concentrated solutions in order to measure a phenomenological parameter, i.e. the swelling pressure, at different void ratios. The obtained experimental results have been interpreted on the basis of the theoretical model, by assuming that the microscopic deviations of the pore solution state variables from their average values are negligible: in such a way, it was possible to interpret the macroscopic behaviour on the basis of the physical and chemical properties of the bentonite mineralogical components, and, thus, characterize the microstructure of the material.

In the last part of the chapter other oedometer tests are presented, with the aim of analysing the effect of different salt concentrations of the equilibrium solution on the mechanical and swelling behaviour of sodium bentonite.

Chapter 4 – Chemico-osmotic behaviour of bentonites

Membrane behaviour represents a potential benefit in engineered clay-based barriers for geoenvironmental applications, especially if such barriers consist of sodium bentonite. A theoretical and experimental study on membrane behaviour of tested sodium bentonite is presented in the Paper included in this chapter, titled "INFLUENCE OF SPECIMEN POROSITY AND SODIUM CHLORIDE PORE

SOLUTION CONCENTRATION ON CHEMICO-OSMOTIC BEHAVIOUR OF SODIUM BENTONITES". The effects of porosity on two natural sodium bentonite specimens submitted to multiple-stage chemico-osmotic tests were investigated, by evaluating two phenomenological parameters that affect transport properties of bentonite, i.e. the chemico-osmotic reflection coefficient and the osmotic effective diffusion coefficient. The experimental results were compared to literature data and interpreted on the basis of the proposed theoretical approach, under the hypothesis that the microscopic deviations of the state variables from their average values are negligible. Even in this case, it was possible to interpret the macroscopic behaviour on the basis of the physical and chemical properties of the bentonite mineralogical components.

In the last paragraph of the chapter, two further chemico-osmotic tests, by means of a new testing apparatus, are presented: experimental data are interpreted through the proposed theoretical framework and compared with previous results.

References

1. Benson, C.H. (2000). Liners and covers for waste containment. *In* Proceeding 4th Kansai Intl. Geotechnical Forum, Creation of a New Geo-Environmental, Japanese Geotechnical Society, Kyoto, Japan, May 24-26, 2000, 1-40.
2. Bouazza, A. (2002). Geosynthetic clay liners. Review article. *Geotextiles and Geomembranes*, **20**, 3-17.
3. Daniel, D.E., Shan, H.-Y., Anderson, J.D. (1993). Effects of partial wetting on the performance of the bentonite component of a geosynthetic clay liner. Geosynthetics '93. Industrial Fabrics Association International, St. Paul, Minnesota, USA, 3, pp. 1483-1496.
4. Koerner, R.M. (2005). *Designing with Geosynthetics*, 5th ed. Pearson Prentice Hall, Upper Saddle River, New Jersey.

5. Koerner, R.M., Koerner, G.R. (2010). Background and overview of Geosynthetic clay liners, (Chapter 1). In *Geosynthetic Clay Liners for Waste Containment Facilities*, eds A. Bouazza and J.J. Bowders, CRC Press, The Netherlands, pp. 1-16.
6. Shackelford, C.D. (2007). Selected issues affecting the use and performance of GCLs in waste containment applications. In: Geosynthetics and Environment, XXI Geotechnical Conferences of Torino (GCT), Torino, Italy, November 2007.

1. BENTONITE BARRIERS

The term “bentonite” has frequently been used to describe any naturally occurring deposit composed primarily of the clay mineral montmorillonite, which has been derived from alteration of volcanic ash. Strictly speaking, bentonites are rocks composed of the swelling clay mineral smectite and variable amounts of other minerals (Grim and Güven, 1978). Smectite is a class of hydrated 2:1 layer silicate minerals that form stable colloidal suspensions and have an expandable volume due to the retention of hydrated cations. As a consequence of its large specific surface (as high as 850 m^2/g), cation exchange capacity (80-150 meq/100g), and capability for interlayer swelling, the smectite component is responsible for the bentonite desirable physical and chemical attributes for geoenvironmental applications (e.g. landfill barriers).

In the present chapter the mineralogical, chemical and physical properties of sodium bentonite are described. Particular attention is then focused on its swelling and semipermeable membrane behaviour. The experimental results of a laboratory study regarding the difference in the swelling and mechanical behaviour of sodium bentonite in equilibrium with sodium chloride solutions with different molarities are reported. Moreover, the main characteristics concerning Geosynthetic Clay Liners are presented.

1.1 Mineralogy of sodium bentonite

1.1.1 Crystalline structure of montmorillonite

Clay minerals are in general composed by hydrous silicates or alumino-silicates and their structure is comprised of layers of silica and alumina sheets joined together. Silica and alumina represent the two main structural units: the former is a tetrahedral sheet, in which a silicon atom is equidistant from the oxygen atoms or the hydroxyls; the latter is an octahedral structure, in which aluminium, iron or magnesium atoms are equidistant from the oxygen atoms or the hydroxyls. Both networks are repeated indefinitely to form a sheet. The crystalline structure and the microstructure are the main factors which influence the physical and chemical properties of clay minerals.

Bentonite, and in particular sodium bentonite, is a clay soil composed by at least 70% of montmorillonite, which belongs to smectite clay minerals, also called 'three-layer minerals' or 2:1 phyllosilicates. The basic structure of minerals in the smectite group is characterized by having one octahedral sheet joined on either side by two silica tetrahedral sheets (thus the term 2:1 layer silicate) forming a unit layer, as shown in Figure 1.1 and Figure 1.2. In an ideal 2:1 layer, aluminium or magnesium octahedra are coordinated with four oxygen atoms and two hydroxyl ions. The tetrahedra are comprised of silicon atoms coordinated with four oxygen atoms; one of these is also bonded to the octahedra.

Oxygen anions are shared between the central octahedral sheet and the two tetrahedral sheets, thus forming a strong bond which preserves the 2:1 unit layer. The thickness of on unit layer is ≈ 10 Å, whereas the thickness of the interlayer plus one unit layer (i.e. basal spacing) is variable. Several tens or even hundreds of unit layers constitute a crystallite, while many million layers and thousand of crystallites form montmorillonite particles with sixes on the order of 2 μm effective spherical diameter.

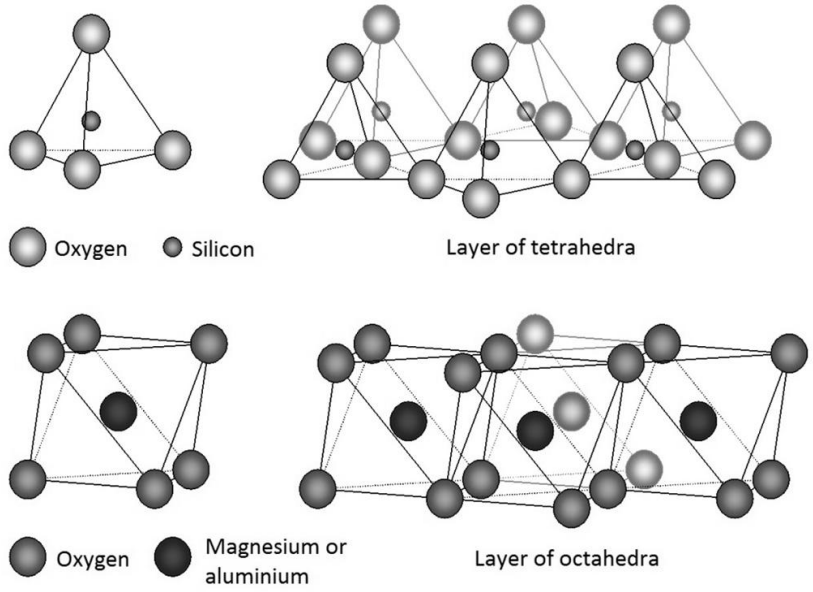

Figure 1.1 Unit layer forming the montmorillonite crystalline structure

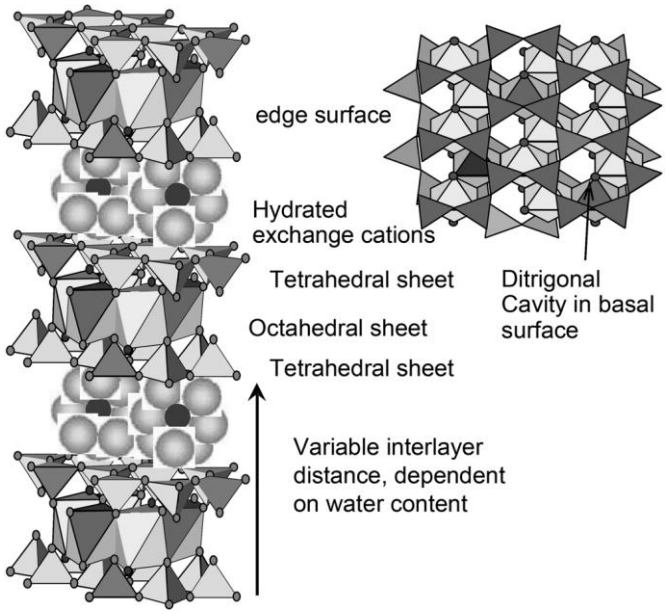

Figure 1.2 Structure of montmorillonite, a hydrated smectite (after Gates, 2007). Hydrated exchange cations, which neutralize charge due to isomorphic substitutions occupy the interlayer surface and enable montmorillonite to swell in water.

Adjacent montmorillonite layers are separated by an interlayer space which spans the distance between opposing basal or interlayer surfaces (see Figure 1.2). These surfaces are elongated flat plates and constitute the largest surface area in smectites. Exchangeable cations required to balance the layer charge reside on these interlayer surfaces. The high hydration energies of the exchange cations enable montmorillonite to absorb large amounts of water. While bonding between unit layers arising from electrostatic and short-range van der Waals attractive forces is relatively weak, the interaction of water with exchangeable cations within the interlayer space can be strong enough to allow partial or complete disassociation of smectite unit layers in aqueous solution, a phenomenon referred to as "interlayer swelling" (Likos et al., 2010). Depending on the extent of interlayer disassociation, montmorillonite particles range in thickness from individual unit layers, upward to thicknesses corresponding to several tens, hundreds, or thousands of stacked unit layers.

1.1.2 **Morphology and microstructure of montmorillonite**

The morphology of montmorillonite is often similar to a thin, crumpled film or flake and it can be difficult to differentiate one "particle" from another. The volume fraction, arrangement, and orientation of the solids and pore spaces on these multiple levels of scale define the fabric (or microstructure) of the system which influences bulk physical properties of the bentonite such as swelling, sealing and hydraulic conductivity, and is critically important in governing the corresponding performance of bentonite as a barrier material (Likos et al., 2010).

The number of layers which constitute a quasi-crystal, its size, shape and interaction with other quasi-crystals are generally dependent on the layer charge characteristics of the mineral, electrolyte concentration, and identity of the exchange cation. The average thickness of Na^+-smectite quasi-crystals is small. The resulting gel fabric (or microstructure) has a distribution of inter-particle pore sizes, which optimizes water

retention, inhibits water flow (Egloffstein, 2001), and influences how interlayer swelling translates to corresponding bulk volume changes (Likos and Lu, 2006).

As observed by Norrish (1954), bentonite can have either a dispersed structure in which clay particles are present as well separated units, or an aggregated structure that consists of packets of particles, or tactoids, within which several clay platelets or lamellae are in a parallel array. Dispersed structures and aggregated structures are characterized respectively by high and low values of the external specific surface of particles.

Swelling clays can absorb >200% their mass in water and increase their original volume many fold. The clay microstructure at high water content is instrumental in translating properties from the individual mineral layer or crystallite level to the macro-scale level. When under confinement, as is the usual condition in geotechnical applications, a Na^+ clay fabric will seal because domains of quasi-crystals will necessarily have to re-arrange and expand into the available inter-particle pore space during wetting. This results in a reduction in void sizes and inter-connectivity of pores with an associated increase in tortuosity. The highly flexible nature of clay platelets enables overlapping face-face associations to dominate the fabric of Na^+ saturated smectite gels.

1.1.3 **Layer charge and exchangeable cations**

Montmorillonite is characterized by extensive isomorphous substitution which results in charge deficiencies within the crystalline structure. Substitution may occur either in the octahedral sheet (e.g. Mg^{2+}, Fe^{2+} or Mn^{2+} for Al^{3+}) or in the tetrahedral sheet (e.g. Al^{3+} or Fe^{3+} for Si^{4+}), such that the overall structure carries a net negative layer charge. Thus, the ideal unit cell formula of montmorillonite is $\{(OH)_4Si_8Al_{3.44}Mg_{0.66}O_{20}\cdot nH_2O^{0.66-}\}$ with a typical surface charge of 0.66 equivalents per unit cell.

The net negative charge arising from isomorphous substitution is offset by exchangeable interlayer cations, which are predominantly located between the unit layers within the interlayer space, but can also exist between particles or crystallites within the interparticle pore space. The exchangeability of exchange cations is governed by their valence, size, hydration energies and concentration (Teppen and Miller, 2005). For equivalent concentrations, the propensity for one type of cation to replace another follows the sequence:

$$Li^+ < Na^+ < K^+ < Mg^{2+} < Ca^{2+} < Al^{3+} < Fe^{3+}$$

The predominant type of exchangeable cation may constitute a qualifier for differentiating one form of the same mineral from another, and often reflects the environment within which mineral formation took place. For example, bentonites altered from volcanic ash in a seawater environment are predominantly sodium form, while calcium is predominant in bentonites which formed within a freshwater environment.

Bentonites used in GCLs commonly have approximately equal fractions of Ca^{2+} and Na^+ cations on the exchange complex when delivered from the GCL factory (Shackelford et al., 2000). Naturally predominant Na^+-bentonites or activated (i.e. Na^+ exchanged) Ca^{2+}-bentonites are preferred for barrier applications due to the beneficial swelling, sealing, and hydrologic characteristics associated with sodium in the exchange complex. Moreover, the higher affinity for polyvalent cations (e.g. Ca^{2+} over Na^+) leads to important considerations regarding ion exchange and the corresponding changes in microstructure and, thus, in engineering behaviour (e.g. increases in hydraulic conductivity) that may occur over the service life of a GCL (e.g. Shackelford et al., 2000).

The magnitude and equivalency of charge in montmorillonite is usually quantified by cation exchange capacity (CEC) rather than by layer charge. The CEC represents the total amount of cations necessary to compensate the negative clay charge and is expressed in milliequivalents per 100 grams of dry clay (meq/100g). A typical CEC

value for montmorillonite is 80-100 meq/ 100g. A higher CEC reflects a greater layer charge and a consequently larger surface activity for exchange. A related property, surface charge density, σ, is defined as CEC divided by specific surface area, and thus has units of meq/100 m^2. It must be stressed that high CEC (and therefore high layer charges or surface charge densities) are not necessarily indicative of bentonite quality for optimal barrier performance.

1.2 **Adsorption and swelling behaviour of sodium bentonite**

Sodium bentonite may exhibit very low hydraulic conductivity values (on the order of 10^{-10} m/s to 10^{-12} m/s) which result primarily from the montmorillonite component's small particle size, large surface area, swelling potential, and capability to adsorb and effectively immobilize pore water through a variety of short-range and long-range hydration mechanisms (Likos et al., 2010). The adsorption and swelling behaviour of bentonite is affected by many factors that are inherent to the bentonite in its natural state, i.e. layer charge (CEC), the location of layer charge, exchange cation identity, the clay microstructure in its natural state, and impurities presence.

Montmorillonite particles are capable of significant interactions with water on the external particle surfaces and on the interlayer surfaces, as a consequence of their large specific surface area values. The initial hydration of a montmorillonite surface involves four basic short-range interaction mechanisms: (i) hydrogen bonding, (ii) dipole-charged surface attraction, (iii) van der Waals attraction, and (iv) hydration of exchangeable cations (Mitchell, 1993).

Hydrogen bonding occurs between water dipoles and oxygens along the surface of the interlayer, and most importantly between water molecules. Charged surface-dipole attraction occurs as water dipoles become attracted to and oriented with the negative electrical field emanating from the mineral surface. Van der Waals attractive fields arise from instantaneous atomic interactions between the atoms comprising the mineral surface and the atoms comprising the pore water.

For montmorillonite hydration of exchangeable cations occurs as the positively charged ions attract water dipoles, which form a hydration shell surrounding the cation. The energy associated with cation hydration is a function primarily of the cation size and valence, where small size, yet low valence provides favourable energetics for hydration (Bohn et al., 1985). Secondary layers of water can H-bond with the primary layer of hydration water, forming multiple hydration shells. These H-bonds decrease in strength rapidly with the number of layers, and, beyond two or three layers, the water of these shells behaves as bulk water.

The physical consequence of these short-range solid-liquid interaction mechanisms is to attract, align, and impart some order into the molecular arrangement of the near surface pore water (Likos et al., 2010).

Moreover, in particular for Na^+, the attraction of additional water may result in "crystalline swelling" at relatively low water contents and in "osmotic swelling" at higher water contents (e.g. when more 3 hydration shells occur).

1.2.1 **Crystalline swelling**

Crystalline swelling is a process whereby expandable 2:1 phyllosilicates sequentially intercalate one, two, three or four discrete layers of water molecules between the mineral interlayers (Norrish, 1954). It occurs prior to osmotic swelling associated with longer-range electrical diffuse double layer effects. Interlayer hydration and dehydration in the crystalline swelling regime has been explored extensively by using a variety of approaches (e.g. through basal spacing measurements using X-Ray Diffraction).

Crystalline swelling is the result of the balance between forces of attraction and repulsion operating between adjacent interlayer surfaces (Norrish, 1954). The net potential energy of interaction (Laird, 2006) is dominated by electrostatic attraction between the exchange cations and the basal surfaces of the clay. The net potential energy of repulsion, on the other hand, is dominated by the hydration energy of the

exchange cations. The exchange cations will attract or release water of hydration until the net potential energies of attraction and repulsion are balanced. Unsaturated conditions or saturated conditions with high electrolyte concentrations favour the dominance of net forces of attraction, while fully saturated conditions of low electrolyte concentration favour the dominance of net forces of repulsion (Likos et al., 2010).

Interlayer attractive energy is proportional to the surface charge density of the mineral, to the interlayer cation valence and to the elementary charge, whereas it is inversely proportional to the half distance between the unit layers and to the permittivity of the intervening fluid. As a consequence, high surface charge density, high cation valence, and small separations distance produce stronger attractive forces that must be overcome by cation hydration for the interlayer to separate.

For monovalent mineral forms, such as Na^+-montmorillonite, where the interlayer attractive forces are relatively weak, interlayer sorption may continue beyond the three or four layers of water associated with crystalline swelling. Additional interlayer separation continues under an osmotic mechanism driven by a gradient in chemical potential between the interlayer water and bulk pore water residing in the interparticle pore space. It is this transition into the osmotic swelling regime that allows for more complete disassociation of the mineral interlayers, large macroscopic volume changes (up to 1660% for free swell), high Atterberg indices, and gelling behaviour partly responsible for the self-healing and low hydraulic conductivity characteristics required for barrier applications (Likos et al., 2010).

1.2.2 **Osmotic swelling**

Osmotic swelling occurs as the result of pore water flow driven by a gradient in dissolved solute concentration between the interparticle pore fluid and the interlayer pore fluid. Figure 1.3 shows a schematic view for the distribution of ions relative to a charged surface in aqueous solution. The charge field emanating from charge

deficiencies in montmorillonite is greatest at the surface and decays with increasing distance. As a result, cations are concentrated near the surface and tend to be diffused at distance.

The Gouy-Chapman diffuse double layer theory (DDL) is considered the most successful approach for this distribution (e.g. Mitchell, 1993). The thickness (1/K) of the DDL, whose decay is modelled exponentially, is:

$$\frac{1}{K} = \sqrt{\frac{\varepsilon_0 DkT}{2n_0 e^2 \nu^2}} \qquad (1.1)$$

where ε_0 is the permittivity of vacuum ($8.8542 \cdot 10^{-12}$ $C^2J^{-1}m^{-1}$), D is the dielectric constant of the pore fluid ($D_{H2O} = 80$), k is the Boltzmann constant ($1.38 \cdot 10^{-23}$ J K^{-1}), T is absolute temperature (K), n_0 is the far-field (bulk pore fluid) ion concentration (ions/m^3), e is the electronic charge ($1.602 \cdot 10^{-19}$ C), and ν is the ion valence. As a result of Eq. (1.1) a double layer will generally decrease in thickness if ion concentration is increased, if the ion valence is increased (e.g if sodium is replaced with calcium), or if the dielectric constant of the pore fluid is decreased. The DDL thickness is very important, since it affects the net interlayer and interparticle interaction force, the corresponding particle and pore microstructure, and the engineering behaviour of the clay.

When two charged surfaces in an electrolyte solution approach each other, their electrical double layers at some point begin to interact and may overlap, if the energetics of the two surfaces favor attraction. Overlapping double layers in clay-water-ion systems may occur on both the particle scale (i.e. between adjacent parallel or non-parallel particles in the interparticle pore space), and on the sub-particle scale (i.e. between quasi-crystals, crystallites, and unit layers in the interlayer pore space): the region of overlapping is characterized by a relatively high concentration of cations, since they are restrained from diffusing to other regions of the pore fluid. This concentration gradient results in osmotic pressure which drives

additional water into the interlayer and allows for disassociation of the unit layers, large bulk volume change, and the formation of a gelled fabric.

In bentonites characterized by high content in montmorillonite the effect of an imperfect semi-permeable membrane is introduced by the restraint in ion mobility that the negatively charged mineral surfaces impose on the interlayer cations in overlapping double layers. Once sufficient separation distances between unit layers are achieved during crystalline swelling, attractive forces no longer dominate, and the interlayer can be considered a region of high concentration compared to the external bulk solution. If cations are retained in the interlayer space in concentrations greater than in the bulk pore fluid, osmotic pressure arises from the difference in ion concentration, thus causing water to be drawn into the zone of relatively high concentration. The volume change associated with this process is referred to as osmotic swelling (e.g. Bolt, 1956).

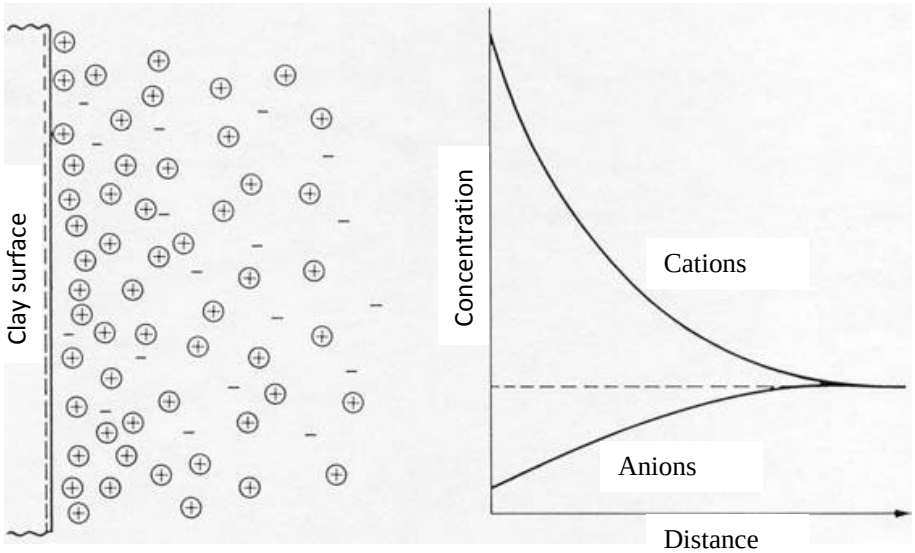

Figure 1.3 Schematic view of the clay-water-ion double layer system (after Mitchell, 1993)

During osmotic swelling, bentonites can form a stable gel phase, i.e. a material which has reduced void sizes and minimal inter-connectivity of pores, and therefore exhibits increased tortuosity of flow path. During wetting, domains of quasi-crystals must be able to re-arrange and expand into the available inter-particle pore space in order to effectively seal under confinement. Typically wetting with low ionic strength solutions forms optimal bentonite gels: in fact, low solution concentrations of counter ions fail to fully shield repulsive forces operating between adjacent clay layers, and enable repulsive forces to override the attractive forces.

1.3 **Engineering properties and their measurement**

A variety of techniques may be employed for evaluating the composition, properties, and quality of bentonite, in particular for use in GCL applications.

X-ray diffraction (XRD), which relies on the interaction of X-rays with atomic planes in the mineral crystalline structure, is commonly used for determining the mineral composition of clayey materials. Reflections defining atomic plane spacings, or basal spacing, in combination with their integrated area, become the primary criteria for mineral identification. The basal spacing of montmorillonite may vary depending on the extent of interlayer separation.

Cation exchange capacity (CEC) is most commonly determined by replacing the cations in the natural exchange complex with a solution of a known or “index” cation species. The quantity of index cations required to satisfy the exchange sites is determined analytically. CEC is generally determined using the ammonium displacement method, but an alternative method is represented by Methylene Blue titration method.

The specific surface area is defined as the combined area of all surfaces as determined by some experimental technique or combination of techniques. A

specific surface area measurement rarely represents a true surface area and each experimental method will provide a different value because (i) the solid surface can be altered during preparation for analysis (e.g. drying exposes more surface) and (ii) if the measurement requires a specific reaction (i.e. a surface complexation reaction), only the surfaces involved in the reaction will be measured (Likos et al., 2010). A variety of methods exist for estimating specific surface area of bentonites: these include physical methods, such as X-ray diffraction to determine crystallographic information, or electron microscopic measurements to determine shape and dimension of particles. These methods tend to provide information on total specific surface area. Knowledge of the structural formula, as well as unit cell information determined by X-ray powder diffraction, enables estimation of the crystallographic surface area, as well as surfaces associated with the interlayer and edge surfaces.

Non-hydrated GCLs contain bentonite in either granular (aggregated) or powdered form. High quality of bentonite is comprised of 70% to 90% particles less than 2 μm. The aggregate particle size of a bentonite product may impact its initial hydration.

The water content of GCL bentonite is an important quality control parameter because of its role in governing mass per unit area. Water content is expressed gravimetrically and may be determined by oven drying to constant mass following ASTM D2216. Drying may take significantly longer than 24 hours for highly plastic soils such as bentonite, as Post (1989) noted. The water content of GCLs in the "dry" or non-prehydrated state typically range from about 10%-18% (Koerner, 1998).

Atterberg Limits are water contents of soil which represent qualitatively the passage between two different states of aggregation. The liquid limit (LL), in particular, is the water content, in percent, of a soil at the boundary between the semi-liquid and plastic state. LL represents how much moisture a soil material can hold until reaching a liquid state. Under a qualitative point of view, LL value can be related to

the external specific surface, S' of montmorillonite particles (Farrar and Coleman, 1967).

Free swell test procedures are described in ASTM Standard D5890. The result of such a test is an index value (Swell Index, SI) which may be used to assess bentonite swell potential as an indirect measure of its effectiveness as a hydraulic barrier. High SI values mean high swelling performance of bentonite in equilibrium with a specific electrolyte solution at a specific molarity. Testing involves grinding the bentonite to pass a #200 (i.e. 75 μm) sieve, filling a 100 ml graduated cylinder with ~90 ml of distilled, de-ionized water, adding 2 grams of oven-dried, powdered bentonite to the cylinder in 0.1 g increments, filling the cylinder to the 100 ml mark, and recording the equilibrium volume (in ml/2g) of the hydrated clay mass that has settled to the bottom of the cylinder after 16 to 48 h. Na^+-bentonites may exhibit swell indices of 25-35 ml/2g.

1.3.1 **Engineering properties of tested sodium bentonite**

The powdered sodium bentonite tested during the PhD laboratory activity is the same described by Puma (2013), Dominijanni et al. (2013) and Puma et al. (2015), i.e. an Indian sodium bentonite which is used for the production of a needle-punched GCL.

The mineralogical composition of the material was evaluated through X-ray diffraction analysis (Puma, 2013): such sodium bentonite presents primarily smectite, with traces of calcite, quartz, mica and gypsum.

The bentonite is characterized by a cation exchange capacity (CEC, measured using the methylene blue adsorption method) of 105 meq/100g (Puma, 2013).

Atterberg Limits, in particular LL, were determined by Puma (2013) by means of Casagrande's device, in accordance with procedures of ASTM 4318 (multipoint liquid limit method). Sodium bentonite was hydrated with DW and sodium chloride solutions characterized by salt concentration of 10 mM and 500 mM.

Experimental results are resumed in Table 1.1 and show that LL decreases when bentonite is exposed to high molarities electrolyte solutions. Such a behaviour is a direct consequence of the reduction of the external specific surface, S' of montmorillonite particles that tend to form tactoids. Tactoid formation is induced by decrease in DDL thickness of particles which decreases the water adsorption capacity of montmorillonite at the microscopic scale, as a consequence of the reduction in S'.

Farrar and Coleman (1967) gave the following regression equation (with the 95% confidence limit in the brackets) between the surface area, S, and the liquid limit, LL, of several British clay soils:

$$S = -14 + 1.48 \cdot LL \ \ (\pm 33), \quad \text{where } [S] = m^2/g \ ; \ [LL] = \% \tag{1.2}$$

The values of specific surface, S, found for sodium bentonite on the basis of the results of LL test using Eq. (1.2) are reported in Table 1.1. They resulted to be within the typical range 700-840 m^2/g (Mitchell and Soga, 2005).

Moreover, the tested sodium bentonite is characterized by a plastic limit (PL) of 63%, measured according to ASTM 4318.

Table 1.1 Liquid limit of powdered sodium bentonite with sodium chloride solutions (ASTM 4318), and evaluation of the corresponding specific surface value obtained, on the basis of LL test, using Eq. (1.2) proposed by Farrar and Coleman (1967) (after Puma, 2013)

	***Salt concentration,* c_s (mM)**	**Liquid limit, LL (%)**	***Specific surface, S (± 33) (m^2/g)***
sodium bentonite + NaCl solutions	DW	525	763
	10	524	762
	500	111	150

Puma (2013) also performed swell index tests (accordingly to ASTM D 5890) on sodium bentonite regarding the equilibrium conditions with de-ionized water (DW) and with sodium chloride solutions (2 mM, 5 mM, 10 mM, 20 mM, 50 mM, 100 mM, 500 mM and 1 M). The swell index trend obtained is reported in Figure 1.4 as a function of the NaCl concentration.

Na^+-bentonites hydrated by NaCl solutions exhibited SI values of 35-25 ml/2g in a range of concentration ranging from 10 mM to 50 mM: stability of bentonite suspensions decreases when the electrolyte concentration increases, since the material behaves as a stable suspension for very low molarity values and for de-ionized water, while swelling behaviour is inhibited for a NaCl concentration higher than 0.5 M. Moreover, the swelling behaviour of the sodium bentonite shows turbid samples ('T' in the graph), which do not present a precise interface between the settled bentonite and the upper clear solution: in these cases, bentonite forms a stable suspension and it is not possible to evaluate a value of SI. As a consequence, a conventional value of SI of 100 ml/2g was assigned to the turbid solutions (actually, without recognizing how much the suspension is turbid).

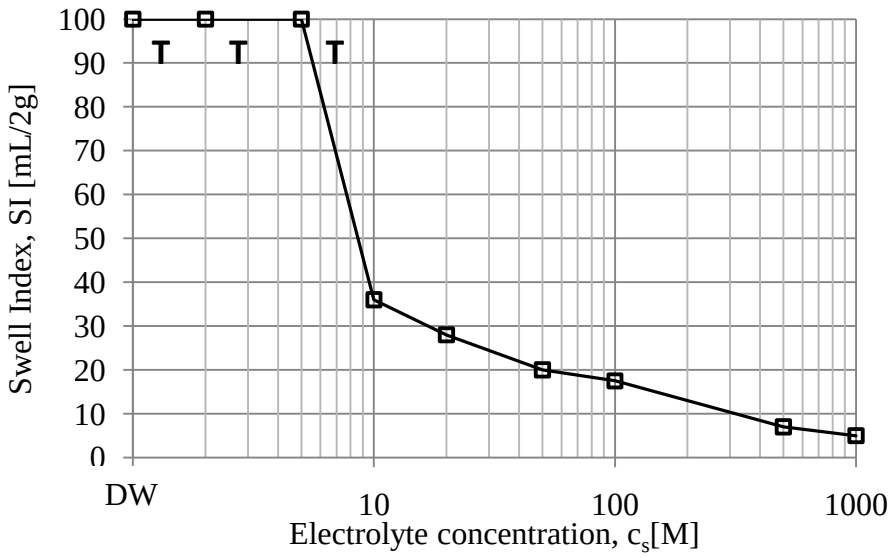

Figure 1.4 Swell index as a function of the NaCl concentration for sodium bentonite (ASTM D5890) (Puma, 2013)

1.4 Swelling behaviour of bentonite under oedometric conditions

The main results of a laboratory study, developed at the beginning of the PhD activity and aimed at analyzing the influence of the equilibrium salt solution concentration and the confining stress on the swelling behaviour of bentonite, are resumed in this paragraph.

Nine swelling tests on powdered sodium bentonite specimens (i.e. SQ_NaB_HS1-9, Table 1.2) under oedometric conditions in equilibrium with NaCl solutions at different molarities were performed using a traditional oedometer, as shown in Figure 1.5.

Table 1.2 Initial and final physical properties of oven-dried squeezed sodium bentonite specimens submitted to swelling tests, under oedometric conditions, in equilibrium with different NaCl solutions

SPECIMEN	σ_v **(kPa)**	c_s **(mM)**	m_d *(g)*	h_0 **(mm)**	e_0 **(-)**	m_f *(g)*	h_f **(mm)**	w_f **(-)**	e_f **(-)**
SQ_NaB_HS1	**12.3**	10	9.04	4.50	1.59	30.06	11.63	2.15	5.70
SQ_NaB_HS2		50	8.97	4.50	1.61	23.70	8.78	1.54	4.09
SQ_NaB_HS3		250	9.09	4.50	1.58	20.25	6.96	1.13	2.98
SQ_NaB_HS4	**24.5**	10	9.08	4.50	1.58	24.26	9.41	1.66	4.39
SQ_NaB_HS5		50	8.98	4.50	1.61	21.08	7.99	1.37	3.63
SQ_NaB_HS6		250	9.10	4.50	1.57	19.45	6.37	1.00	2.64
SQ_NaB_HS7	**49.0**	10	9.00	4.50	1.60	22.23	7.70	1.30	3.45
SQ_NaB_HS8		50	9.00	4.50	1.60	20.11	6.62	1.07	2.83
SQ_NaB_HS9		250	9.07	4.50	1.58	18.15	5.77	0.87	2.31

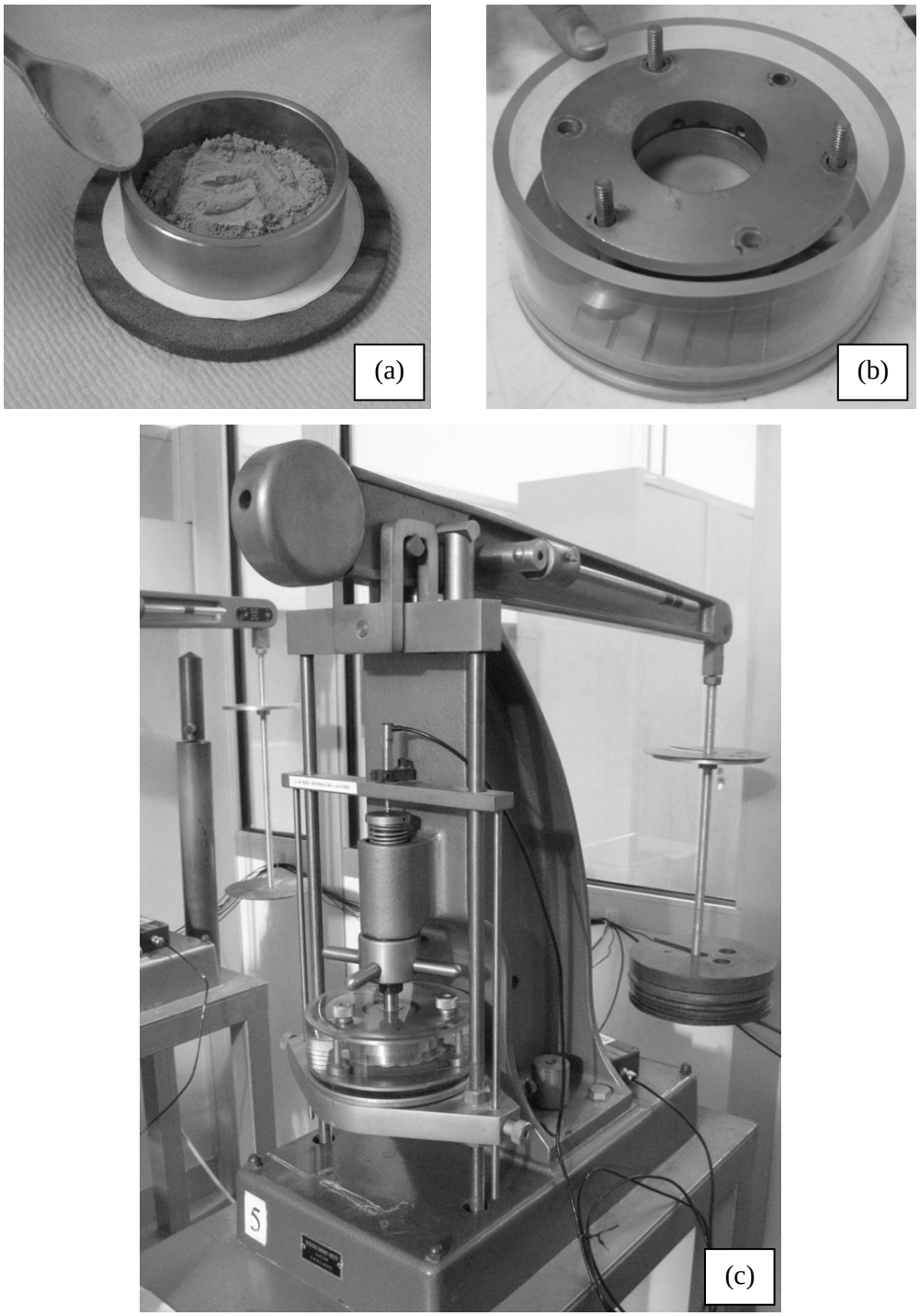

Figure 1.5 Oedometric testing device: (a) stainless steel ring, (b) plexiglass cell, and (c) full oedometric apparatus

In a preliminary phase, the sodium bentonite was submitted to the same 'squeezing' process described in Dominijanni et al. (2013) (see chapters 3 and 4), in order to remove the soluble salts which are naturally present inside the powdered material, as a consequence of its marine origin, and to prevent them from affecting the determination of the swelling properties of the sodium bentonite.

All the samples were then prepared by dusting a dry mass, $m_d \cong 9$ g of sodium bentonite inside the stainless steel ring in the plexiglass cell: specimens reached an initial height, h_0 of 4.5 mm. Samples SQ_NaB_HS1-3 were saturated under a total axial stress of 12.3 kPa respectively with NaCl 0.01, 0.05 and 0.25 concentrated solutions, samples SQ_NaB_HS4-6 under a total stress of 24.5 kPa respectively with NaCl 0.01, 0.05 and 0.25 concentrated solutions, and samples SQ_NaB_HS7-9 under a total stress of 49.0 kPa respectively with NaCl 0.01, 0.05 and 0.25 concentrated solutions.

Figure 1.6 (i.e. specimens SQ_NaB_HS1-3), Figure 1.7 (i.e. specimens SQ_NaB_HS4-6) and Figure 1.8 (i.e. specimens SQ_NaB_HS7-9), represent the axial displacement, referred to the initial height of the specimens and measured by LVDT transducer, as a function of time, for the three different concentrations of NaCl solutions. All the specimens were allowed to swell for several days and the tests were stopped when the specimen volume ceased to increase, reaching a stable value of height, h_f.

As expected from the Gouy-Chapman DDL theory, bentonite specimens have reached higher final heights for decreasing total vertical stresses and for decreasing concentrations of salt solution, which have allowed for the formation of thicker double layers during hydration.

At the end of each test, sodium bentonite was taken from the plexiglass cell in order to measure the final mass, m_f, of wet specimen and derive the final water content, w_f, and the final void ratio, e_f: such experimental measures are resumed in Table 1.2

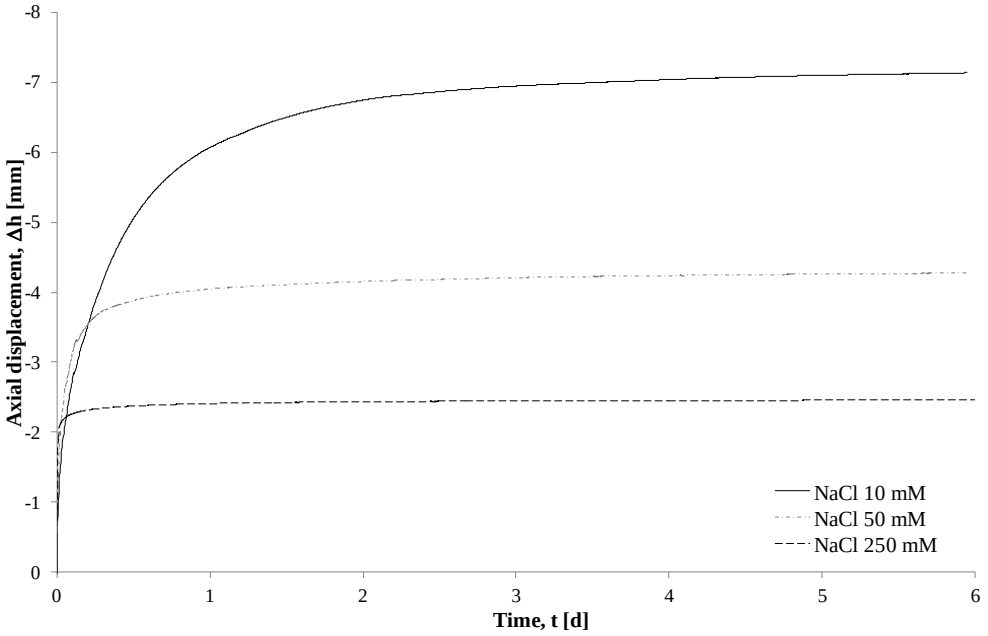

Figure 1.6 Axial displacement measures as a function of time of specimens SQ_NaB_HS1-3, under a total vertical stress of 12.3 kPa with different concentrations of NaCl solution

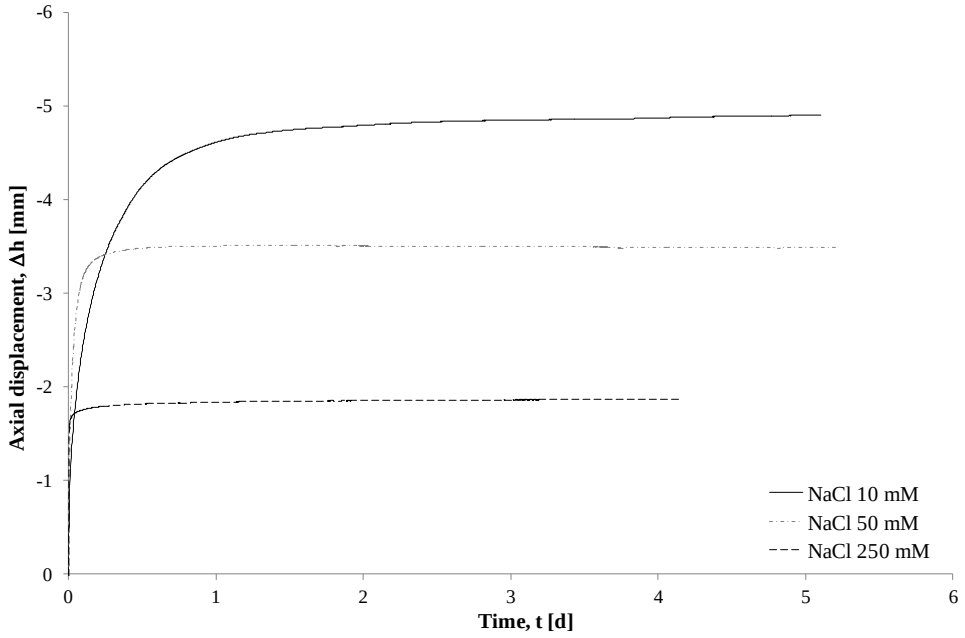

Figure 1.7 Axial displacement measures as a function of time of specimens SQ_NaB_HS4-6, under a total vertical stress of 24.5 kPa with different concentrations of NaCl solution

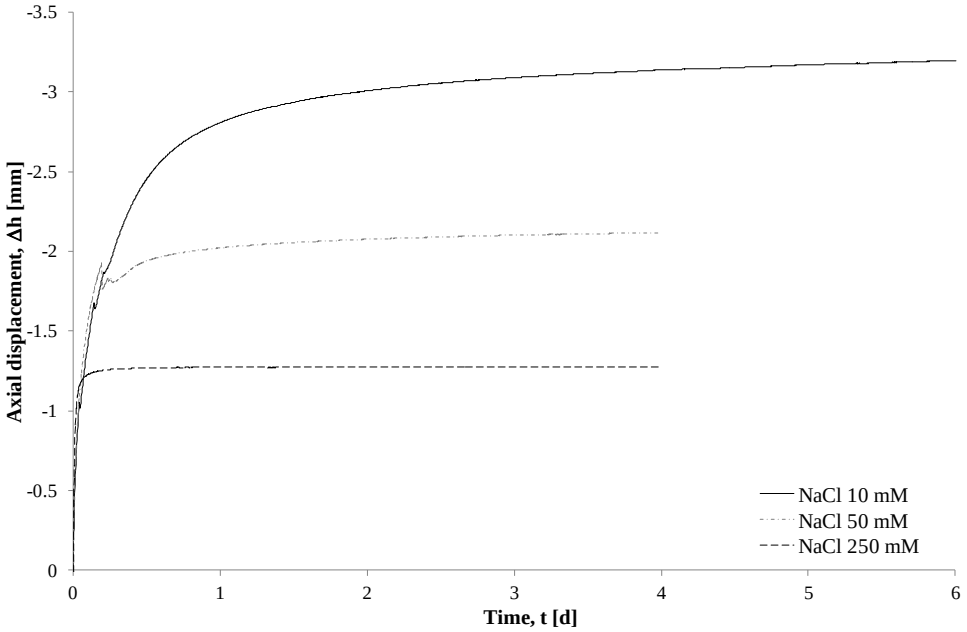

Figure 1.8 Axial displacement measures as a function of time of specimens SQ_NaB_HS7-9, under a total vertical stress of 49.0 kPa with different concentrations of NaCl solution

1.5 **Geosynthetic Clay Liners (GCLs)**

Geosynthetic clay liners (GCLs) are manufactured hydraulic barriers typically consisting of a thin layer (~5-15 mm) of natural or treated bentonite (sodium or calcium) sandwiched between two geotextiles and/or glued to a geomembrane (Daniel et al., 1993; Koerner and Daniel, 1995; Bouazza, 2002; Koerner, 2005). The primary differences among GCLs are the mineralogy (e.g., content of montmorillonite) and form (e.g., powdery versus granular) of bentonite used in the GCL, the type of geotextile (e.g., woven versus non-woven), the hydration condition (e.g., non-prehydrated versus prehydrated), and the method of bonding the component materials together (e.g., Daniel et al., 1993; Koerner and Daniel, 1995; Shackelford et al., 2000; Lee and Shackelford, 2005).

The preferential use of GCLs in applications relative to alternative barriers or barrier components, such as compacted clay liners (CCLs) and geomembrane liners

(GMLs), has increased over the past decades due to several advantages. The two primary motivations are a savings in cost, and an establishment of technical equivalency relative to CCLs (e.g. Daniel et al., 1993; Koerner and Daniel, 1995; Lee and Shackelford, 2005; Kang and Shackelford, 2011). The savings in cost results essentially from the ease of installation of GCLs relative to both CCLs and GMLs as well as from the maximization of disposal space due to the thinness of GCLs relative to CCLs. In terms of technical equivalency (see Figure 1.9), there are a number of technical advantages for preferring GCLs relative to CCLs and/or GMLs (e.g., Bouazza 2002).

	Criterion	Equivalency of GCL to CCL			
Category	for Evaluation	GCL Probably Superior	GCL Probably Equivalent	GCL Probably Inferior	Site or Product Dependent
Construction Issues	Ease of Placement	X			
	Material Availability	X			
	Puncture Resistance			X	
	Quality Assurance	X			
	Speed of Construction	X			X
	Subgrade Condition	X			
	Water Requirements				X
	Weather Constraints				
Contaminant Transport Issues	*Attenuation Capacity*			X(1)	X
	Gas Permeability				X
	Solute Flux and Breakthrough Time	X(2)		X	
Hydraulic Issues	*Compatibility*	X(2)		X	
	Consolidation Water	X			
	Steady Flux of Water		X		
	Water Breakthrough Time				X
Physical/ Mechanical Issues	Bearing Capacity				X
	Erosion				X
	Freeze-Thaw	X			
	Settlement-Total		X		
	Settlement-Differential	X			
	Slope Stability				X
	Wet-Dry	X			

(1) Based only on total exchange capacity, TEC
(2) Only for GCLs with a geomembrane

Figure 1.9 Equivalency between Geosynthetic clay liners, GCLs, and compacted clay liners, CCLs (after Daniel and Koerner, 1995; Shackelford and Nelson, 1996)

However, the primary technical justification probably has been the extremely low hydraulic conductivity, k, of GCLs when permeated with de-ionized water, which is typically less than approximately 3.0×10^{-11} m/s (e.g., Daniel et al. 1997).

Another technical aspect, which favours the use of GCLs, is the greater self-healing capability of the bentonite in GCLs relative to CCLs constructed with typically lower plasticity natural clay soils, and a generally greater ability to withstand relatively large differential settlements compared with CCLs (Shackelford, 2007). The greater self-healing capability of GCLs allows them to overcome small defects, such as puncture holes and generally leads to greater resistance of GCLs to increases in k resulting from climatological distress due to repeated freezing-thawing and/or wetting-drying cycles. Finally, the ability to seal containment facilities by simply overlapping adjacent GCL panels and placing dry bentonite between the panels favours the installation of GCLs relative to GMLs, where such adjacent panels must be welded together to ensure an intact, continuous seam.

In addition, GCLs also have been found to behave as semipermeable membrane, thereby restricting the migration of solutes (Malusis and Shackelford, 2002a,b). Since the purpose of clay barriers used in hydraulic containment applications is to restrict the migration of aqueous miscible contaminants (i.e. solutes), the existence of membrane behaviour in GCLs represents a potentially significant beneficial aspect in the use of GCLs for such applications (Kang and Shackelford, 2011).

GCLs typically are categorized as either unreinforced or reinforced. In the former case, they are held together by mixing an adhesive (i.e. glue) with the bentonite to affix it to the adjacent geotextiles or a geomembrane; in the latter case, they are bonded by stitching or needle-punching fibres through the geotextiles adjacent to each side of a layer of bentonite. The existence of the stitched or needle-punched fibres in reinforced GCLs provides greater internal resistance to shear than in unreinforced ones: as a result, such GCLs can be used as liners or liner system components on the side slopes of waste containment systems.

Geosynthetic clay liners also may be categorized as either single-barrier GCLs or composite barrier GCLs (Figure 1.10). In single-barrier GCLs bentonite is encased or sandwiched between two geotextiles, and its hydraulic performance depends primarily on the bentonite hydraulic resistance. In contrast, in composite-barrier GCLs, two hydraulic resistant materials are included, i.e., bentonite and a polymer sheet such as a geomembrane or other polyethylene geofilm (Figure 1.11). Although both the bentonite and the polymer sheet likely provide hydraulic resistance in composite barrier GCLs, the overall hydraulic resistance likely is dominated by the polymer sheet (Shackelford, 2007).

The geotextiles used in GCLs may be either woven or non-woven, although at least one of the geotextiles in a needle-punched GCL must be non-woven to ensure the fibres from this geotextile can be punched through the bentonite layer in order to create an interlocking system (Hsuan, 2002). Moreover, geomembranes may be either textured or non-textured, with the former consisting of a roughened surface aimed at increasing the interface frictional resistance for use on side slopes.

The type of polymer commonly used for fibres and geotextiles in reinforced GCLs is polypropylene (PP), although polyethylene (PE) geotextiles and fibres also have been used in some cases (Hsuan, 2002). Since both PP and PR are sensitive to oxidative degradation, antioxidants are routinely incorporated into the polymer resin for protection (Hsuan, 2002).

The quality of the bentonite increases with increase in smectite (i.e. montmorillonite) content, surface area (decrease in particle size), surface charge deficiency, and/or percentage of sodium (Na^+) on the exchange complex (Shackelford, 2007). The effect of these factors on the quality of the bentonite generally is indicated macroscopically by an increase in cation exchange capacity (CEC), an increase in plasticity, an increase in swell capacity in the presence of water, and a decrease in hydraulic conductivity, k, based on permeation with water.

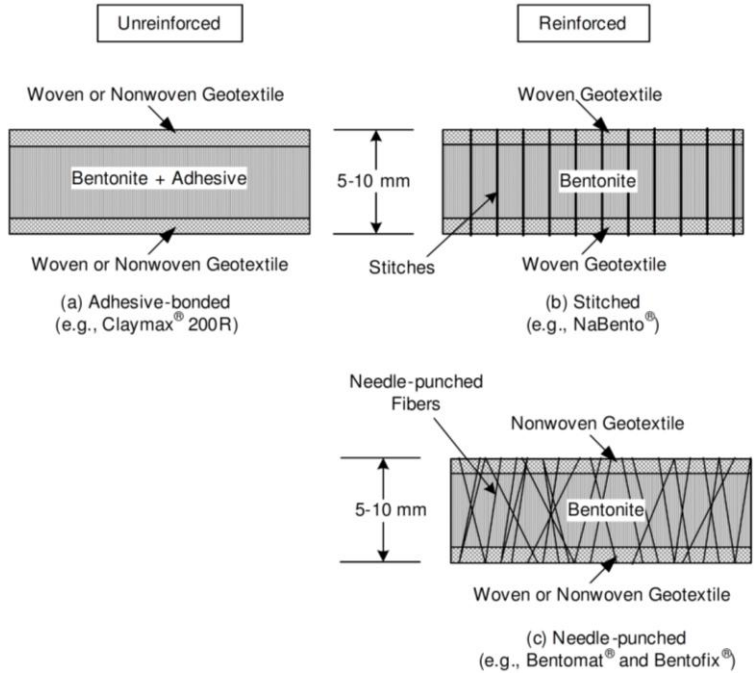

Figure 1.10 Types of single-barrier GCLs (not to scale, after Shackelford, 2007)

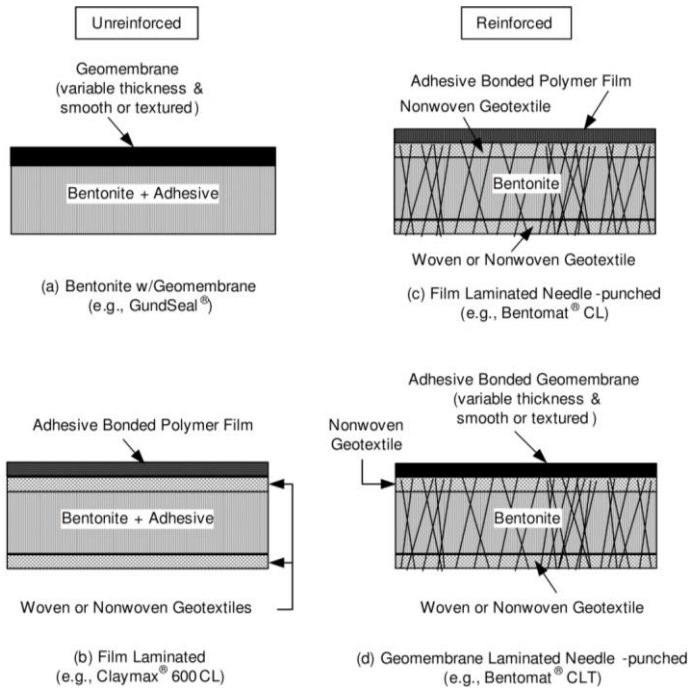

Figure 1.11 Common types of composite-barrier GCLs (not to scale, after Shackelford, 2007)

However, as noted by Lee and Shackelford (2005) and by Puma et al. (2015), even though so-called higher quality bentonites typically result in lower k upon permeation with water, such bentonites are also more susceptible to chemical attack (i.e. cation exchange) upon permeation with non-standard liquids (i.e., liquids different from water, for example $CaCl_2$ solutions), resulting in greater increases in k (i.e., $\Delta k > 0$) for higher quality bentonites relative to those that occur with lower quality bentonites.

1.6 **Clay membrane barriers**

In the last decades, great research efforts have been devoted to the potential benefits arising from the existence of semi-permeable membrane behaviour in bentonite and bentonite-based barrier materials (Malusis, 2001; Malusis et al., 2001; Malusis and Shackelford, 2002a,b; Van Impe, 2002; Malusis et al., 2003; Manassero and Dominijanni, 2003; Shackelford et al., 2003; Shackelford and Lee, 2003; Henning, 2004; Lu et al., 2004; Dominijanni, 2005; Yeo et al., 2005; Dominijanni et al., 2006; Kang and Shackelford, 2009, 2010, 2011; Di Emidio, 2010; Dominijanni and Manassero, 2012a,b; Bohnhoff and Shackelford, 2013; Dominijanni et al., 2013; Malusis et al., 2012, 2013; Puma, 2013; Shackelford, 2013; Malusis and Daniyarov, 2014; Manassero et al., 2014; Meier et al., 2014).

The electric interaction between the montmorillonite lamellae and the ions contained in the pore solution generates macroscopic phenomena which cannot be modelled with the classical constitutive equations of soil mechanics (Mitchell, 1993). For instance, when a bentonite layer is put in equilibrium with an electrolyte solution, swelling or shrinkage is observed depending on the salt concentration, without any apparent modifying of the effective stresses. Moreover, if a bentonite layer is interposed between two electrolyte solutions with different salt concentrations, a volumetric flux of water can be observed, even in the absence of a hydraulic gradient.

The mechanical and transport behaviour of bentonites has more affinity with that of biological tissues, reverse-osmosis membranes, or polyelectrolyte gels than with that of sands or gravels, since clays are characterized by membrane behaviour.

Clay soils in general are semipermeable porous media, since they are permeable to only some components of a solution. Referring to a permeating solution constituted by a solvent and a single solute, a semipermeable membrane is "ideal" or "perfect" if is able to prevent completely the passage of the solute. However the ability to restrict the movement of solutes is only one of the so-called "osmotic properties" of clay soils. The movement of the permeating solution through a semipermeable membrane, for example, may be driven by a solute concentration gradient (chemico-osmosis) or by an electric potential gradient (electro-osmosis).

Nowadays, we know that all osmotic properties of semipermeable membranes are due to the ability of the solid skeleton to "interact" differently with the components of the fluid phase. The simplest "interaction" is that to hinder the passage of molecules having size greater than the pore size (steric hindrance). For clays the main source of osmotic phenomena is recognized to be the electrostatic interaction between the ions in the pore solution and the solid skeleton, having generally a negative electric charge.

The materials characterized by similar properties are very common. Clay soils are an example of mineral semipermeable membranes or, preferentially, semipermeable porous media, considering that: (i) they are characterized by a system of interconnected pores; (ii) they may have an appreciable thickness (Dominijanni, 2005).

Clay membrane behaviour is quantified in terms of reflection coefficient, ω. The value of ω for a clay soil exhibiting no solute restriction is zero ($\omega = 0$), corresponding to zero membrane efficiency, whereas the value of ω for clay soil exhibiting complete solute restriction is unity ($\omega = 1$), corresponding to 100% membrane efficiency. In general, the value of ω for naturally occurring clay soils that exhibit membrane behaviour range from greater than zero to less than unity because of the variation in the pore sizes that exist in such soils (Shackelford, 2005).

Clay membrane behaviour is a function of several mechanical, physical and chemical factors, such as stress-strain properties of clay, boundary and initial salt concentrations, type of solute species (ions) and mineralogy of the soil (Shackelford et al., 2003). In general, the potential for the existence of membrane behaviour increases with (a) an increase in stress (decrease in porosity), (b) an increase in content of high activity clay minerals, particularly sodium montmorillonite, and (c) a decrease in the salt concentration in the pore water (Shackelford et al., 2003).

References

1. ASTM, 2002. Standard Test Method for Laboratory Determination of Water (Moisture) Content of Soil and Rock by Mass, D 2216-98: 2000 Annual Book of ASTM Standards, Vol. 04.08. American Society for Testing and Materials, West Conshohocken, PA.
2. ASTM, 2002. Standard Test Methods for Liquid Limit, Plastic Limit, and Plasticity Index of Soils, D 4318-00: 2000 Annual Book of ASTM Standards, Vol. 04.08. American Society for Testing and Materials, West Conshohocken, PA.
3. ASTM, 2011. Standard Test Method for Swell Index of Clay Mineral Component of Geosynthetic Clay Liners, D 5890-11: 2011 Annual Book of ASTM Standards, Vol. 04.13. American Society for Testing and Materials, West Conshohocken, PA.
4. Bohn, H.L., McNeal, B.L., O'Connor, G.A. (1985). *Soil chemistry*, 2nd Edition, John Wiley and Sons, New York.
5. Bohnoff, G.L., Shackelford, C.D. (2013). Improving membrane performance via bentonite polymer nanocomposite. *Applied Clay Science* **86**, 83-98.
6. Bolt, G.H. (1956). Physicho-chemical analysis of the compressibility of pure clays. *Géotechnique* **6**(2): 86-93.

7. Bouazza, A. (2002). Geosynthetic clay liners. Review article. *Geotextiles and Geomembranes* **20**, 3-17.
8. Daniel, D.E., Bowders, J.J., Jr., Gilbert, R.B. (1997). Laboratory hydraulic conductivity testing of GCLs in flexible-wall permeameters. *Testing and Acceptance Criteria for Geosynthetic Clay Liners*, L.W. Well, ed., ASTM STP 1308, 208-226.
9. Daniel, D.E., Shan, H.-Y., Anderson, J.D. (1993). Effects of partial wetting on the performance of the bentonite component of a geosynthetic clay liner. Geosynthetics '93. Industrial Fabrics Association International, St. Paul, Minnesota, USA, 3, pp. 1483-1496.
10. Daniel, D.E., Koerner, R.M. (1995). Waste Containment Facilities: Guidance for Construction, Quality Assurance and Quality Control of Liner and Cover Systems. ASCE, New York.
11. Dominijanni, A. (2005). Osmotic properties of clay soils. PhD Dissertation. Politecnico di Torino, Torino, Italy.
12. Dominijanni, A., Manassero, M. (2012,a). Modelling the swelling and osmotic properties of clay soils. Part I: The phenomenological approach. *International Journal of Engineering Scienc*e, **51**, 32-50.
13. Dominijanni, A., Manassero, M. (2012,b). Modelling the swelling and osmotic properties of clay soils. Part I: The physical approach. *International Journal of Engineering Science*, **51**, 51-73.
14. Dominijanni, A., Manassero, M., Puma, S. (2013). Coupled chemical-hydraulic-mechanical behaviour of bentonites. *Géotechnique*, **63**(3), 191-205.
15. Egloffstein, T.A. (2001). Natural bentonite-influence of the ion exchange and partial desiccation on permeability and self-healing capacity of bentonites used in GCLs. *Geotextiles and Geomembranes*, **19**, 427-444.
16. Farrar, D., M., Coleman, J., D., (1967). The correlation of surface area with other properties of nineteen British clay soils. *Journal or Soil Science*, **18**(1), 118-124.

17. Gates, W.P. (2007). Geosynthetic Clay Liner Technology: Understanding Bentonite. National Landfill & Transfer Stations Conference, 2007, Melbourne, Australia.
18. Grim, R.E., Güven, N. (1978). *Bentonites: Geology, Mineralogy, Properties and Uses*. Chapter 4. Elsevier, Amsterdam.
19. Henning, J. T. (2004). Chemico-osmotic efficiency of two real word slurry trench cutoff wall backfills. MS Thesis, Bucknell University, Lewisburg, Pennsylvania, USA.
20. Hsuan, Y.G. (2002). Approach to the study of durability of reinforcement fibers and yarns in geosynthetic clay liners. *Geotextiles and Geomembranes* **20**(1), 63-76.
21. Kang, J.-B., Shackelford, C.D. (2009). Clay membrane testing using a flexible-wall cell under closed-system boundary conditions. *Applied clay science*, **44**, 43-58.
22. Kang, J.-B., Shackelford, C.D. (2010). Membrane behaviour of compacted clay liners. *Journal of geotechnical and geoenvironmental engineering*, **136**(10), 1368-1382.
23. Kang, J.-B., Shackelford, C.D. (2011). Consolidation enhanced membrane behavior of a geosynthetic clay liner. *Geotextiles and Geomembranes*, **29**(6), 544-556.
24. Koerner, R.M. (1998). *Designing with Geosynthetics*, 4th Edition, Prentice Hall, Upper Saddle River, New Jersey.
25. Koerner, R.M. (2005). *Designing with Geosynthetics*, 5th ed. Pearson Prentice Hall, Upper Saddle River, New Jersey.
26. Koerner, R.M., Daniel, D.E. (1995). A suggested methodology for assessing the technical equivalency of GCLs to CCLs. In: Koerner, R.M., Gartung, E., Zanzinger, H. (Eds.), Geosynthetic Clay Liners. Balkema, Rotterdam, pp. 73-98.
27. Laird, D.A. (2006). Influence of layer charge on swelling of smectites. *Applied Clay Science* **34**, 74-87.

28. Lee, J.-Y., Shackelford, C.D. (2005). Impact of bentonite quality on hydraulic conductivity of geosynthetic clay liners. *Journal of Geotechnical and Geoenvironmental Engineering* **131**(1), 64-77.
29. Likos, W.J., and Lu, N. (2006). Pore-scale analysis of bulk volume change from crystalline interlayer swelling in Na and Ca-smectite. *Clays and Clay Minerals* **54**(4): 516-529.
30. Likos, W.J., Bowders, J.J., Gates, W.P. (2010). Mineralogy and engineering properties of bentonite, (Chapter 3). In *Geosynthetic Clay Liners for Waste Containment Facilities*, eds A. Bouazza and J.J. Bowders, CRC Press, The Netherlands, pp. 31-53.
31. Malusis, M.A. (2001). Membrane behaviour and coupled solute transport through a Geosynthetic Clay Liner. PhD Dissertation, Colorado State University, Fort Collins, Colorado, USA.
32. Malusis, M.A., Shackelford, C.D., Olsen, H.W. (2001). A laboratory apparatus to measure chemico-osmotic efficiency coefficients for clay soils. *Geotechnical Testing Journal* **24**, 229-242.
33. Malusis, M.A. & Shackelford, C.D. (2002a). Chemico-osmotic efficiency of a geosynthetic clay liner. *Journal of Geotechnical and Geoenvironmental Engineering* **128**, No. 2, 97–106.
34. Malusis, M.A. & Shackelford, C.D. (2002b). Coupling effects during steady-state solute diffusion through a semipermeable clay membrane. *Environmental Science and Technology* **36**, No. 6, 1312–1319.
35. Malusis, M.A., Shackelford, C.D., Olsen, H.W. (2003). Flow and transport through clay membrane barriers. *Engineering geology*, **70**, 235-248.
36. Malusis, M.A., Shackelford, C.D., Maneval, J.E. (2012). Critical review of coupled flux formulations for clay membranes based on nonequilibrium thermodynamics. *Journal of Contaminant Hydrology* **138-139**, 40-59.
37. Malusis, M.A., Kang, J.-B., Shackelford, C.D. (2013). Influence of membrane behavior on solute diffusion through GCLs. Coupled Phenomena in Environmental Geotechnics, M. Manassero, A. Dominijanni, S. Foti and

G. Musso, Eds., July 1-3, 2013, Torino, Italy, CRC Press/Balkema, Taylor & Francis Group, London, 267-274.

38. Malusis, M.A., Daniyarov, A.S. (2014). Membrane efficiency of a dense, prehydrated GCL. 7th International Congress on Environmental Geotechnics, A. Bouazza, S. Yuen and B. Brown, Eds, November 10-14, 2014, Melbourne, Australia, 2014 Engineers Australia, 1166-1173.
39. Manassero, M., Dominijanni, A. (2003). Modelling the osmosis effect on solute migration through porous media. *Géotechnique*, **53**(5), 481-492.
40. Manassero, M., Dominijanni, A., Musso, G., Puma, S. (2014). Coupled phenomena in contaminant transport. 7th International Congress on Environmental Geotechnics, A. Bouazza, S. Yuen and B. Brown, Eds, November 10-14, 2014, Melbourne, Australia, 2014 Engineers Australia, 144-169.
41. Meier, A., Sample-Lord, K. M., Castelbaum, D., Kallase, S., Moran, B., Ray, T., Shackelford, C. D. (2014). Persistence of semipermeable membrane behavior for a geosynthetic clay liner. 7th International Congress on Environmental Geotechnics, A. Bouazza, S. Yuen and B. Brown, Eds, November 10-14, 2014, Melbourne, Australia, 2014 Engineers Australia, 496-503.
42. Mitchell, J.K. (1993). *Fundamentals of soil behavior* (2nd ed.). New York: Wiley.
43. Mitchell, J.K., Soga, K. (2005). *Fundamentals of soil behaviour* (3rd ed.) New York: Wiley & Sons.
44. Norrish, K. (1954). The swelling of montmorillonite. Discussions of the Faraday Society, **18**, 120-134.
45. Post, J.L. (1989). Moisture content and density of smectites. *Geotechnical Testing Journal* **12**(3): 217-221.
46. Puma, S. (2013). Chemico-mechanical improvement of bentonite barriers for pollutant containment. PhD Dissertation. Politecnico di Torino, Torino, Italy.

47. Puma, S., Dominijanni, A., Manassero, M., Zaninetta, L. (2015). The role of physical pretreatments on the hydraulic conductivity of natural sodium bentonites. *Geotextiles and Geomembranes*, **43**, 263-271.
48. Shackelford, C.D., Nelson, J.D. (1996). Geoenvironmental design considerations for tailings dams. *In* Proceedings Seismic and environmental design of earth dams, concrete dams and tailings dams. Santiago, Chile.
49. Shackelford, C.D., Benson, C.H., Katsumi, T., Edil, T.B., Lin, L. (2000). Evaluating the hydraulic conductivity of GCLs permeated with non-standard liquids. *Geotextiles and Geomembranes* **18** (2-4), 133-161.
50. Shackelford, C.D., Malusis, M.A., Olsen, H.W. (2003). Clay membrane behaviour for geoenvironmental containment. Soil and rock America conference 2003 (*in* Proceedings of the joint 12th Panamerican Conference on Soil Mechanics and Geotechnical Engineering and the 39th U.S. Rock Symposium), Culligan, P. J., Einstein, H. H., and Whittle, A. J. (Eds), Verlag Glückauf GMBH, Essen, Germany, **1**, 767-774.
51. Shackelford, C.D. (2005). Environmental issues in geotechnical engineering. 16th International conference on soil mechanics and geotechnical engineering, **1**, Osaka, Japan, September 12-16, Millpress, Rotterdam, Netherlands, 95-122.
52. Shackelford, C.D. (2007). Selected issues affecting the use and performance of GCLs in waste containment applications. In: Geosynthetics and Environment, XXI Geotechnical Conferences of Torino (GCT), Torino, Italy, November 2007.
53. Teppen, B.J., Miller, D.M. (2005). Hydration energy determines isovalent cation exchange selectivity by clay minerals. *Soil Science Society America Journal* **70**, 31-40.
54. Van Impe P. O. (2002). Consolidation, contaminant transport and chemico-osmotic effects in liner materials. PhD Dissertation, Ancona University, Ancona, Italy.

55. Yeo, S. S., Shackelford, C. D., Evans, J. C. (2005). Membrane behaviour of model soil-bentonite backfills. *Journal of geotechnical and geoenvironmental engineering*, **131**(4), 418-429.

2. THEORETICAL MODELS FOR MECHANICAL AND OSMOTIC BEHAVIOUR OF BENTONITES

The present chapter is focused on the theoretical approaches (Dominijanni and Manassero, 2012a,b; Dominijanni et al., 2013) which can be adopted with the aim of modelling mechanical behaviour and transport properties of bentonite contained in Geosynthetic Clay Liners.

2.1 Introduction

The electric interaction between montmorillonite particles, which represent the main mineralogical component of bentonite, and the ions in pore solution determines macroscopic phenomena which cannot be modelled on the basis of the classical theories of Soil Mechanics used to describe the movement of water and solutes through porous media (Mitchell, 1993). For instance, when a bentonite layer is put in equilibrium with an electrolyte solution, swelling or shrinkage occurs depending on the salt concentration, without any apparent modification of the effective stresses; moreover, if a bentonite layer is interposed between two electrolyte solutions with different salt concentrations, a volumetric flux of water can be observed, even under a condition of null hydraulic gradient (i.e. membrane behaviour). The evaluation of bentonite performances requires an adequate theoretical approach which is able to

model the simultaneous migration of water and solutes, and to account for the deformations of the solid skeleton (Dominijanni and Manassero, 2012a).

Two different theoretical approaches can be adopted with the aim of modelling mechanical behaviour and transport properties of bentonite. The first one is called *phenomenological*, because it is finalized to describe how phenomena occur at the macroscopic scale of observation, without explaining why. The second one is called *physical*, because it has the scope of explaining macroscopic phenomena on the basis of a picture of the physical and chemical interactions which occur at the microscopic or pore scale.

The *phenomenological approach* is based on the formalism of the Thermodynamics of irreversible processes and allows for the identification of macroscopic parameters which govern mechanical, hydraulic and transport behaviour of bentonite. The *physical approach* is based on a conceptual picture of the bentonite structure and Donnan's equations of equilibrium between membranes and electrolyte solutions.

In Dominijanni and Manassero (2012a) a *phenomenological approach* was developed with reference to a solution containing N ion species, and by accounting for both mechanical and transport constitutive equations, under the following simplifying assumptions:

1. unidimensional geometry (spatial coordinate, x), representing the reference problem (Figure 2.1);
2. infinitesimal strains of the solid skeleton;
3. saturated porous medium (the voids are filled with an electrolyte solution);
4. incompressible solid and liquid phase;
5. infinitely diluted electrolyte solution;
6. complete dissociation of the salts in the solution;
7. absence of chemical reactions.

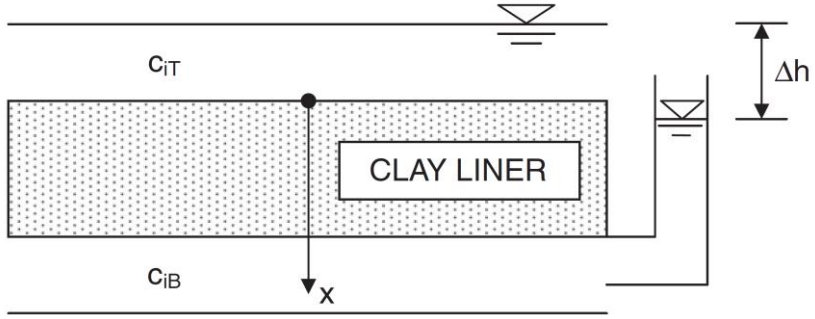

Figure 2.1 Reference problem representing a horizontal clay barrier separating two electrolyte solutions containing different concentrations of ions (Dominijanni and Manassero, 2012a). Symbols: c_{iT} = concentration of the *i*th ion in the solution at the top of the liner; c_{iB} = concentration of the *i*th ion in the solution at the bottom of the liner; Δh = difference in the hydraulic head between the top and bottom electrolyte solutions; x = spatial coordinate.

In order to maintain the purely *phenomenological approach*, it was necessary to refer the state variables of the system (i.e. the hydraulic pressure, the ion concentrations and the electric potential) to a virtual solution, which was considered to be in thermodynamic equilibrium with the real pore solution at any point of the porous medium. Such approach results to be consistent, since it is possible to formulate the boundary conditions for the virtual solution, in terms of the values assumed by the state variables in the external real bulk solutions in contact with the porous medium. The obtained constitutive equations were characterized by the phenomenological parameters, which were assumed to be measured by means of macroscopic experimental tests, without any identification of the physical mechanisms that influence them at the microscopic scale.

A *physical approach* was proposed by Dominijanni and Manassero (2012b), in order to provide an interpretation of phenomenological parameters, which can be obtained from laboratory tests. Chemical equilibrium was assumed to be established between the bulk electrolyte solution and the internal pore solution at the macroscopic scale: in such a way, the hydraulic pressure and ion concentrations can be evaluated through Donnan's equations. Water and ion transport were described at the pore

scale through the generalized Navier-Stokes equations and the generalized Nernst-Planck equations, respectively; mechanical behaviour was modelled taking into account intergranular contact stresses.

The two approaches are complementary and represent a very useful tool for the interpretation of experimental data, in order to reduce the number of tests, which needs to be carried out, and simulate the performances of GCLs in applications, under boundary conditions that are different from those adopted in laboratory.

2.2 **Bentonite structure and partition effect**

Montmorillonite crystals consist of parallel-aligned elementary alumino-silicate lamellae, which are approximately 10 Å thick and 1000-2000 Å in the lateral extent. The unit cell parameters are a = 5.17 Å and b = 8.95 Å, which correspond to a unit cell area of 92.5 $Å^2$, or one unit charge per 140 $Å^2$. The corresponding surface charge, σ, is equal to 0.114 $C \cdot m^{-2}$. The total specific surface, S, available for water adsorption is approximately equal to 760 $m^2 \cdot g^{-1}$, assuming a solid density, ρ_{sk} = 2.65 $g \cdot cm^{-3}$ (Dominijanni and Manassero, 2012b).

Montmorillonite particles can be represented as infinitely extended platy particles. The half distance, b (m), between the montmorillonite particles can be estimated from the total porosity, n (-), or the void ratio, e = n/(1-n) (-). Norrish (1954) showed that bentonite can have a dispersed structure in which clay particles are present, as well separated units, or an aggregated structure that consists of packets of particles, or tactoids, within which several clay platelets or lamellae are in a parallel array, with a characteristic interparticle distance of 9 Å.

The formation of tactoids has the net result of reducing the surface area of the montmorillonite, which then behaves like a much larger particle with the diffuse double layer only fully manifesting itself on the outside surfaces of the tactoids (see Figure 2.2).

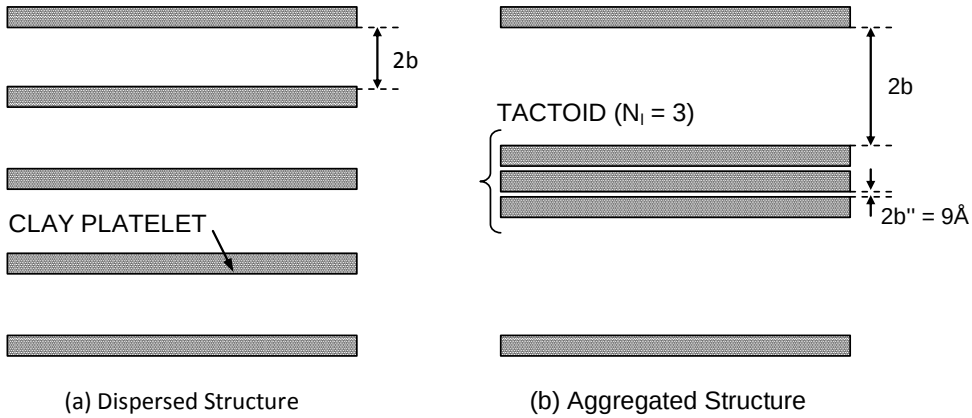

Figure 2.2 Microscopic structure of clay soils containing montmorillonite as the main mineralogical component. The structure can be dispersed (a), if the lamellae of montmorillonite (or clay platelets) are present as individual units, or aggregated (b), if the lamellae are condensed to form the so-called tactoids. Symbols: N_l = number of clay platelets per tactoid; b = half-spacing of the conducting pores; b'' = half spacing of the intra-tactoid pores containing immobile water (after Dominijanni and Manassero, 2012b)

The formation of tactoids is due to internal flocculation of the clay platelets, and depends on the concentration and the valence of the ions in the soil solution. The number, N_l, of clay platelets or lamellae forming tactoids increases with an increase of the ion concentration and valence of cations in the soil solution. Unfortunately, the number of platelets in a tactoid cannot be predicted and has to be estimated from macroscopic measurements of the transport parameters. For example Guyonnet et al. (2005), through a comparison of the results of hydraulic conductivity tests and microscopic analyses of bentonite structure based on small angle X-ray scattering and transmission electron microscopy, showed that high values of the hydraulic conductivity are related to an aggregated structure (also called the hydrated-solid phase), while low values of the hydraulic conductivity are related to a dispersed structure (also called the gel phase). These experimental results can be explained by the increase in the average pore size, due to tactoid formation.

The average half spacing, b, in dispersed clays may be estimated assuming a uniform distribution of the clay platelets in a parallel orientation, from the relation:

$$b = \frac{e}{\rho_{sk} S} \tag{2.1}$$

If the clay has an aggregated structure, only the external surface of the tactoids is in contact with the mobile fluid, therefore the void space within the platelets in the tactoids should be subtracted from the total void space to obtain the void space with reference to the conducting pores (see Figure 2.2). If N_l is the number of platelets per tactoid, the external specific surface, S', and the internal specific surface, S'', are given by:

$$S' = \frac{S}{N_l} \tag{2.2a}$$

$$S'' = S - S' = \frac{(N_l - 1)}{N_l} S \tag{2.2b}$$

The average half spacing between the platelets in the tactoids, as determined by means of X-ray measurements, is b'' = 4.5 Å (Shainberg et al., 1971). The total void index, e_T, of the bentonite is given by the sum of the void ratio inside the tactoid, e'', and the void ratio, e, of the conducting pores. The water in the tactoids can be considered part of the solid particles and is excluded from the transport mechanisms. The void ratio associated with the internal surfaces of the tactoid, e'', can be estimated as follows:

$$e'' = b'' \rho_{sk} S'' \tag{2.3}$$

where ρ_{sk} = density of the solid particles (kg/m^3).

The corrected half spacing, b, between the tactoids, in the case of an aggregate microstructure of bentonite, can be estimated from a similar equation to Eq.1.1:

$$b = \frac{e}{\rho_{sk} S'} \tag{2.4}$$

where $e = e_T - e_0$ = void ratio referring to the void space between the tactoids and S' = effective specific surface of the tactoids.

When the number, N_l, of clay platelets in the tactoids increases, the external specific surface decreases and the half spacing, b, between the tactoids increases, even though the total void ratio remains constant and the void ratio referring to the pore volume available for the transport decreases.

Montmorillonite lamellae are characterized by a negative electric charge per unit solid volume, which can be expressed as $F \cdot \bar{c}_{sk,0}$, where F is Faraday's constant (96,485 C·mol^{-1}) and $\bar{c}_{sk,0}$ is the molar concentration per unit solid volume of the solid skeleton electric charge, which is assumed to have unit valence (i.e. $z_{sk} = -1$). $\bar{c}_{sk,0}$ represents the moles of solid skeleton electric charge per volume of solids and, in order to be compared with the ion concentrations of the pore solution, it needs to be divided by the void ratio, e, which represents the pore volume per volume of solids. Dominijanni and Manassero (2012b) have shown that $\bar{c}_{sk,0}$ is proportional to the effective specific surface of the solid particles and decreases when the montmorillonite lamellae aggregate to form the so-called tactoids, through the following expression:

$$\bar{c}_{sk,0} = \frac{\left(1 - f_{Stern}\right)\sigma}{F} \rho_{sk} S' \tag{2.5}$$

where F = Faraday's constant (96.485 C mol^{-1}), σ is the surface charge of the single lamella (0.114 C m^{-2}), $f_{Stern} = \frac{\sigma_{Stern}}{\sigma}$ is the fraction of electric charge compensated by

the cations specifically adsorbed in the Stern layer (typically ranging from 0.80 to 0.90 in the case for Na^+ ions), ρ_{sk} is the solid density of bentonite (assumed equal to 2.65 g cm^{-3}), and S' is the external specific surface of the tactoid, which corresponds to the total specific surface, S, of the single platelet (760 m^2 g^{-1}) over the number of lamellae per tactoid, N_l.

By dividing $\bar{c}_{sk,0}$ by the void ratio, e, the solid skeleton charge concentration referring to the pore volume, $\bar{c}_{sk}$ (mol m^{-3}) can be obtained. If we introduce the cation exchange capacity, $CEC = \frac{\sigma S}{F}$, $\bar{c}_{sk}$ can be expressed as follows:

$$\bar{c}_{sk} = \frac{\bar{c}_{sk,0}}{e} = \phi_{sk} \cdot CEC \cdot \rho_{sk} \frac{1}{e} \qquad (2.6)$$

where $\phi_{sk} = \frac{(1 - f_{Stern})S'}{S}$ is the solid skeleton charge coefficient (-).

If the pore solution contains a single salt that is completely dissociated with the following stoichiometric reaction:

$$(Cation)_{z_1}^{\nu_1} (Anion)_{z_2}^{\nu_2} \rightarrow \nu_1 (Cation)^{z_1} + \nu_2 (Anion)^{z_2}$$

where z_1 and z_2 are the electrochemical valences of the cation and the anion, and ν_1 and ν_2 are the stoichiometric coefficients of the cation and the anion, respectively, the following condition has to be satisfied in order to preserve electroneutrality within a saturated porous medium, even in the presence of the solid skeleton electric charge:

$$z_1 \bar{c}_1 + z_2 \bar{c}_2 = \frac{\bar{c}_{sk,0}}{e} \qquad (2.7)$$

where $\bar{c}_1$ and $\bar{c}_2$ are the molar concentrations of the cation and the anion, respectively, and e is the void ratio.

As a consequence, the solid skeleton electric charge influences the distribution of the ions contained in the pore solution. This phenomenon is known as the ion-partition effect and is expected to be more relevant for porous media characterized by higher solid skeleton charge concentrations.

2.3 **Equilibrium conditions**

When an electrically charged porous medium is placed in contact with an external bulk solution that contains the same ions that are present in the pore solution, a thermodynamic equilibrium condition is reached, after a certain period of time, in which the water chemical potential and the ion electrochemical potentials between the two solutions are equal. The external bulk solution can be considered as a "chemical thermometer" in order to evaluate the equilibrium conditions of the porous medium (Coussy, 2004). The electroneutrality condition in the external solution is given by:

$$z_1 c_1 + z_2 c_2 = 0 \tag{2.8}$$

where c_1 and c_2 are the molar concentrations of the cation and the anion that are contained in the bulk solution.

It is convenient to define the salt concentration, c_s, of the external solution as follows:

$$c_s = \frac{c_1}{\nu_1} = \frac{c_2}{\nu_2} \tag{2.9}$$

Using Eq. (2.9), the electroneutrality condition, Eq. (2.8), provides the relation between the electrochemical valences and the stoichiometric coefficients:

$$z_1\nu_1 + z_2\nu_2 = 0\,. \tag{2.10}$$

As a result, the equilibrium condition can be characterized by the following state variables of the external bulk solution: the absolute temperature, T, the hydraulic pressure (referenced to the atmospheric pressure, as is usual in soil mechanics), u, and the salt concentration, c_s. The corresponding variables of the pore solution can be evaluated from the following conditions:

$$\bar{T} = T \tag{2.11}$$

$$\bar{\mu}_w = \mu_w \tag{2.12}$$

$$\bar{\mu}_i^{ec} = \mu_i^{ec} \qquad i = 1,2 \tag{2.13}$$

where $\bar{T}$ and T are the absolute temperature in the pore solution and in the external bulk solution, respectively; $\bar{\mu}_w$ and μ_w are the water chemical potential in the pore solution and in the external bulk solution, respectively; $\bar{\mu}_i^{ec}$ and μ_i^{ec} are the electrochemical potentials of the i-th ion in the pore solution and in the external bulk solution, respectively.

The water chemical potential, μ_w, and the ion electrochemical potentials, μ_i^{ec}, of the external solution can be related to the hydraulic pressure, u, and the salt concentration, c_s, for a dilute solution, as follows (Katchalsky and Curran, 1965; Dominijanni and Manassero, 2012a):

$$\mu_w = \mu_w^0(T) + \frac{(u - \Pi)}{c_w} \tag{2.14}$$

$$\mu_i^{ec} = \mu_i + z_i F\varphi = \mu_i^0(T) + RT\ln(\nu_i c_s) + z_i F\varphi \qquad i = 1,2 \qquad (2.15)$$

where μ_w^0 and μ_i^0 are integration constants that only depend on the absolute temperature T; c_w is the water molar concentration; $\Pi = RT\sum_{i=1}^{2}\nu_i c_s$ is the osmotic pressure; μ_i is the chemical potential of the i-th ion; R is the universal gas constant (8.314 J·mol^{-1}·K^{-1}); and φ is the electric potential.

The state variables in the external bulk solution can be measured easily, whereas it is very difficult to determine the corresponding variables in the pore solution. Moreover, the relations obtained by linking the chemical potentials to the state variables of the pore solution are more uncertain, due to the interaction with the solid skeleton charge, which alters the ion concentration distribution near the solid particles. The simplest assumption that can be adopted involves using analogous relations to Eqs. (2.14) and (2.15), as they are also considered valid for the pore solution. This assumption, which was first proposed by Donnan (1911), neglects the microscopic deviations of the ion concentrations from their average values that are induced by the electric potential distribution within the pores. If this approximation is accepted, the water chemical potential, $\bar{\mu}_w$, and the ion electrochemical potentials, $\bar{\mu}_i^{ec}$, of the pore solution can be expressed as follows:

$$\bar{\mu}_w = \bar{\mu}_w^0(T) + \frac{\left(\bar{u} - \bar{\Pi}\right)}{\bar{c}_w} \qquad (2.16)$$

$$\bar{\mu}_i^{ec} = \bar{\mu}_i + z_i F\bar{\varphi} = \bar{\mu}_i^0(T) + RT\ln(\bar{c}_i) + z_i F\bar{\varphi} \qquad i = 1,2 \qquad (2.17)$$

where $\bar{\mu}_w^0$ and $\bar{\mu}_i^0$ are integration constants that only depend on the absolute temperature T; $\bar{c}_w$ is the molar concentration of the water in the pore solution, which can be taken equal to the molar concentration of the water in the external bulk

solution, i.e. $\bar{c}_w \cong c_w$; $\bar{\Pi} = RT\sum_{i=1}^{2}\bar{c}_i$ is the osmotic pressure of the pore solution; $\bar{\mu}_i$ is the chemical potential of the i-th ion in the pore solution; and $\bar{\varphi}$ is the electric potential in the pore solution.

The hydraulic pressure of the pore solution, $\bar{u}$, and the ion partition factors, Γ_i, defined as the ratio between the ion concentration of the pore solution and the ion concentration of the external bulk solution, can therefore be expressed on the basis of Eqs. (2.12) and (2.13), and using Eqs. (2.14)-(2.17), as follows:

$$\bar{u} = u + (\bar{\Pi} - \Pi) \tag{2.18}$$

$$\Gamma_i = \frac{\bar{c}_i}{c_i} = \frac{\bar{c}_i}{\nu_i c_s} = \exp\left(-z_i \frac{F}{RT}\bar{\psi}\right) \qquad i = 1,2 \tag{2.19}$$

where $\bar{\psi} = \bar{\varphi} - \varphi$ is the electric potential of the porous medium, which is also called Donnan's potential.

On the basis of this approach, the hydraulic pressure of the pore solution is different from the hydraulic pressure of the external solution that is in equilibrium with it. The pressure difference between the pore solution and the external solution is called swelling pressure, u_{sw}, and is given by:

$$u_{sw} = \bar{\Pi} - \Pi \,. \tag{2.20}$$

Eqs. (2.18) and (2.19) for i= 1,2, together with Eq. (2.7), constitute a set of four equations that can be solved to find the four unknown variables: the hydraulic pressure, $\bar{u}$, the ion concentrations, $\bar{c}_i$ for i= 1,2, and the electric potential, $\bar{\psi}$.

When the ion electrochemical valences are both unitary, such as for NaCl, Eq. (2.19) implies that

$$\Gamma_1 = \Gamma_2^{-1}. \tag{2.21}$$

Inserting Eq. (2.21) into Eq. (2.7) results in the following equation:

$$\Gamma_2^{-1} - \Gamma_2 - \frac{\overline{c}_{sk,0}}{e \cdot c_s} = 0, \tag{2.22}$$

which has a positive solution of the following form:

$$\Gamma_2 = -\frac{\overline{c}_{sk,0}}{2 \cdot e \cdot c_s} + \sqrt{\left(\frac{\overline{c}_{sk,0}}{2 \cdot e \cdot c_s}\right)^2 + 1} \tag{2.23}$$

and

$$\Gamma_1 = \Gamma_2^{-1} = \frac{\overline{c}_{sk,0}}{2 \cdot e \cdot c_s} + \sqrt{\left(\frac{\overline{c}_{sk,0}}{2 \cdot e \cdot c_s}\right)^2 + 1}. \tag{2.24}$$

On the basis of Eqs. (2.23) and (2.24), the swelling pressure can be expressed as follows:

$$u_{sw} = RTc_s\left(\Gamma_1 + \Gamma_2 - 2\right) = 2RTc_s\left[\sqrt{\left(\frac{\overline{c}_{sk,0}}{2 \cdot e \cdot c_s}\right)^2 + 1} - 1\right]. \tag{2.25}$$

As a consequence, the effective stress principle proposed by Terzaghi (see Figure 2.3(a)) is modified for a charged porous medium, such as bentonite, and can be expressed as (see Figure 2.3(b)):

$$\sigma' = \sigma - \bar{u} = \sigma - u - u_{sw}, \tag{2.26}$$

where σ' is the effective stress and σ is the total stress. The effective stress can be considered as the intergranular stress which is transmitted through the intergranular contacts between the solid particles. The pore solution pressure, $\bar{u}$ can be associated to the ion concentrations and the concentration of the charge of the solid particles (i.e. the moles of solid skeleton electric charge per volume of solid, $\bar{c}_{sk,0}$) through Donnan's equation (2.18).

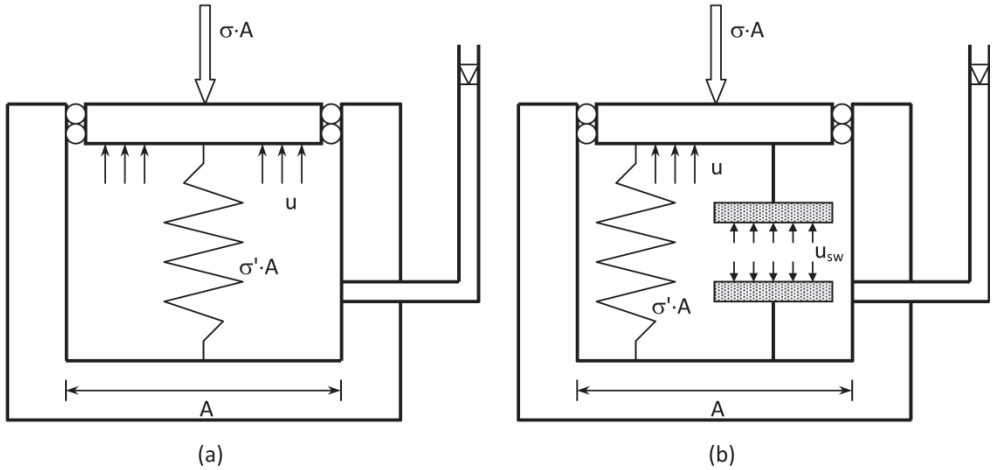

Figure 2.3 Mechanical model for (a) an uncharged porous medium and (b) a charged porous medium (Dominijanni and Manassero, 2012b).

2.4 **Transport equations**

If clay is interposed between two reservoirs with different hydraulic pressures or ion concentrations, a pore solution volumetric flux, q, and an ion mass flux, J_i, relative to the solid skeleton, are generated. The most general approach for modelling coupled fluxes is to invoke phenomenological equations by applying the formalism of the Thermodynamics of Irreversible Processes (Katchalsky and Curran, 1965;

Yaroshchuk, 1995; Dominijanni and Manassero, 2012a,b). The main advantage of this approach is to avoid any specification of physical properties of the membrane, maintaining the model as general as possible. Using such formalism, Dominijanni et al. (2013) derived the following equations for the volumetric flux, q, and the salt flux, J_s, for a semipermeable porous medium permeated by a solution containing a single salt (e.g. NaCl):

$$q = -\frac{k}{\gamma_w}\left(\frac{\partial u}{\partial x} - \omega\frac{\partial \Pi}{\partial x}\right) \tag{2.27}$$

$$J_s = (1-\omega)qc_s - nD_\omega^* \frac{\partial c_s}{\partial x} \tag{2.28}$$

where

$$k = \frac{n \cdot \gamma_w}{\alpha\left[1 + \frac{RT}{\alpha}\frac{(\Gamma_1 - \Gamma_2)^2 \nu_1 \nu_2 c_s}{\nu_1\Gamma_2 D_2 + \nu_2\Gamma_1 D_1}\right]} = \text{hydraulic conductivity;} \tag{2.29}$$

$$\omega = 1 - \frac{\nu_1 D_2 + \nu_2 D_1}{\nu_1\Gamma_2 D_2 + \nu_2\Gamma_1 D_1}\Gamma_1\Gamma_2 = \text{reflection coefficient;} \tag{2.30}$$

$$J_s = \frac{J_1}{\nu_1} = \frac{J_2}{\nu_2} = \text{salt molar flux;} \tag{2.31}$$

$$D_\omega^* = (1-\omega)\cdot D_s = \text{osmotic effective diffusion coefficient;} \tag{2.32}$$

$$D_s = \frac{(\nu_1 + \nu_2)D_1 D_2}{\nu_1 D_2 + \nu_2 D_1} = \text{macroscopic salt diffusion coefficient;} \tag{2.33}$$

α = friction coefficient (Dominijanni et al., 2013);

n = soil porosity.

Dominijanni and Manassero (2012b) have demonstrated that, if the microscopic deviations of the variables from their average values are assumed to be negligible,

the macroscopic ion diffusion coefficients, D_i, result to be equal to the ion effective diffusion coefficients, D_i^*:

$$D_i = D_i^* = \tau_m D_{i,0} \qquad i=1,2 \tag{2.34}$$

$$D_s = D_s^* = \frac{(\nu_1+\nu_2)D_1^* D_2^*}{\nu_1 D_2^* + \nu_2 D_1^*} = \tau_m \frac{(\nu_1+\nu_2)D_{1,0}D_{2,0}}{\nu_1 D_{2,0} + \nu_2 D_{1,0}} = \tau_m D_{s,0} \tag{2.35}$$

where τ_m is the dimensionless matrix tortuosity factor that accounts for the tortuous nature of the actual diffusive pathway through the porous medium (Malusis and Shackelford, 2002), $D_{i,0}$ is the free (aqueous) solution diffusion coefficient of the i-th ion, D_s^* is the salt effective diffusion coefficient and $D_{s,0}$ is the free solution diffusion coefficient of the salt.

An interesting observation is that the reflection coefficient, ω, results to be equal to the swelling pressure coefficient, ϖ, when the ion free solution diffusion coefficients are equal.

When the solid skeleton electric charge is equal to zero, the ion partition coefficients, Γ_i, are equal to 1 and Eqs. (2.27) and (2.28) reduce to the Darcy equation and the classical advective-diffusion equation, respectively.

The osmotic effective diffusion coefficient, D_ω^*, results to be related to the reflection coefficient, ω, through Eq. (2.32), so that $D_\omega^* = 0$ when ω=1. As a result, the condition ω=1 implies a null salt flux through the porous medium, which, in this case, can be said to act as a "perfect" or "ideal" barrier.

If Eq. (2.32) is compared with the expression of D_ω^* proposed by Malusis and Shackelford (2002) and Malusis et al. (2012):

$$D_\omega^* = \tau_r D_s^* \tag{2.36}$$

Where τ_r is the restrictive tortuosity factor, τ_r results to be given by:

$$\tau_r = (1-\omega)\frac{D_s}{D_s^*}. \tag{2.37}$$

Moreover, if the hypotheses implied by Eq. (2.35) are adopted, the expression of τ_r reduces to:

$$\tau_r = (1-\omega). \tag{2.38}$$

The coefficient k can be measured, under steady state conditions, using traditional permeameters. Malusis et al. (2001) developed a testing apparatus to determine ω and D_ω^*. This apparatus is able to impose the condition of no-volumetric flux (q = 0) through a soil sample in contact with two external solutions, maintained at constant salt concentrations, so that the global or averaged values of the coefficients can be measured. The global values of ω and D_ω^* are defined as follows (Auclair et al., 2002):

$$\omega_g = \frac{1}{\Delta c_s}\int_{c_b}^{c_t} \omega \cdot dc_s \tag{2.39}$$

$$D_{\omega g}^* = \frac{1}{\Delta c_s}\int_{c_b}^{c_t} D_\omega^* \cdot dc_s \tag{2.40}$$

where c_t and c_b represent the salt concentration at the top and the bottom boundaries of the clay sample, respectively, and $\Delta c_s = c_t - c_b$ is their difference.

These coefficients can be determined by means of the following relations under steady state conditions:

$$\omega_g = \left(\frac{\Delta u}{\Delta \Pi} \right)_{q=0} \tag{2.41}$$

$$D^*_{\omega g} = \frac{L}{n} \left(\frac{J_s}{\Delta c_s} \right)_{q=0} \tag{2.42}$$

where $\Delta u = u_t - u_b$ and $\Delta \Pi = \Pi_t - \Pi_b$ represent the differences between the hydraulic pressure and the osmotic pressure at the boundaries of the clay sample, and L is the length of the sample.

It is interesting to observe that the relationship between D^*_ω and ω is also maintained between their corresponding global values: in fact, inserting Eq. (2.32) into Eq. (2.39) with $D_s = D^*_s$ leads to:

$$D^*_{\omega g} = (1 - \omega_g) \cdot D^*_s = (1 - \omega_g) \cdot \tau_m \cdot D_{s,0} . \tag{2.43}$$

In the case of a salt constituted by monovalent ions, inserting Eq. (2.30) into Eq. (2.41) and using Eqs. (2.23) and (2.24), the following expression of ω_g is obtained:

$$\omega_g = 1 + \frac{\bar{c}_{sk,0}}{2 \cdot \Delta c_s \cdot e} \left[Z_2 - Z_1 - (2t_1 - 1) \cdot \ln \left(\frac{Z_2 + 2t_1 - 1}{Z_1 + 2t_1 - 1} \right) \right] \tag{2.44}$$

where

$$t_1 = \frac{D_{1,0}}{D_{1,0} + D_{2,0}} \text{ = cation transport number,} \tag{2.45}$$

$$Z_1 = \sqrt{1 + \left(\frac{2 \cdot c_t \cdot e}{\bar{c}_{sk,0}} \right)^2} \,, \tag{2.46}$$

$$Z_2 = \sqrt{1 + \left(\frac{2 \cdot c_b \cdot e}{\bar{c}_{sk,0}} \right)^2} \,. \tag{2.47}$$

References

1. Auclair, B., Nikonenko, V., Larchet, C., Métayer, M., Dammak, L. (2002). Correlation between transport parameters of ion-exchange membranes. *Journal of Membrane Science* **195**, 89-102.
2. Coussy, O. (2004). *Poromechanics*. Chichester: Wiley.
3. Dominijanni, A., Manassero, M. (2010). Chemico-osmosis and solute transport through geosynthetic clay liners. In: A. Bouazza and J.J. Bowders (Eds.), Geosynthetic clay liners for waste containment, 105-125. Leiden: CRC Press.
4. Dominijanni, A., Manassero, M. (2012a). Modelling the swelling and osmotic properties of clay soils. Part I: The phenomenological approach. *International Journal of Engineering Science* **51**, 32-50.
5. Dominijanni, A., Manassero, M. (2012b). Modelling the swelling and osmotic properties of clay soils. Part II: The physical approach. *International Journal of Engineering Science* **51**, 51-73.
6. Dominijanni, A., Manassero, M., Puma, S. (2013). Coupled chemical-hydraulic-mechanical behaviour of bentonites. *Géotechnique* **63**, No. 3, 191-205.
7. Donnan, F.G. (1911). Theorie der Membrangleichgewichte und Membranpotentiale bei Vorhandensein von nicht dialysierenden Elektrolyten. Ein Beitrag zur physikalisch-chemischen Physiologie [Theory of membrane equilibria and membrane potentials in the presence of non-dialysing electrolytes. A contribution to physical-chemical physiology],

Zeitschrift für Elektrochemie und angewandte physikalische Chemie **17**, 572-581. English translation republished in *Journal of Membrane Science* **100** (1995), 45-55.

8. Guyonnet, D., Gaucher, E., Gaboriau, H., Pons, C.H., Clinard, C., Norotte, V., and Didier, G. (2005). Geosynthetic clay liner interaction with leachate: correlation between permeability, microstructure and surface chemistry. *Journal of Geotechnical and Geoenvironmental Engineering*, **131** (6), 740-749.
9. Katchalsky, A., Curran, P.F. (1965). *Nonequilibrium thermodynamics in biophysics*. Cambridge: Harvard University.
10. Malusis, M.A., Shackelford, C.D. & Olsen, H.W. (2001). A laboratory apparatus to measure chemico-osmotic efficiency coefficients for clay soils. *Geotechnical Testing Journal* **24**, 229-242.
11. Malusis, M.A., Shackelford, C.D. (2002). Coupling effects during steady-state solute diffusion through a semipermeable clay membrane. *Environmental Science and Technology* **36**, No. 6, 1312–1319.
12. Malusis, M.A., Shackelford, C.D., Maneval, J.E. (2012). Critical review of coupled flux formulations for clay membranes based on nonequilibrium thermodynamics. *Journal of Contaminant Hydrology* **138-139**, 40-59.
13. Mitchell, J. K. (1993). *Fundamentals of soil behavior* (2nd ed.). New York: Wiley.
14. Norrish, K. (1954). The swelling of montmorillonite. Discussions of the Faraday Society, **18**, 120-134.
15. Shainberg, I., Bresler, E., Klausner, Y. (1971). Studies on Na/Ca montmorillonite systems. 1. The swelling pressure. *Soil Science*, **111** (4), 214-219.
16. Yaroshchuk, A.E. (1995). Osmosis and reverse osmosis in fine-charged diaphragms and membranes. *Advances in Colloid and Interface Science* **60**, 1-93.

3. MECHANICAL AND SWELLING BEHAVIOUR OF BENTONITES

This chapter reports the contents of the SUBMITTED Paper:

Boffa, G., Dominijanni, A., Manassero, M., Marangon, M., Zaninetta, L. (2016). Mechanical and swelling behaviour of sodium bentonites in equilibrium with low molarity NaCl solutions under oedometric conditions. *Acta Geotechnica*.

In the last paragraphs, some other experimental results of conventional oedometer tests and swelling tests under oedometric conditions in equilibrium sodium chloride solutions with different concentrations are reported.

Mechanical and swelling behaviour of sodium bentonites in equilibrium with low molarity NaCl solutions under oedometric conditions

Giacomo Boffa[a], Andrea Dominijanni[b], Mario Manassero[c], Manuel Marangon[d], Luciano Zaninetta[e]

[a] *Corresponding author*, Ph.D. Candidate, Politecnico di Torino, c.so Duca degli Abruzzi 24, 10129 - Torino, Italy, tel. number +390110907705, fax number +390110904899, e-mail address giacomo.boffa@polito.it

[b] Research Fellow, Politecnico di Torino, c.so Duca degli Abruzzi 24, 10129 - Torino, Italy, tel. number +390110907705, fax number +390110904899, e-mail address andrea.dominijanni@polito.it

[c] Professor, Politecnico di Torino, c.so Duca degli Abruzzi 24, 10129 - Torino, Italy, tel. number +390110904820, fax number +390110904899, e-mail address mario.manassero@polito.it

[d] Engineer, Syndial S.p.A. (ENI Group), Piazza Marcello Boldrini 1, 20097 - San Donato Milanese, MI, Italy, e-mail address Manuel.Marangon@syndial.it

[e] Engineer, Syndial S.p.A. (ENI Group), Piazza Marcello Boldrini 1, 20097 - San Donato Milanese, MI, Italy, e-mail address Luciano.Zaninetta@syndial.it

Keywords: sodium bentonites, oedometer tests, swelling behaviour, clay microstructure, interpretative model

Abstract

Geosynthetic Clay Liners (GCLs) represent a valid alternative to traditional compacted clay liners in engineered clay-based barriers for geoenvironmental applications. The swelling properties of sodium bentonite contained in the GCLs are fundamental, because they affect the efficiency of waste landfills barriers. In the present paper, the effects of different preparation methods of natural sodium bentonite specimens for oedometer tests were investigated. Swelling pressure values were measured for different void ratios of specimens, which were tested in 2 types of oedometers, in equilibrium with NaCl 0.01 M concentrated solutions. The interpretation proposed by Cui et al. (2013) of the unloading paths of oedometer tests, performed accordingly to ASTM D 2435-96, was used in order to derive the swelling pressure values associated to the void ratios before each unloading. Other laboratory data were found through the so-called strain-controlled method by using a new testing device and by measuring directly swelling pressure values through a load cell. On the basis of the theoretical model proposed by Dominijanni and Manassero (2012b), the experimental results were interpreted in order to evaluate the microstructure of the tested sodium bentonite, under the hypothesis that the microscopic deviations of the pore solution state variables from their average values are negligible.

3.1 Introduction

Sodium bentonite (Na-B) is the most common type of clay material used for the production of Geosynthetic Clay Liners (GCLs), which are frequently installed in engineered clay-based barriers for geoenvironmental applications (e.g. hydraulic and contaminant barriers), as an alternative to traditional compacted clay liners, due to their reduced costs and ease of installation (Dominijanni & Manassero, 2012b).

GCLs consist of a thin layer of dry bentonite added to a layer or layers of geosynthetics, which can be either geotextiles or geomembranes (Bouazza, 2002).

The functioning of waste landfills barriers depends on the swelling properties of bentonite: for this reason a great number of theoretical and experimental studies has been produced on different types of bentonites or bentonite-aggregate mixtures in both distilled water and saline solutions (Mesri & Olson, 1971; Shainberg et al., 1971; Sridharan & Venkatappa Rao, 1973; Sridharan & Jayadeva, 1982; Di Maio, 1996; Di Maio et al., 2004; Laird, 2006; Kang & Shackelford, 2010a; Di Emidio, 2010; Dominijanni & Manassero, 2012a, Dominijanni & Manassero, 2012b; Cui et al., 2013; Dominijanni et al., 2013; Liu, 2013; Nguyen et al., 2013), in order to evaluate the mechanical behaviour and the swelling pressure of bentonites under different boundary conditions.

Sodium bentonite is a clay soil which usually contains at least 70% of montmorillonite, a smectitic three layered (2:1) clay mineral consisting of an alumina octahedral sheet sandwiched between two silica tetrahedral sheets. The unit layer of montmorillonite has, on the faces, a permanent negative lattice charge which results from isomorphous substitutions of divalent cations (e.g. Mg^{2+} and Fe^{2+}) for trivalent aluminium (Al^{3+}) in the octahedral sheet and trivalent aluminium (Al^{3+}) for tetravalent silicon (Si^{4+}) in the tetrahedral sheet. This permanent negative charge is compensated by the preferential adsorption of exchangeable cations on the layer surfaces, intercalated between the unit layers (van Olphen, 1977): the Cation Exchange Capacity (CEC) is a measure of the quantity of exchangeable cations neutralizing the negative surface charge and it is usually expressed in milliequivalents per 100 g of dry soil.

Montmorillonite crystals consist of parallel-aligned elementary alumino-silicate lamellae, which are approximately 10 Å thick and 1000-2000 Å wide, and this results in a very high specific surface ($\approx$ 760 m^2/g) (Dominijanni & Manassero, 2012a). Norrish (1954) showed that bentonite may have a dispersed structure characterised by separated clay particles with high specific surfaces, or an aggregated structure which consists of packets of particles, the so-called tactoids,

within which several clay platelets or lamellae are in a parallel array, with a characteristic interparticle distance of 9 Å; in the latter case, the specific surface of tactoids depends on the number of lamellae per tactoid and is lower than specific surface of the dispersed structure.

The exchangeable cations are present at some distance from the surface of montmorillonite lamellae: this distance from the surface increases with decreasing valence of cations. Cations are attracted to the negatively charged surface through an electrical force but as a consequence of their thermal energy they diffuse away from this space with a high ion concentration. The balance of Coulomb electrical attraction and thermal diffusion leads to a diffuse double layer (DDL) of cations, with the concentration highest at the surface and gradually decreasing with distance from the surface (Yong & Warkentin, 1975). The Gouy-Chapman theory (Gouy, 1910; Chapman, 1913) is considered as the most successful for the description of the DDL. The interaction of DDLs of adjacent particles gives an explanation for the properties of swelling, plasticity, and water retention of bentonites (Yong & Warkentin, 1975). The interaction force between two double layers depends on the ion concentration at the midplane between two adjacent parallel lamellae and is given by the osmotic pressure in that plane (Bolt, 1956). According to Bolt (1956), the swelling pressure is the difference between the osmotic pressure in the central plane between clay layers and the osmotic pressure in the equilibrium solution.

As a consequence, the compressibility and the mechanical behaviour of a sodium bentonite with a high percentage of montmorillonite depend not only on the mechanical properties of the constituents and on the particle interactions through their direct contacts, but also on physico-chemical factors, i.e. the balance by the physico-chemical interaction between the lamellae and the soil solution (Bolt, 1956; Mesri & Olson, 1971; Sridharan & Venkatappa Rao, 1973; Di Maio, 1996; Nguyen et al., 2013). Bentonite may swell or shrink in response to changes in the chemical composition of the pore solution even if the applied external stress does not change. The amount of smectitic minerals, their orientation, the valence of exchangeable cations and the pore-water salt concentration determine the amount of swelling of

bentonites. It is important to note that the lower the valence of the exchangeable cations and the higher the specific surface of bentonite particles, the higher is bentonite swelling: monovalent exchangeable cations such as sodium cause greater swelling than divalent calcium ions (Yong & Warkentin, 1975).

The hydraulic performances of GCLs containing sodium bentonite are influenced by swelling or shrinkage of the bentonite. A low hydraulic conductivity of the GCLs is generally associated to a great amount of swelling in bentonite when it is hydrated from a dry state: as the material expands and develops a high swelling pressure, the macropores of bentonite can be closed by the formation of a gel which ensures sealing and reduces the permeability of the material (Guyonnet et al., 2005). This occurs principally when bentonite is exposed to water, or to very low concentrated salt solutions; on the contrary, when high concentrated salt solutions are in contact with bentonite, swelling is inhibited and hydraulic conductivity increases; furthermore, when bentonite is dried, shrinkage and cracking occur, with subsequent increase in hydraulic conductivity.

It has been found that the swelling pressure of bentonites determined in the laboratory can be affected by the experimental methods (Sridharan et al., 1986; Wang et al., 2012). In several works, in which authors carried out oedometer tests, different experimental data were found out from the swell-reload, zero-swell, constant-volume, pre-swell methods, as a consequence of the difference in the loading and wetting conditions in each method. For the swell-reload and the zero-swell methods, the equipment employed is a conventional oedometer; for the constant-volume and the pre-swell methods (i.e. strain-controlled tests), the device is a modified oedometer in which axial deformation of bentonite specimens is prevented: typically it consists of a rigid cell confining the sample, with access to water or salt solutions through a porous stone at one end and at the other end a solid piston which allows a pressure measurement. Swelling pressure is measured as the restraint which has to be applied to the piston to prevent movement. (Yong & Warkentin, 1975).

According to Cui et al. (2013), the swelling process of soils is governed by the microstructure variations; they have proposed to derive swelling pressure values from bi-linear unloading and reloading paths of soil compression curves of conventional oedometer tests. The experimental results can be analyzed on the basis of the competition between the mechanical effect and the physico-chemical effect occurring during unloading and reloading loops. They found out a good exponential relationship between the swelling pressure and the void ratio just before the unloading or reloading.

Several models (i.e. empirical models, diffuse double-layer models, thermodynamics models) for predicting swelling pressure in bentonite clays have been proposed. In Dominijanni et al. (2013), on the basis of the phenomenological (Dominijanni & Manassero, 2012a) and on the physical (Dominijanni & Manassero, 2012b) approaches, a new model for the evaluation the coupled chemical-hydraulic-mechanical behaviour of bentonites has been described. In particular, the authors have proposed an expression for determining the swelling pressure of an electrically charged porous medium, i.e. sodium bentonite, in oedometric conditions in equilibrium with an external bulk solution that contains the same ions as are present in the pore solution, i.e. NaCl solutions whose ion electrochemical valences are both unitary. The equation contains a macroscopic parameter (i.e. the moles of solid skeleton electric charge per volume of solid, $\overline{C}_{sk,0}$) which is linked to the microscopic properties (e.g. the effective specific surface of lamellae) of the sodium bentonite.

In the present paper, the effects of different preparation methods of natural sodium bentonite specimens for oedometer tests were investigated. Swelling pressure values were measured for different void ratios of specimens, which were tested in 2 types of oedometers, in equilibrium with NaCl 0.01 M concentrated solutions. Experimental data derived from oedometer tests carried out accordingly to ASTM D 2435- 96 were analysed on the basis of the interpretation proposed by Cui et al. (2013). Other swelling pressure data were obtained through the so-called strain-

controlled method. All the results have been interpreted on the basis of the model proposed by Dominijanni and Manassero (2012b), in order to evaluate a simplified picture of the microstructure of the tested bentonite.

3.2 **Theoretical background**

The effective stress principle, for a charged porous medium, such as the tested sodium bentonite, can be expressed as

$$\sigma' = \sigma - \bar{u}\,, \tag{3.1}$$

where σ' is the effective stress, σ is the total stress and $\bar{u}$ is the pore solution pressure (Dominijanni and Manassero, 2012b). The effective stress can be considered as the intergranular stress which is transmitted through the intergranular contacts between the solid particles. The pore solution pressure can be associated to the ion concentrations and the concentration of the charge of the solid particles (i.e. the moles of solid skeleton electric charge per volume of solid, $\bar{c}_{sk,0}$) through Donnan's equation:

$$\bar{u} = u - \Pi + \bar{\Pi}\,, \tag{3.2}$$

where u is the pressure of the external bulk solution in equilibrium with bentonite, $\bar{\Pi}$ is the osmotic pressure within the bentonite, and Π is the osmotic pressure of the external bulk solution.

The effective stress principle can be formulated as follows:

$$\sigma' = \sigma'_{app} - u_{sw}\,, \tag{3.3}$$

where $\sigma'_{app} = \sigma - u =$ apparent effective stress, evaluated with respect to the pressure of the external bulk solution in equilibrium with the bentonite; $u_{sw} = \bar{\Pi} - \Pi =$ swelling pressure, which depends on the ion concentration of the external bulk solution, c_s, and bentonite void ratio, e. The swelling pressure can be expressed by the following equation (Dominijanni et al., 2013), when the pore solution contains a single salt constituted by monovalent ions (e.g. NaCl):

$$u_{sw} = 2RTc_s \left[\sqrt{\left(\frac{\bar{c}_{sk,0}}{2ec_s} \right)^2 + 1} - 1 \right] \tag{3.4}$$

where R is the universal gas constant (= 8.314 J/(mol K)), T is the absolute temperature of the external bulk solution. The swelling pressure increases when the void ratio, e, and the salt concentration, c_s, decrease, and the reference concentration of the charge of solid particles, $\bar{c}_{sk,0}$, increases (Dominijanni and Manassero, 2012b).

According to the physical approach proposed by Dominijanni and Manassero (2102b), the moles of solid skeleton electric charge per volume of solid, $\bar{c}_{sk,0}$ can be expressed as follows:

$$\bar{c}_{sk,0} = \frac{(1 - f_{Stern})\sigma}{F} \rho_{sk} S' \tag{3.5}$$

where F = Faraday's constant (96.485 C mol^{-1}), σ is the surface charge of the single lamella (0.114 C m^{-2}), $f_{Stern} = \frac{\sigma_{Stern}}{\sigma}$ is the fraction of electric charge compensated by the cations specifically adsorbed in the Stern layer (typically ranging from 0.80 to

0.90 in the case for Na^+ ions), ρ_{sk} is the solid density of bentonite (assumed equal to 2.65 g cm^{-3}), and *S'* is the external specific surface of the tactoid, which corresponds to the total specific surface, *S*, of the single platelet (760 m^2 g^{-1}) over the number of lamellae per tactoide, N_l. The value of $\bar{c}_{sk,0}$ is proportional to the effective specific surface of the solid particles and is expected to decrease in case of aggregated microstructure, in which the montmorillonite lamellae form the tactoids. $\bar{c}_{sk,0}$ is the only new macroscopic material parameter introduced into the model proposed by Dominijanni and Manassero (2012b), in order to account for the electro-chemical phenomena related to the microscopic surface forces.

In bentonites characterized by a very high void ratio, it can be assumed that there are no contacts between the solid particles, therefore the effective stresses can be considered null (Dominijanni and Manassero, 2012b). In this case, from Eq. (3.3) it follows that the swelling pressure is equal to the apparent effective stress.

Further details on the theoretical background can be found in Dominijanni and Manassero (2012a, b) and in Dominijanni et al. (2013).

3.3 Materials and methods

3.3.1 Materials

In this study the same Indian sodium bentonite used by Dominijanni et al. (2013) was tested. The material is characterized by a cation exchange capacity (measured through the methylene blue adsorption method) of 105 meq/100 g. X-ray diffraction analysis revealed the mineralogical composition of the sodium bentonite, which presents primarily smectite, traces of calcite, quartz, mica and gypsum.

The bentonite is characterized by a liquid limit (*LL*) of 525 %, a plastic limit (*PL*) of 63%, and a hydraulic conductivity (*k*) of $8 \cdot 10^{-12}$ m/s, measured at a 27.5 kPa confining effective stress using de-ionized water as the permeant liquid. The specific gravity, G_s is assumed to be equal to 2.65 (Dominijanni et al., 2006).

The salt solutions were prepared with sodium chloride (ACS reagent, purity ≥ 99%) and de-ionized water (DW), at a molarity value of 0.01 M, with the aim of investigating the effect of the monovalent cations (i.e. Na^+) on the swelling behaviour of the sodium bentonite at different void ratios. The DW (*pH* = 6.95; EC at 20 °C = 0.2 mS/m) consisted of tap water processed through a series of activated carbon filters, a reverse osmosis process and, finally, a UV lamp (Elix Water Purification system). Moreover, the DW was de-aerated prior to use, in order to limit the presence of air which could affect the experimental results. The electrical conductivity (*EC*) measured at 20 °C for the NaCl solutions ranged from 116 mS/m to 123 mS/m.

3.3.2 **Bentonite specimens preparation**

In a preliminary phase, the sodium bentonite was submitted to the same 'squeezing' process described in Dominijanni et al. (2013), in order to remove the soluble salts which are naturally present inside the powdered material as a consequence of its marine origin. This procedure is necessary in order to prevent soluble salts from affecting the determination of the swelling properties of the sodium bentonite.

In literature several authors (Malusis et al., 2001; Malusis and Shackelford, 2002a, 2002b; Shackelford and Lee, 2003; Yeo et al., 2005; Kang and Shackelford, 2009; Di Emidio, 2010; Kang and Shackelford, 2010b) used a different process, called 'flushing' method, in order to remove soluble salts. It consists of an initial permeation phase, performed under back-pressure, which takes a long period of time (i.e. from months to a year), due to the low hydraulic conductivity of bentonite.

The 'squeezing' method was preferred, in order to reduce the salt removal time. It consists of a series of consecutive phases of powder sodium bentonite hydration with DW, at a higher water content than the *LL*, and drained consolidation, by using a consolidometer, under a maximum load of 500 kPa (instrumental limit). During the consolidation phase, the drained solution was sampled daily, with the aim of

controlling the *EC* and evaluating the soluble salt concentration in the bentonite pore-water. About 500 g of squeezed dry powder bentonite, characterized by an *EC* value lower than 50 mS/m, was produced in 60-70 days, using a 5 l consolidometer. The monitored *EC* results of the squeezing process are reported in Figure 3.1.

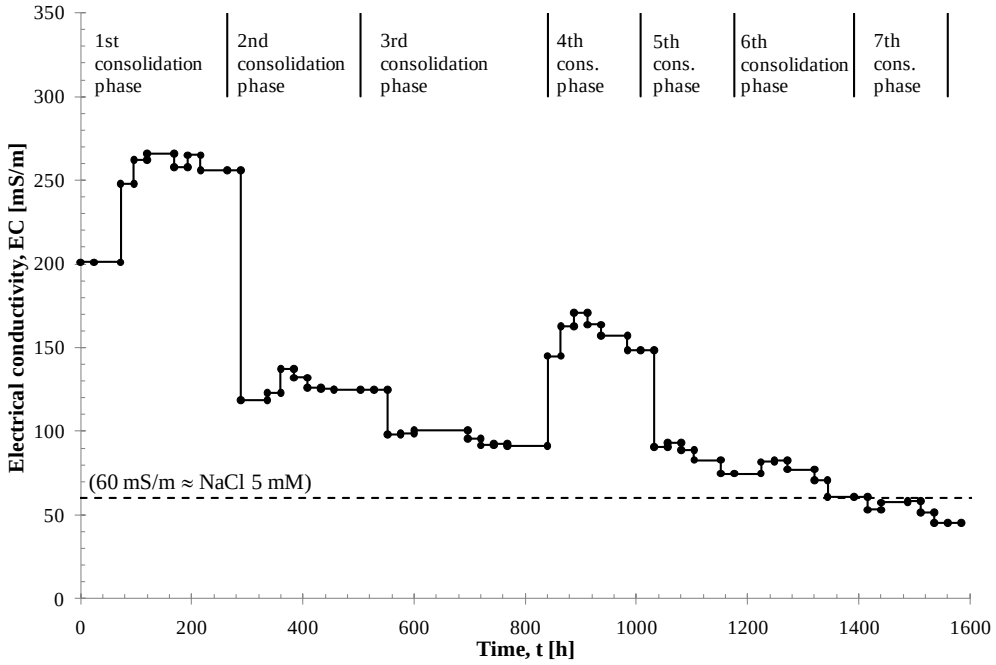

Figure 3.1 Electrical conductivity as a function of time during squeezing process

After the salt removal phase, the material was oven-dried at 105 °C and pulverized once again.

3.3.3 **Conventional oedometer testing apparatus and procedures**

Five oven-dried squeezed sodium bentonite specimens of 50 mm diameter were prepared for conventional oedometer tests, partially accordingly to ASTM D 2435-96. The physical properties of the specimens are shown in Table 3.1.

The samples SQ_NaB_1, SQ_NaB_4, SQ_NaB_5 were prepared by dusting the dry material inside the stainless steel ring in the plexiglass cell: in these cases the specimens reached an initial height of 4.5 mm. Under a total axial stress of 12.3 kPa the sodium bentonite specimens were saturated with NaCl 0.01 M concentrated solutions. The dry material was allowed to swell for several days and later loading, unloading and reloading phases were performed. For specimen SQ_NaB_1, after the initial swelling phase (A-B), step loading up to 49.0 kPa (B-C), unloading to 12.3 kPa (C-D), reloading up to 196.1 kPa (D-E), unloading to 12.3 kPa (E-F), reloading up to 784.4 kPa (F-G), unloading to 12.3 kPa (G-H), reloading up to 3137.6 kPa (H-I) and finally unloading to 12.3 kPa were conducted. The dry specimen SQ_NaB_4 was loaded up to 49 kPa (A-B), later on unloaded to 12.3 kPa (B-C); under this vertical stress the material was saturated with 0.01 M NaCl solution until full swell was achieved (C-D). After swell completion, standard consolidation test was conducted with a loading phase up to 1569.1 kPa (D-E) and finally an unloading phase to 12.3 kPa (E-F). Specimen SQ_NaB_5 was allowed to swell under an axial stress of 12.3 kPa (A-B); afterwards it was loaded up to 98.1 kPa (B-C), unloaded to 12.3 kPa (C-D), reloaded up to 490.4 kPa (D-E), unloaded to 12.3 kPa (E-F), reloaded up to 3628.9 kPa (F-G), and finally unloaded to 12.3 kPa (G-H).

Specimens SQ_NaB_TTw1 and SQ_NaB_TTw2 were prepared by rehydrating the squeezed bentonite in a NaCl 0.01 M concentrated solution at a lower water content (i.e. respectively w_0 = 366.0 and 317.2 %) than the LL value and then by installing the slurry inside the oedometer ring: in these cases the specimen height was 20 mm. The NaCl 0.01 M concentrated solution was supplied in the cell few seconds after the application of the first axial stress of 12.3 kPa. The specimen SQ_NaB_TTw1 was loaded up to 294.2 kPa (A-B), unloaded to 12.3 kPa (B-C), reloaded up to 686.7 kPa (C-D) and finally unloaded to 12.3 kPa (D-E). On the other hand, the specimen SQ_NaB_TTw2 was loaded up to 392.7 kPa (A-B) and then unloaded to 12.3 kPa (B-C).

During all the tests, each load was sustained long enough to reach the end of the consolidation phase. It is to note that only for specimen SQ_NaB_1 the standard

loading schedule consisted of a load increment ratio of one, which is obtained by doubling the pressure on the soil; moreover, in the unloading phases each load was one-fourth as large as the preceding load. In the other tests (i.e. for SQ_NaB_4, SQ_NaB_5, SQ_NaB_TTw1 and SQ_NaB_TTw2), other loading, unloading and reloading schedules were employed in order to obtain a greater definition of some parts of the stress-deformation curve.

3.3.4 **New testing apparatus and procedures**

In this study a new testing apparatus aimed at measuring the swelling pressure, u_{sw}, of bentonite specimens was used. This device allows measures of swelling pressure through the so-called constant-volume and pre-swell method, i.e. strain-controlled tests. Moreover, this type of testing apparatus can be employed for chemico-osmotic tests, in order to evaluate transport properties (i.e. global reflection coefficient and global osmotic effective diffusion coefficient) of bentonites.

The main components of the device are shown in Figures 3.2 and 3.3, and are partially the same as those described in detail in Malusis et al. (2001). The new testing apparatus includes a stainless steel oedometer, a flow pump accumulator, two bladders, three pressure transducers, a displacement transducer (i.e. a Linear Variable Differential Transformer, LVDT), a load cell and a pneumatic piston.

The stainless steel oedometer (diameter = 70 mm) replaces the modified rigid-wall permeameter used by Dominijanni et al. (2013). The oedometer matches with the need of containment of bentonite specimens characterized by very high swelling pressure without allowing loss of material. The top piston and the bottom pedestal of the oedometric cell are endowed of 3 drainage lines. They allow for the circulation of the solutions in the porous stones (i.e. through the 2 peripheral lines), in order to maintain a constant pressure of solutions at the top and bottom boundaries of the specimen, and, moreover, to establish a constant concentration gradient across the bentonite specimen, and the simultaneous measurement of the differential pressure

between the porous stones (i.e. through the central line with the differential pressure transducer). The other two pressure transducers allow the control of the pressure in the lines during all the testing phases.

Bentonite specimens can be back-pressurized during the tests through two bladders, which are connected to the flow pump accumulator, in order to limit the presence of air in the system.

The displacement transducer allows the specimen height to be monitored, both during the preliminary phase (i.e. compaction/swelling stage), and during the effective testing phase, with the aim of controlling the porosity of the material.

The rigid piston of the oedometer is connected to the load cell, which measures the pressure that has to be applied in order to hinder the axial strain of the specimen. The maximum pressure which can be measured by the load cell is of 500 kPa.

Three oven-dried squeezed sodium bentonite specimens of 70 mm diameter were prepared for the new testing apparatus. The physical properties of the specimens are resumed in Table 3.2.

For samples SQ_NaB_NTA1,2 a known amount of dry material was dusted inside the oedometer ring and the 0.01 M NaCl solution was supplied in order to saturate the material. Each specimen was allowed to swell freely in the axial direction to a certain value of height, which corresponds to a fixed void ratio. The piston was then blocked and the steady-state pressure was recorded by the load cell after a transitional phase of several hours. This procedure can be repeated several times, just by allowing bentonite swell to other fixed heights.

Specimen SQ_NaB_NTAw was prepared by rehydrating the squeezed pulverized bentonite in a NaCl 0.01 M concentrated solution at a lower water content (i.e. w_0 = 323.0 %) than the *LL* value, then putting the slurry inside the oedometer ring and consolidating the material to a fixed height (i.e. to e = 3.45). After the compaction stage, the bentonite was subsequently allowed to swell for few micrometers (i.e. to e_i = 3.48), the piston was then blocked and the load cell measured the swelling pressure after a transitional phase, as described above.

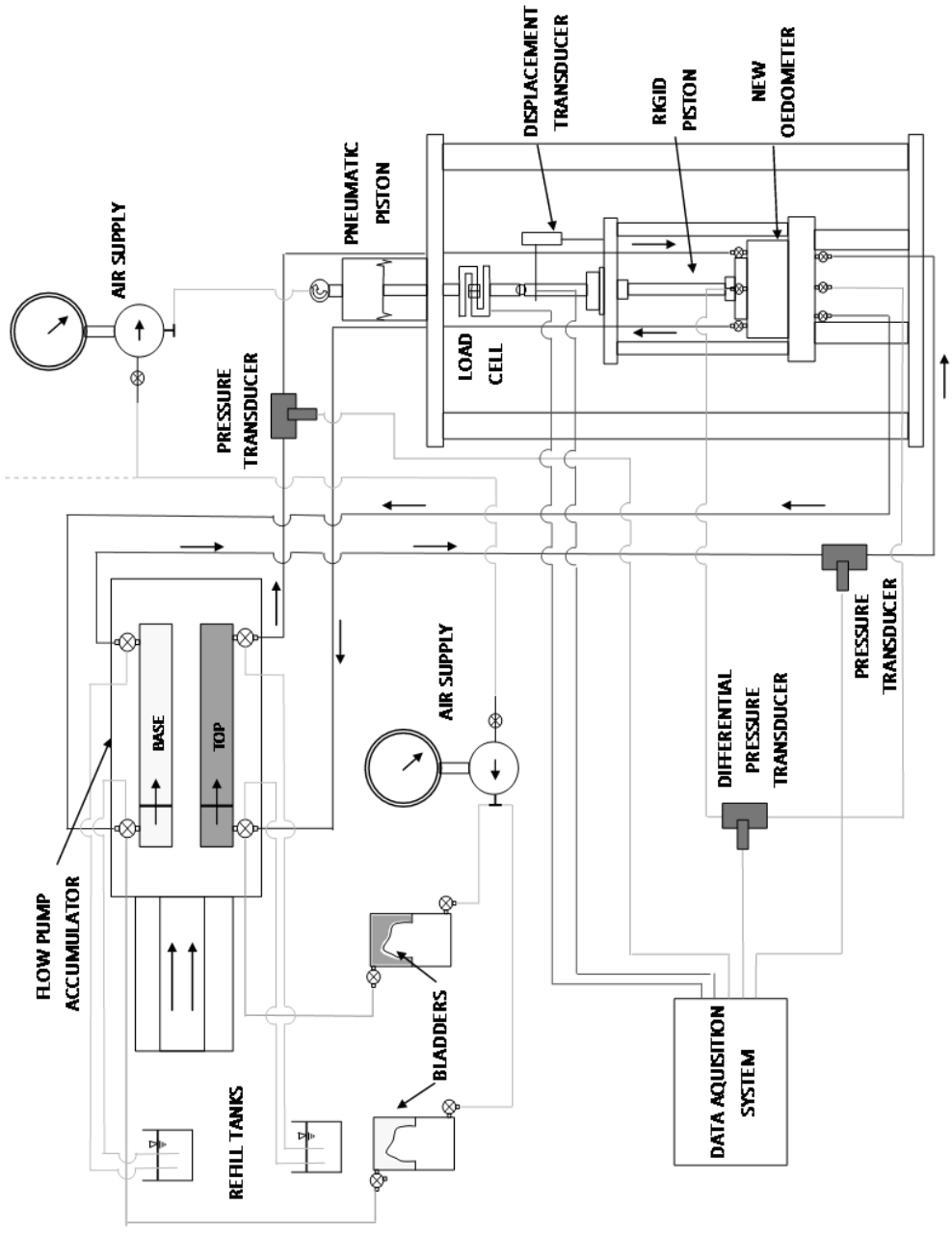

Figure 3.2 Schematic view of the new testing apparatus (not to scale)

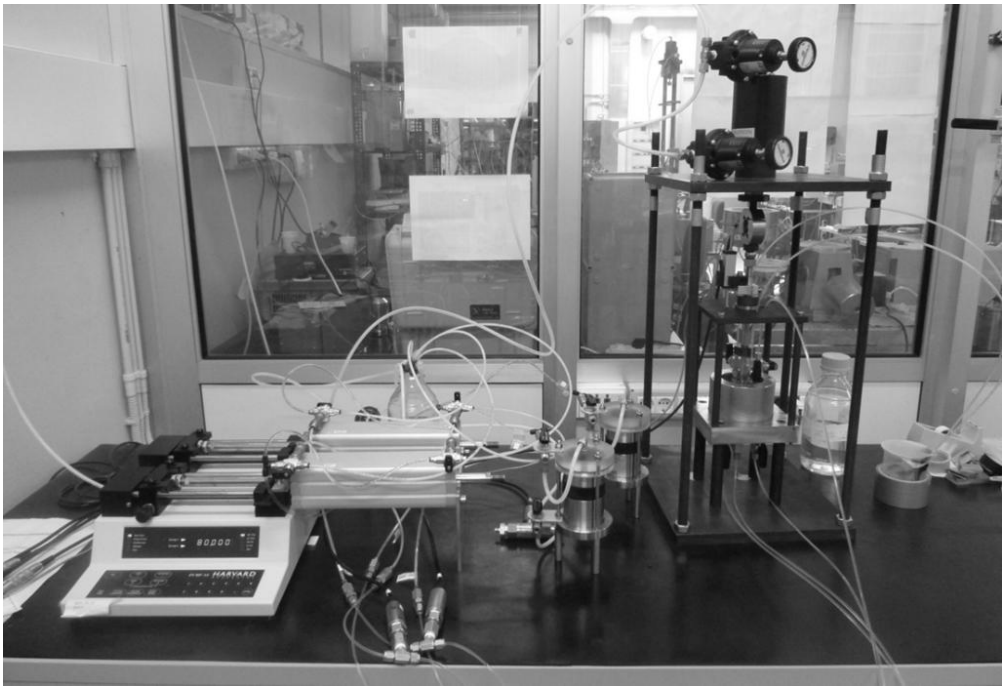

Figure 3.3 Pictorial view of the new testing apparatus

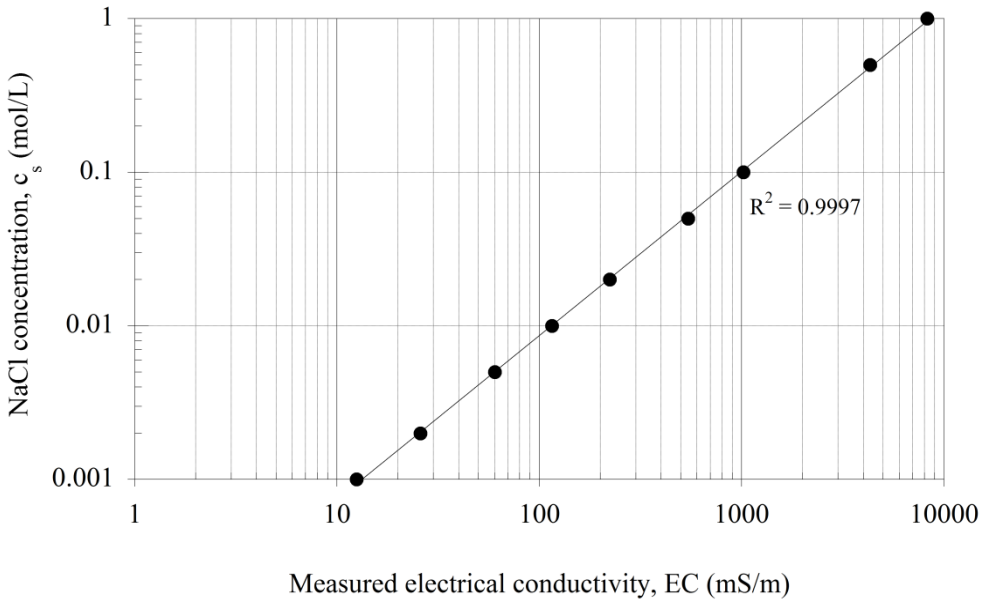

Figure 3.4 Calibration of sodium chloride (NaCl) concentration with electrical conductivity. R^2 is the coefficient of determination of the regression line

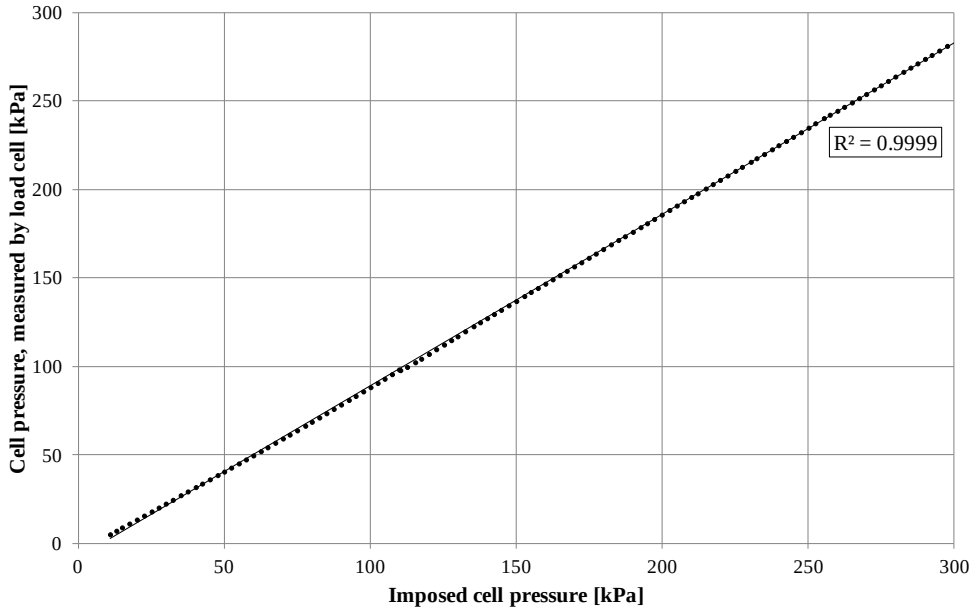

Figure 3.5 Calibration of load cell with imposed cell pressure. R^2 is the coefficient of determination of the regression line

3.4 Experimental results

3.4.1 Conventional oedometer tests

Figure 3.6 (i.e. (a) SQ_NaB_1, (b) SQ_NaB_4, (c) SQ_NaB_5, (d) SQ_NaB_TTw1 and (e) SQ_NaB_TTw2) represent the axial displacement, referred to the initial height of the specimens and measured by LVDT transducer, as a function of time. From the graphs it is possible to observe that each load was sustained long enough to reach the end of the consolidation phase.

The *EC* of the equilibrium solutions was monitored by sampling daily the solution in the plexiglass cell, and the sodium chloride molar concentration was derived using a linear relation represented in Figure 3.4.

Figure 3.7 (i.e. (a) SQ_NaB_1, (b) SQ_NaB_4, (c) SQ_NaB_5, (d) SQ_NaB_TTw1 and (e) SQ_NaB_TTw2) show the compression curves for the five specimens. It must be stressed that, since the values of the pressure of the external bulk solution

can be considered negligible (i.e. u = 0.2 kPa), it is possible to refer to total vertical stresses, σ_v instead of apparent effective vertical stresses, $\sigma_{v,app}$.

Under a total vertical stress of 12.3 kPa, sample SQ_NaB_1 swelled, during the saturation phase, from an initial void ratio e_0 = 1.60 (i.e. dry state), to e_{sat} = 5.51, SQ_NaB_4 from e_0 = 1.31 to e_{sat} = 4.97, and SQ_NaB_5 from e_0 = 1.54 to e_{sat} = 5.32: in the three cases the volumetric strain was about -150%.

Upon unloading and reloading samples SQ_NaB_1,5 and SQ_NaB_TTw1, a sort of hysteresis was observed from non-linear unloading/reloading paths. Similar trends of unloading/reloading loops in conventional oedometer tests were observed in clayey soils (Holtz et al., 1986), in bentonites (Borgesson et al., 1996), in bentonite/sand mixtures (Tong and Yin, 2011), in kaolin/bentonite mixtures (Di Maio et al., 2004) and in stiff clays (Cui et al., 2013). Cui et al. (2013) observed a certain bi-linearity of the unloading and reloading paths on some Ypresian clay specimens withdrawn at different depths.

The values of threshold stress (identified as u_{sw}) derived from the unloading paths of Figure 3.7, according to the method proposed by Cui et al. (2013), are resumed in Table 3.1 as a function of the void ratio just before each unloading.

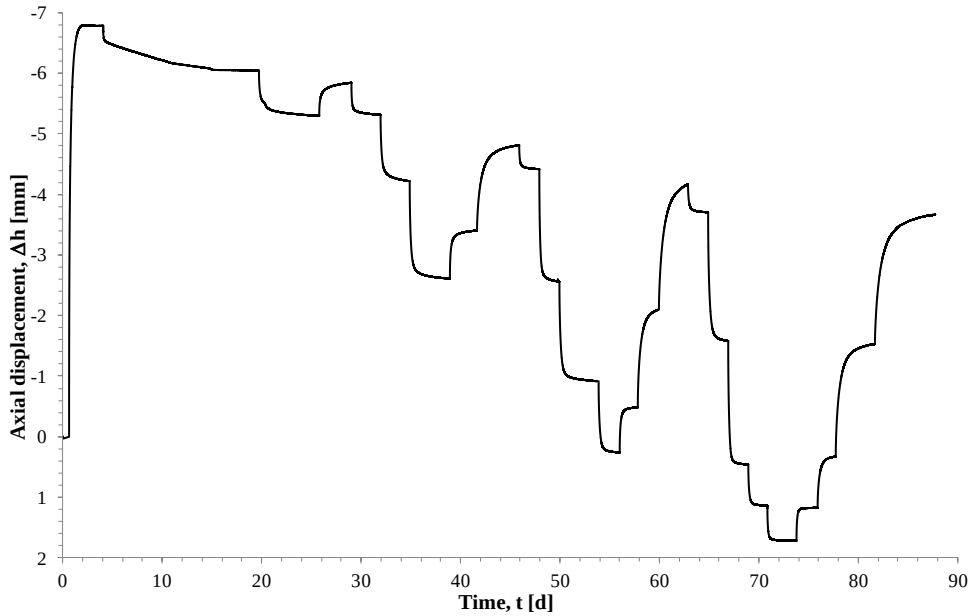

Figure 3.6 (a) Axial displacement measures of specimen SQ_NaB_1 as a function of time

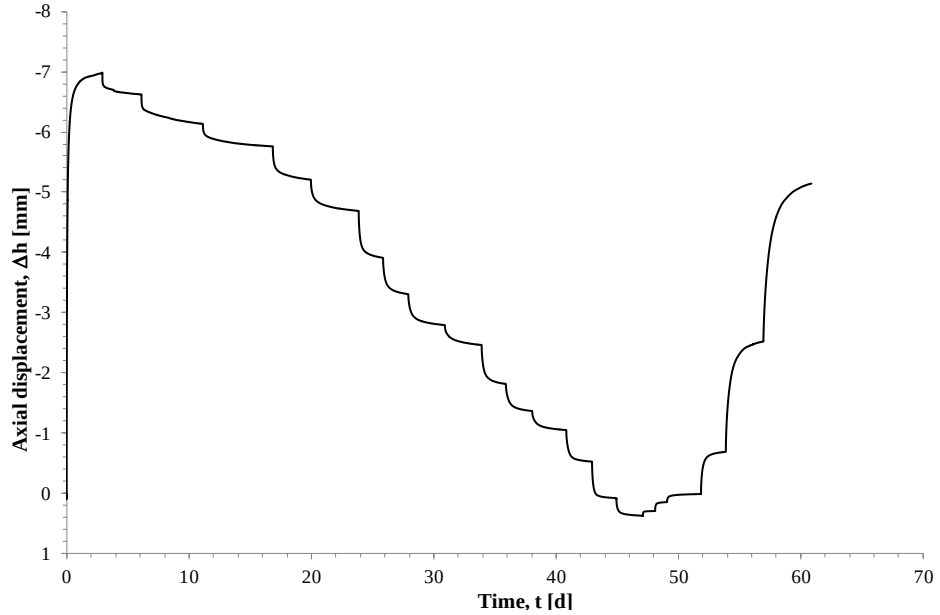

Figure 3.6 (b) Axial displacement measures of specimen SQ_NaB_4 as a function of time

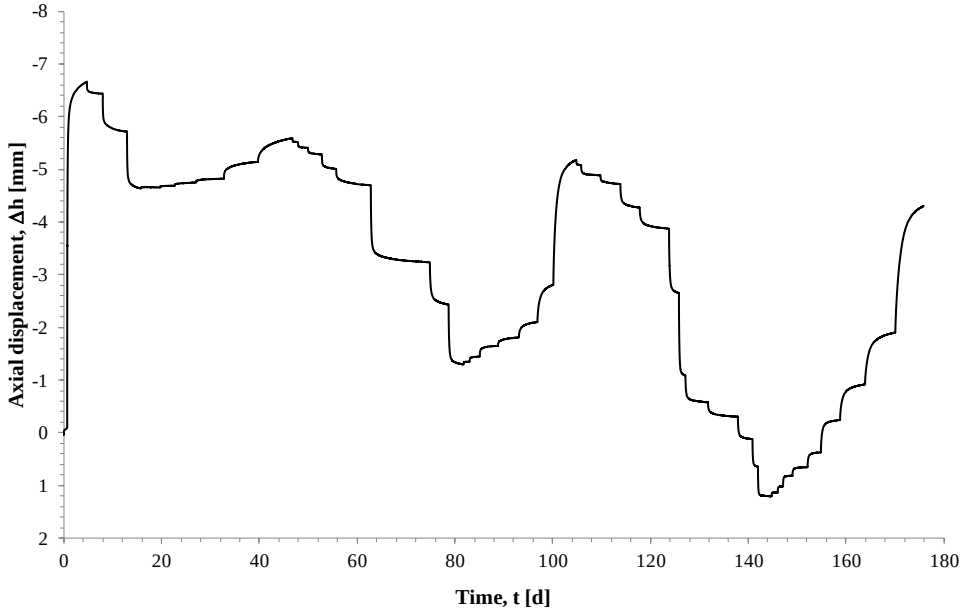

Figure 3.6 (c) Axial displacement measures of specimen SQ_NaB_5 as a function of time

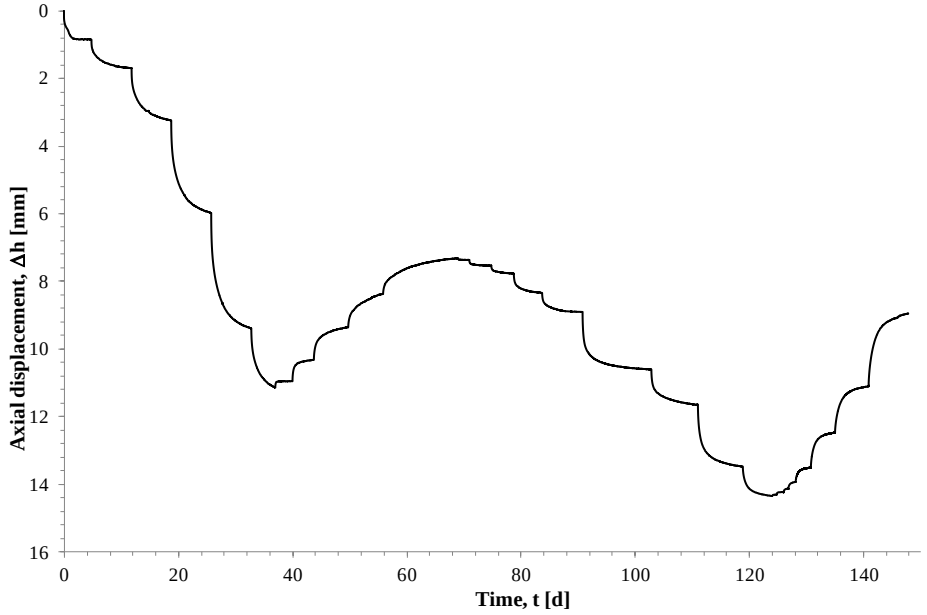

Figure 3.6 (d) Axial displacement measures of specimen SQ_NaB_TTw1 as a function of time

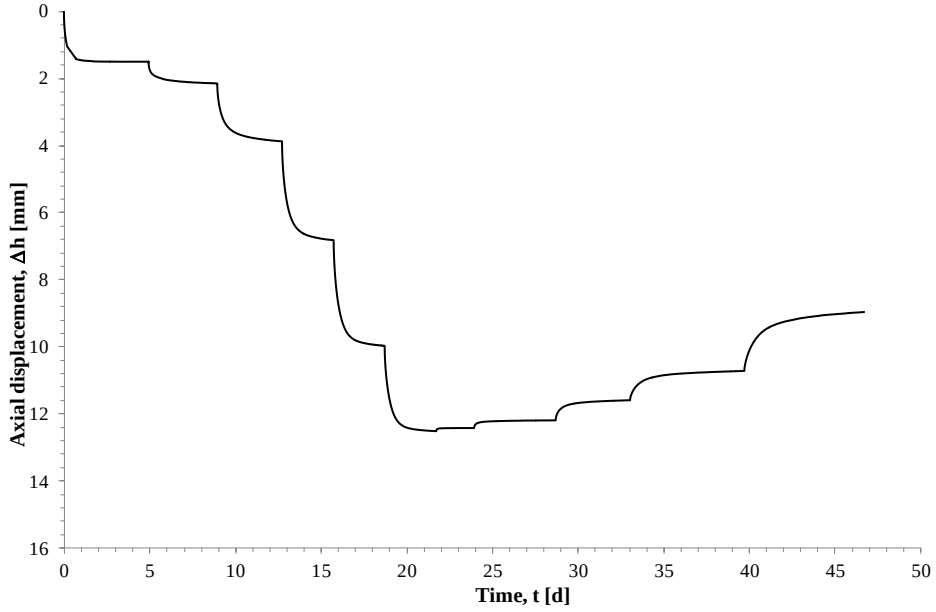

Figure 3.6 (e) Axial displacement measures of specimen SQ_NaB_TTw2 as a function of time

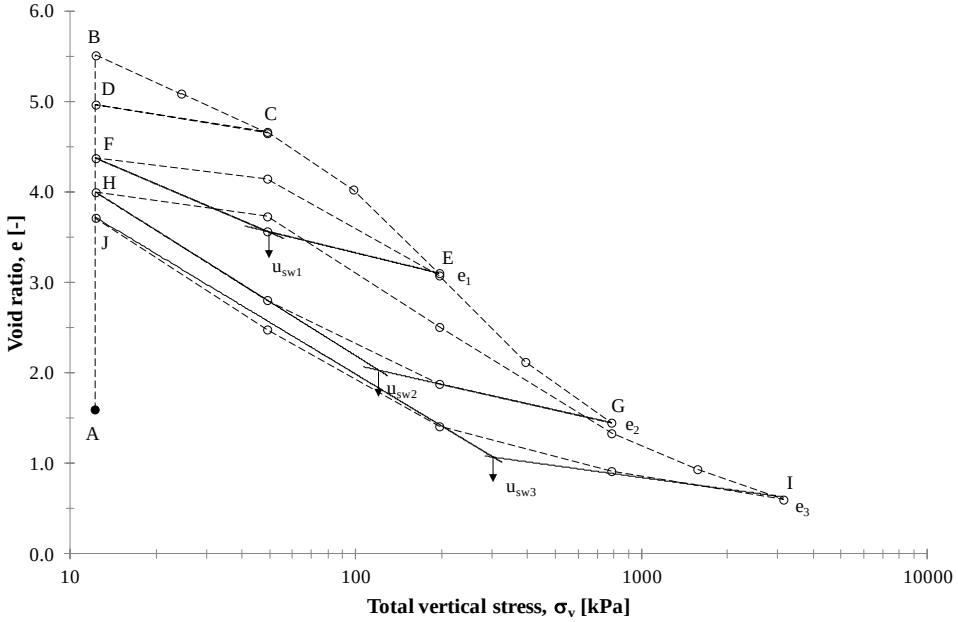

Figure 3.7 (a) Oedometer test with unloading regression lines on specimen SQ_NaB_1

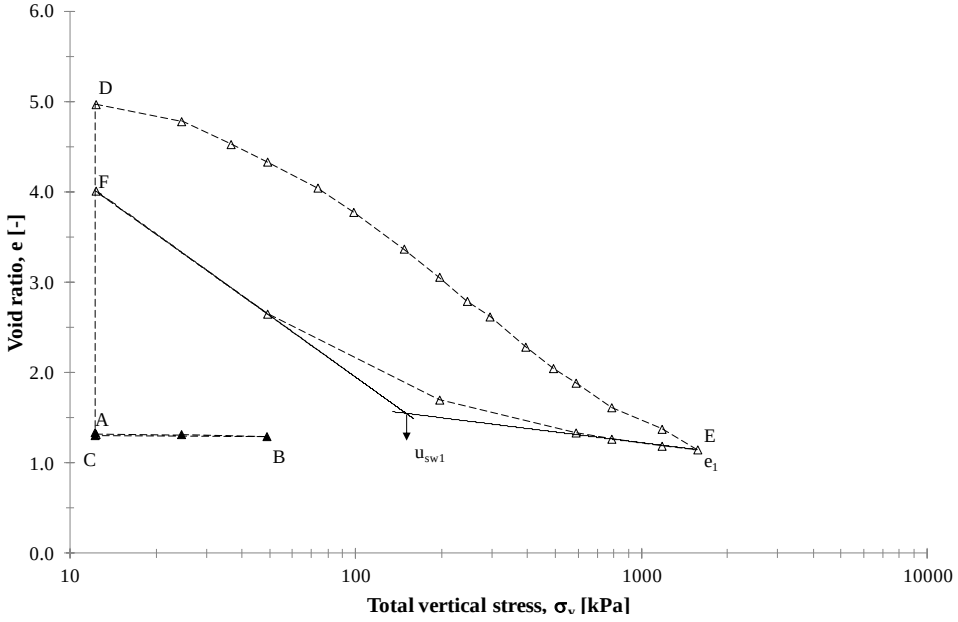

Figure 3.7 (b) Oedometer test with unloading regression lines on SQ_NaB_4

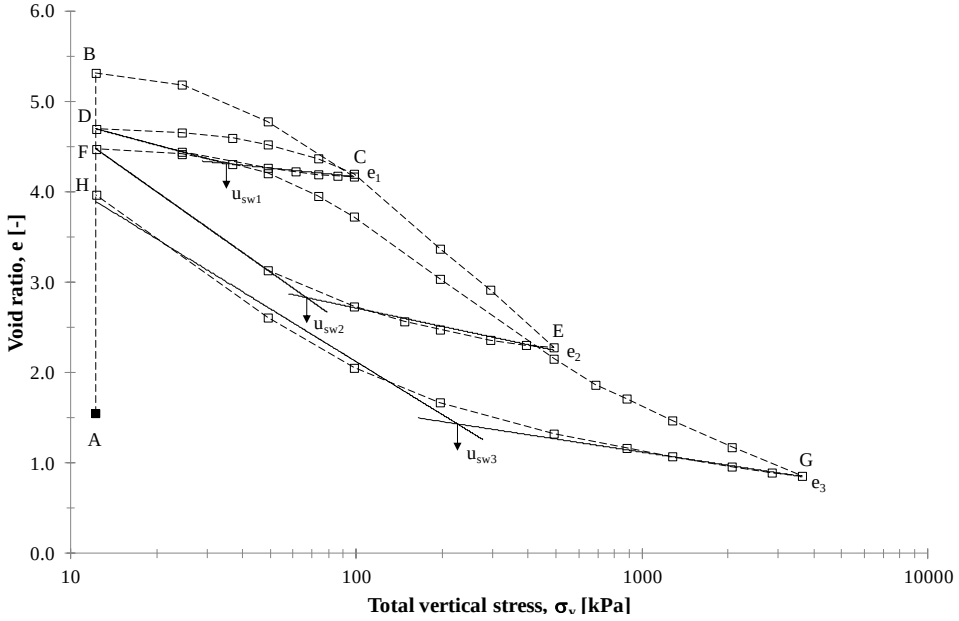

Figure 3.7 (c) Oedometer test with unloading regression lines on SQ_NaB_5

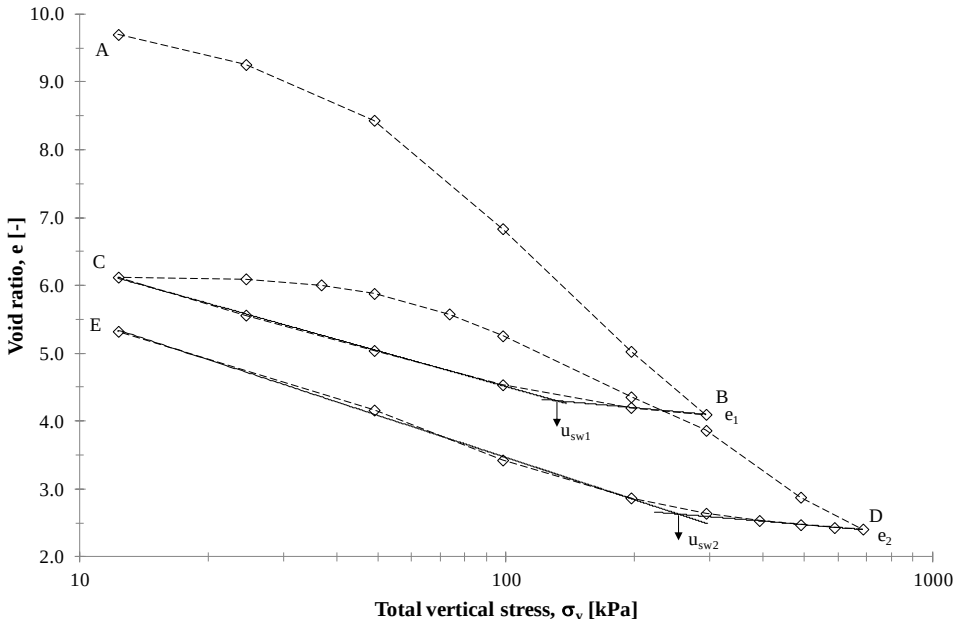

Figure 3.7 (d) Oedometer test with unloading regression lines on SQ_NaB_TTw1

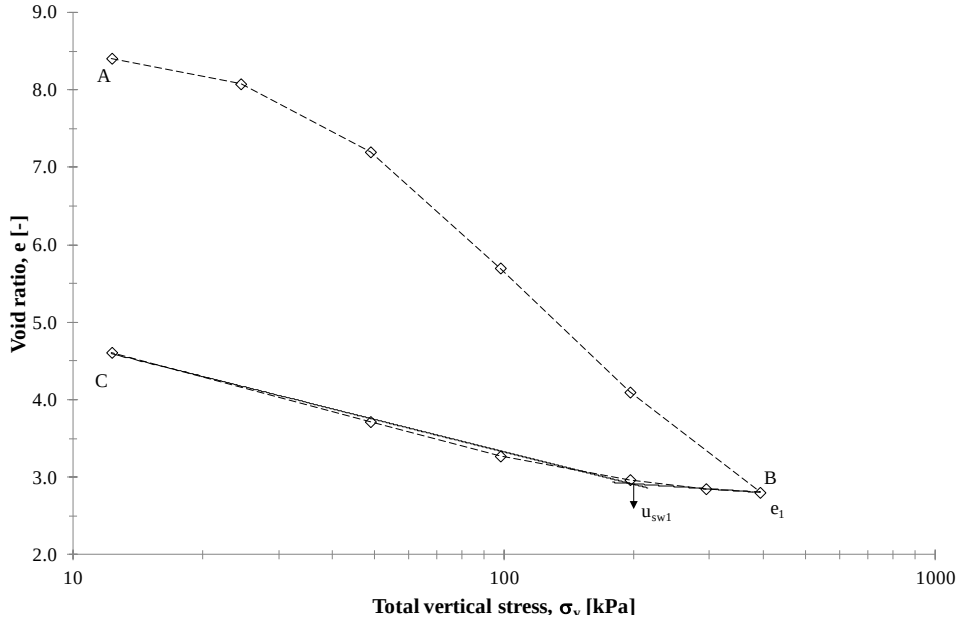

Figure 3.7 (e) Oedometer test with unloading regression lines on SQ_NaB_TTw2

Table 3.1 Physical properties and measured swelling pressures of oven-dried squeezed sodium bentonite specimens submitted to conventional oedometer tests, in equilibrium with NaCl 0.01 M concentrated solutions.

Sample	m_d [g]	w_0 [%]	e_0 [-]	e_{sat} [-]	e_i [-]	$u_{sw}(e_i)$ [kPa]	w_{fin} [%]
SQ_NaB_1	9.0	-	1.60	5.51	3.10 1.45 0.60	49 120.7 310	140.2
SQ_NaB_4	10.0	-	1.31	4.97	1.15	150	151.5
SQ_NaB_5	9.2	-	1.54	5.32	4.17 2.28 0.86	33.0 66.0 228	149.8
SQ_NaB_TTw1	9.9	366.0	-	10.28	4.10 2.41	130.7 264.9	200.9
SQ_NaB_TTw2	10.4	317.2	-	8.41	2.80	200.0	174.0

3.4.2 **Strain-controlled tests**

The swelling pressure tests in the new testing device were performed dusting dry specimens (i.e. SQ_NaB_NTA1-2), prepared with the squeezed, oven-dried sodium bentonite, allowed to swell to a fixed void ratio (i.e. respectively 3.98 and 3.32) during the hydration phase with NaCl 0.01 M solutions. Otherwise, for sample SQ_NaB_NTAw the sodium bentonite was rehydrated in a NaCl 0.01 M solution at a water content w_0 = 323.0 %, then put inside the cell and consolidated to a void ratio equal to 3.45; after this compaction stage the material was allowed to swell to e_i = 3.48, the specimen volume change was prevented and the value of the swelling pressure was measured at the stationary state.

In Figure 3.8 (i.e. (a) SQ_NaB_NTA1, (b) SQ_NaB_NTA2, (c) SQ_NaB_NTAw) the swelling pressure trend of each test is reported as a function of time. The swelling/hydration phase (i.e. from e_0 to e_{sat}) was characterised by null swelling pressure values, because the load cell was unloaded until the specimen swelled to the fixed height. From the graphs of Figure 3.8 (a) and (b) it is evident that the swelling pressure increases for several hours, when the volumetric strain is inhibited, and that the equilibrium swelling pressure is reached when the hydration phase is concluded.

During all phases of the tests, the swelling pressure was measured using the load cell. A calibration of the instrument was necessary before the testing phase in order to take into account the o-ring friction of the top piston. A linear relation was obtained by measuring the back-pressure of a volume of de-aired water inside the cell both with the pressure transducers and the load cell, as represented in Figure 3.5. The swelling pressure data measured through the strain-controlled method are resumed in Table 3.2 as a function of the fixed final void ratio, e_{sat}.

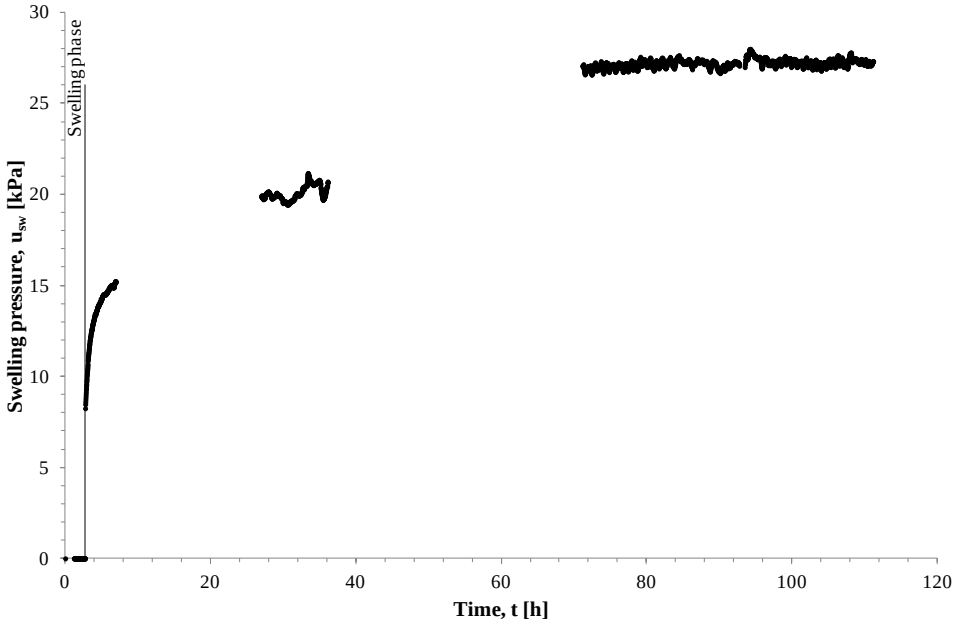

Figure 3.8 (a) Swelling pressure as a function of time (e_i = 3.98)

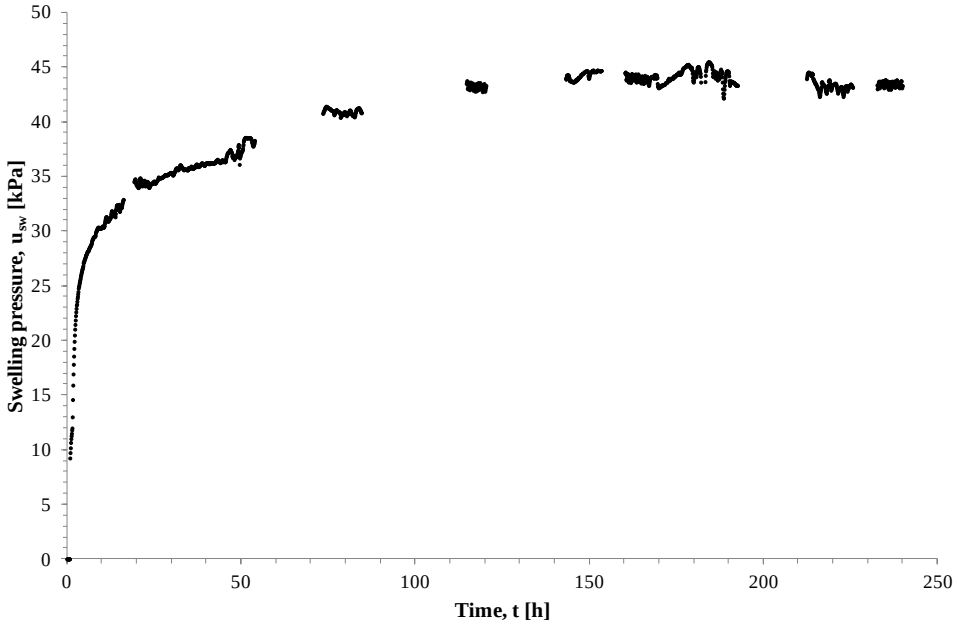

Figure 3.8 (b) Swelling pressure as a function of time (e_i = 3.32)

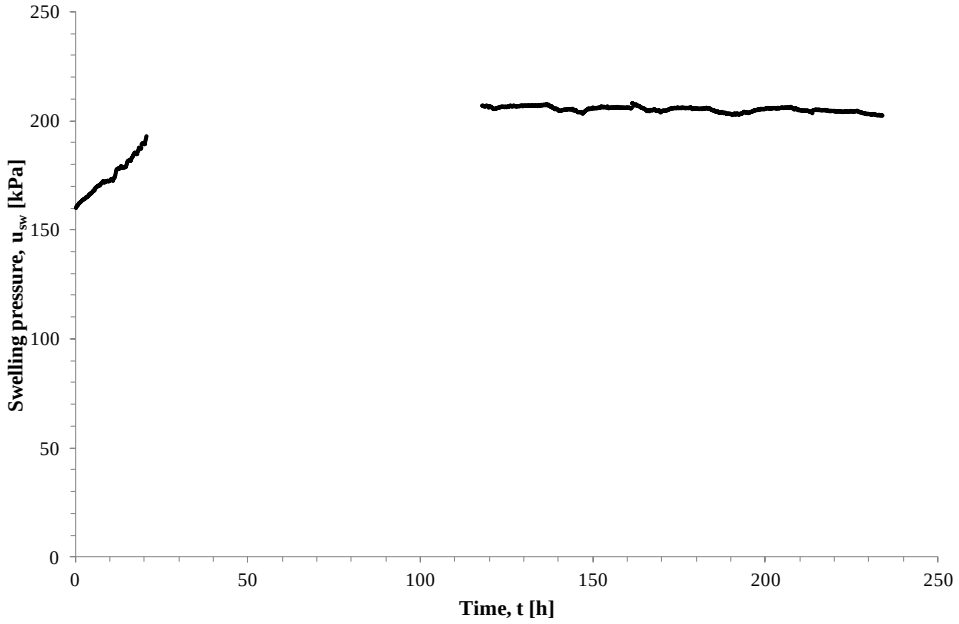

Figure 3.8 (c) Swelling pressure as a function of time (e_i = 3.48)

Table 3.2 Physical properties and measured swelling pressures of oven-dried squeezed sodium bentonite specimens tested in the new testing apparatus with the pre-swell method, in equilibrium with NaCl 0.01 M concentrated solutions.

Sample	m_d [g]	w_0 [%]	e_0 [-]	e_{sat} [-]	e_i [-]	$u_{sw}(e_i)$ [kPa]	w_{fin} [%]
SQ_NaB_NTA1	18.0	-	2.93	3.98	3.98	27.0	105.5
SQ_NaB_NTA2	21.8	-	2.11	3.32	3.32	43.0	125.3
SQ_NaB_NTAw	36.0	323.0	-	8.56	3.48	203.0	131.3

3.5 **Interpretation of test results and discussion**

Conventional oedometer tests allow to study the mechanical and the volume change behaviour of bentonite specimens. During these tests clay platelets are subjected to external forces (i.e. total vertical stresses) and interact through intergranular contact forces (i.e. apparent effective stresses) and electrostatic repulsion forces within the pore solution, which, at the macroscopic scale, determine the swelling pressure.

According to Olson and Mesri (1970) the particles geometric arrangement (i.e. the contact angle between particles) influences the competition between the mechanical effect and the physico-chemical effect on soil volume change behaviour: the mechanical effect is predominant when the contact angle between particles is large (i.e. random microstructure), on the contrary, the physico-chemical effect, governed by the soil particle-water interaction, becomes more evident when the particles are more parallel with a small contact angle (i.e. oriented microstructure). Thereby, upon mechanical loading in oedometer the contact angle is decreasing, leading to an increase of the physico-chemical effect, which can be more appreciated during unloading: the more oriented particles undergo higher repulsion forces and thus show more significant swelling (Cui et al., 2013).

Basically, the unloading path of oedometer tests can be subdivided in two distinct zones: the threshold stress (or swelling pressure, u_{sw}) separates the zone characterized by a more pronounced physico-chemical effect from that with predominant mechanical effect. When the external stress, σ_v is higher than the repulsive forces related to the soil particle–water interaction, low swelling volume change occurs; otherwise, higher swelling volume change can be expected (Cui et al., 2013). It follows that the volume change is characterized by the mechanical rebound, when $\sigma_v > u_{sw}$, whereas it is controlled by the physico-chemical swelling, for $\sigma_v < u_{sw}$. In the first case, the microstructure pattern of the soil remains rather orientated with dominated face-to-face particle contacts; in the latter case, the physico-chemical effect becomes more important and leads to a significant microstructure change (i.e. a larger soil swelling), characterized by more face-to-edge particle contacts.

A qualitative understanding of this mechanism can be proposed looking at Figure 3.9, in which a representation of clay particles and forces acting at the microscopic scale is reported. Under loading conditions, the external total stress is transferred to contact forces and electro-chemical repulsive forces. When unloading starts, the decrease of the external stress is expected to determine an initial reduction in contact stress until the external stress is equal to the swelling pressure related to the electro-chemical repulsive forces. When $\sigma_v < u_{sw}$, the clay particles undergo a significant

deformation with consequent increase of void ratio and decrease of the corresponding swelling pressure.

Even if the unloading paths of the conventional oedometer tests performed in this study are curvilinear, it is possible to simplify them in two linear paths and derive a swelling pressure value through their intersection, ad illustrated by Cui et al. (2013). Although specimen SQ_NaB_4 was tested according to Method A of ASTM D 4546-96, the swelling pressure value was obtained through the method described above. In fact, as in ASTM D 4546-96 the swelling pressure is defined as the pressure required to compress the specimen back to void ratio equal to e_0, it follows that the definition accounts for the contributions of both the direct contact between the soil particles and of the electrical forces. Therefore, in order to consider a swelling pressure value associated just to the physico-chemical swelling behaviour, the interpretation proposed by Cui et al. (2013) was preferred.

The experimental results of this study were plotted in a semi-logarithmic plane (i.e. e-log u_{sw}). The swelling pressure datum (i.e. u_{sw} = 23 kPa) obtained by Dominijanni et al. (2013) during a similar strain-controlled test on a oven-dried squeezed sodium bentonite specimen, characterised by a void ratio, e_{sat} = 4.26, in equilibrium with a 0.01 M concentrated NaCl solution, was added in the same graph.

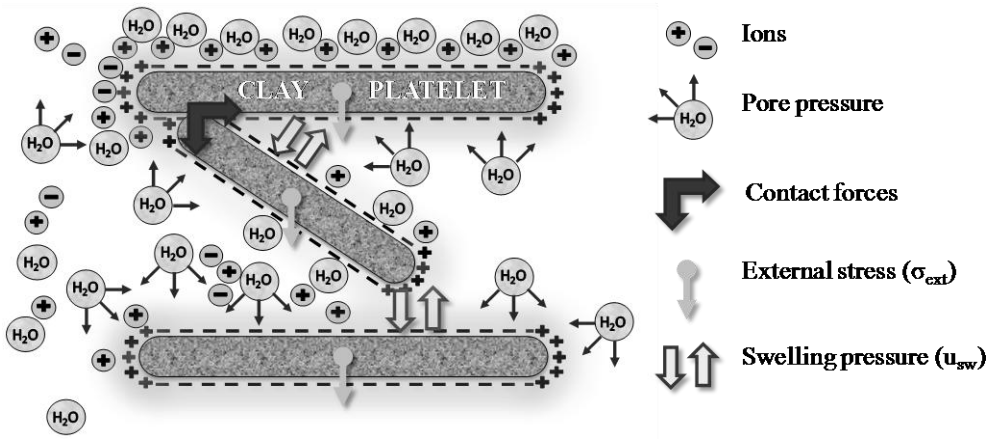

Figure 3.9 Representation of clay particles and forces acting at the microscopic scale

According to Dominijanni and Manassero (2012b), it is possible to relate the experimental swelling pressure results of the two types of tests to the physical and chemical properties of the tested bentonite specimens, by assuming that the microscopic deviations of the state variables from their average values are negligible. In such a case, on the basis of the proposed theoretical model, the swelling pressure depends on the solid skeleton electric charge, $\overline{C}_{sk,0}$ through Eq. (3.4). Therefore, from the best-fitting of the theoretical curves with the experimental results (Figure 3.10), two different constant values of $\overline{C}_{sk,0}$ were found, respectively equal to 95 mM for specimens SQ_NaB_1,4,5 and SQ_NaB_NTA1,2, and to 305 mM for specimens SQ_NaB_TTw1,2 and SQ_NaB_NTAw, in accordance with the theoretical background. In fact, from Eq. (4.5), assuming σ = 0.114 C m^{-2}, f_{Stern} = 0.85, ρ_{sk} = 2.65 g cm^{-3}, S = 760 m^2 g^{-1}, it follows that, in the case of $\overline{C}_{sk,0}$ = 95 mM, the number of lamellae per tactoid, N_l is equal to 4, corresponding to an aggregated structure; otherwise, in the case of $\overline{C}_{sk,0}$ = 305 mM, N_l is equal to 1, corresponding to a dispersed structure. The results are a direct consequence of the initial process of saturation of specimens SQ_NaB_TTw1,2 and SQ_NaB_NTAw, which leaded to a dispersed microstructure of the bentonite, characterized by single lamellae and, consequently, more relevant physico-chemical phenomena. The interpretation of the previous results (i.e. u_{sw} data from tests on specimens SQ_NaB_1, 4, 5 and SQ_NaB_NTA1,2) is in accordance with the study carried out by Dominijanni et al. (2013), in which the authors obtained a similar value of $\overline{C}_{sk,0}$ (i.e. 90 mM), interpreting experimental swelling pressure data from similar strain-controlled tests on sodium bentonite specimens in equilibrium with NaCl solutions at different molar concentrations (i.e. 5, 10, 20 50, 100 mM).

The possibility of fitting swelling pressure results, obtained from two different types of tests, with a single value of $\overline{C}_{sk,0}$ is an indication of the ability of the theoretical approach, proposed by Dominijanni and Manassero (2012b), to simulate the bentonite behaviour.

It should be pointed out that the solid skeleton electric charge, $\overline{C}_{sk,0}$, can assume different values as a function of void ratio and, in particular, of salt concentration due to the bentonite fabric changes. Nevertheless, considering the constant concentration and high dilution of the salt solution, within this study, the obtained data have been interpreted, in a first approximation, with a constant value of $\overline{C}_{sk,0}$. Despite these approximations, experimental results are quite well fitted by the theoretical curves.

Finally, it is important to stress that the physical approach should not be mistaken for a microscopic modelling of soil behaviour: it's a tool which can be used in order to understand why sodium bentonites behave in a given way at the macroscopic scale on the basis of a simplified picture of their microstructure.

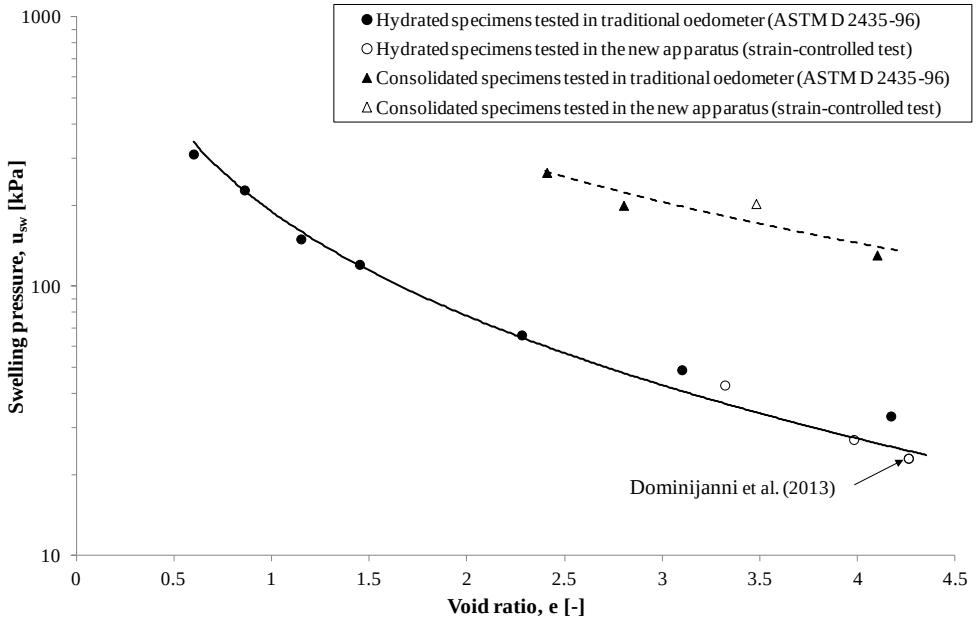

Figure 3.10 Swelling pressure, u_{sw}, as a function of void ratio, with best-fitting theoretical curve, obtained for $\overline{C}_{sk,0}$ = 95 mM (continuous line) and for $\overline{C}_{sk,0}$ = 305 mM (dotted line) in Eq. (3.4)

3.6 **Conclusions**

In this study the mechanical behaviour of sodium bentonites in equilibrium with NaCl 0.01 M solutions was analyzed by performing two types of oedometer tests. Several swelling pressure data were derived from conventional oedometer tests accordingly to the interpretation proposed by Cui et al. (2013), other results were obtained through the so-called strain-controlled method, by using a new oedometer testing device. The experimental data were interpreted on the basis of the theoretical approach proposed by Dominijanni and Manassero (2012b). The results are in agreement with the trends given by the model, under the assumption that the microscopic deviations of the pore solution state variables from their average values are negligible. By accepting this hypothesis, from the experimental value of swelling pressure it was possible to derive two different electric charge of the solid skeleton (per unit solid volume), $\overline{C}_{sk,0}$, indication of the different (i.e. dispersed and aggregated) microstructure of the tested bentonite specimens. However, the physical model proposed by Dominijanni and Manassero (2012b) represents a simplified picture of the real bentonite microstructure: a direct measurement of its properties at the microscopic scale could be very difficult. Further experimental tests are recommended in order to verify the applicability of the proposed theoretical model under different boundary conditions and for different salts contained in the pore solution.

References

1. ASTM, 2002. Test Method for One-Dimensional Consolidation Properties of Soils, D 2435-96: 2000 Annual Book of ASTM Standards, Vol. 04.08. American Society for Testing and Materials, West Conshohocken, PA.
2. ASTM, 2002. Standard Test Methods for One-Dimensional Swell or Settlement Potential of Cohesive Soils, D 4546-96: 2000 Annual Book of ASTM Standards, Vol. 04.08. American Society for Testing and Materials, West Conshohocken, PA.
3. Bolt, G.H. (1956). Physico-chemical analysis of the compressibility of pure clays. *Géotechnique* **6**(2), 86-93.
4. Borgesson, L., Karnland, O., Johannesson, L.E. (1996). Modelling of the physical behaviour of clay barriers close to water saturation. *Engineering Geology* **41**, 127-144.
5. Bouazza, A. (2002). Geosynthetic clay liners. Review article. *Geotextiles and Geomembranes* **20**, 3-17.
6. Chapman, L. (1913). A contribution to the theory of electrocapillarity. *Philosophical Magazine*, 25, 475–481.
7. Cui, Y.J., Nguyen, X.P., Tang, A.M., Li X.L. (2013). An insight into the unloading/reloading loops on the compression curve of natural stiff clays. *Applied Clay Science* **83-84**, 343-348.
8. Di Emidio, G. (2010). Hydraulic and chemico-osmotic performance of polymer treated clays. PhD Thesis, Ghent: Ghent University.
9. Di Maio, C. (1996). Exposure of bentonite to salt solution: osmotic and mechanical effects. *Géotechnique* **46**(4), 695-707.
10. Di Maio, C., Santoli, L., Schiavone, P. (2004). Volume change behaviour of clays: the influence of mineral composition, pore fluid composition and stress rate. Mechanics of Materials **36**, 435-451.
11. Dominijanni, A., Manassero, M., Vanni, D. (2006). Micro/macro modeling of electrolyte transport through semipermeable bentonite layers. In: Thomas, H.R. (Ed.), Proceedings of the 5th International Congress of

Environmental Geotechnics, 26th-30th June, 2006, Cardiff, Wales, UK, vol. II. Thomas Telford, London, pp. 1123-1130.

12. Dominijanni, A. & Manassero, M. (2012a). Modelling the swelling and osmotic properties of clay soils. Part I: The phenomenological approach. *International Journal of Engineering Science* **51**, 32-50.
13. Dominijanni, A. & Manassero, M. (2012b). Modelling the swelling and osmotic properties of clay soils. Part II: The physical approach. *International Journal of Engineering Science* **51**, 51-73.
14. Dominijanni, A., Manassero, M., Puma, S. (2013). Coupled chemical-hydraulic-mechanical behaviour of bentonites. *Géotechnique* **63**(3), 191-205.
15. Gouy, G. (1910). Sur la constitution de la charge électrique à la surface d'un electrolyte. *Journal de Physique Théorique et Appliquée*, 9, 457–468.
16. Guyonnet, D., Gaucher, E., Gaboriau, H., Pons, C.H., Clinard, C., Norotte, V. and Didier, G. (2005). Geosynthetic clay liner interaction with leachate: correlation between permeability, microstructure and surface chemistry. *Journal of Geotechnical and Geoenvironmental Engineering*, **131**(6), 740-749.
17. Holtz, R.D., Jamiolkowski, M.B., Lancellotta, R. (1986). Lessons from oedometer tests on high quality samples. *Journal of Geotechnical Engineering* **112**(8), 768-776.
18. Kang, J.-B., Shackelford, C. D. (2009). Clay membrane testing using a flexible-wall cell under closed system boundary conditions. *Applied Clay Science* **44**(1-2), 43-58.
19. Kang, J.-B., Shackelford, C. D. (2010a). Consolidation of a geosynthetic clay liner under isotropic states of stress. *Journal of Geotechnical and Geoenvironmental Engineering* **136**(1), January 1, 2010, 253-259.
20. Kang, J.-B., Shackelford, C. D. (2010b). Membrane behavior of compacted clay liners. *Journal of Geotechnical and Geoenvironmental Engineering* **136**(10), 1368-1382.

21. Laird, D.A. (2006). Influence of layer charge on swelling of smectites. *Applied Clay Science* **34**, 74-87.
22. Liu, L. (2013). Prediction of swelling pressures of different types of bentonite in dilute solutions. *Colloids and Surfaces A: Physicochemical and Engineering Aspects* **434**, 303-318.
23. Malusis, M.A., Shackelford, C.D. & Olsen, H.W. (2001). A laboratory apparatus to measure chemico-osmotic efficiency coefficients for clay soils. *Geotechnical Testing Journal* **24**, 229-242.
24. Malusis, M.A. & Shackelford, C.D. (2002a). Chemico-osmotic efficiency of a geosynthetic clay liner. *Journal of Geotechnical and Geoenvironmental Engineering* **128**, No. 2, 97–106.
25. Malusis, M.A. & Shackelford, C.D. (2002b). Coupling effects during steady-state solute diffusion through a semipermeable clay membrane. *Environmental Science and Technology* **36**, No. 6, 1312–1319.
26. Mesri, G., Olson, R. E. (1971). Consolidation characteristics of montmorillonite. *Géotechnique* **21**(4), 341-352.
27. Nguyen, X.P., Cui, Y.J., Tang, A.M., Deng, Y.F., Li, X.L., Wouters, L. (2013). Effects of pore water chemical composition on the hydro-mechanical behavior of natural stiff clays. *Engineering Geology* **166**, 52-64.
28. Norrish, K. (1954). The swelling of montmorillonite. Discussions of the Faraday Society, **18**, 120-134.
29. Olson R.E., Mesri G. (1970). Mechanisms controlling the compressibility of clays. *Journal of Soil Mechanics and Foundation Division*, ASCE **96**(6), 1863-1878.
30. Shackelford, C.D. & Lee, J.-M. (2003). The destructive role of diffusion on clay membrane behavior. *Clays and Clay Minerals* **51**, No. 2, 186–196.
31. Shainberg, I., Caiserman, A. (1971). Studies on Na/Ca montmorillonite systems. 1. The hydraulic conductivity. *Soil Science* **111**(5), 276-281.
32. Sridharan, A., Jayadeva, M. S. (1982). Double layer theory and compressibility of clays. *Géotechnique* **32**(2), 133-144.

33. Sridharan, A., Rao, S., Sivapullaiah, P.V. (1986). Swelling pressure of clays. *Geotech. Test. J.* **9**, 24-33.
34. Sridharan, A., Venkatappa Rao, G. (1973). Mechanisms controlling volume change of saturated clays and the role of the effective stress concept. *Géotechnique* **23**(3), 359-382.
35. Tong, F., Yin, J.H., (2011). Nonlinear creep and swelling behavior of bentonite mixed with different sand contents under oedometric condition. *Marine Georesources & Geotechnology* **29**(4), 346-363.
36. Van Olphen, H. (1977). An introduction to Clay Colloid Chemistry: For Clay Technologists, Geologists, and Soils Scientists, John Wiley and Sons, New York.
37. Wang, Q., Tang, A.M., Cui, Y.J., Delage, P., Gatmiri, B. (2012). Experimental study on the swelling behavior of bentonite/claystone mixture. *Engineering Geology* **124**, 59-66.
38. Yeo, S.-S., Shackelford, C. D., Evans, J. C. (2005). Membrane behavior of model soil-bentonite backfills. *Journal of Geotechnical and Geoenvironmental Engineering* **131**(4), 418-429.
39. Yong, R.N., Warkentin B.P. (1975). *Soil properties and behaviour. Developments in geotechnical engineering (vol. 5)*. Elsevier Scientific Publishing Company.

3.7 Further results of oedometer tests

Several further oedometer tests (i.e. conventional oedometer tests and swelling tests under oedometric conditions) were performed during the PhD research activity, in order to evaluate the mechanical and swelling behaviour of sodium bentonites at different void ratios and, in particular, the consequences on the microstructure of bentonites produced by the change in NaCl solution concentrations during conventional oedometer tests.

3.7.1 Effect of change of the pore solution concentration on bentonite microstructure

Two oven-dried squeezed sodium bentonite specimens (i.e. SQ_NaB_2 and SQ_NaB_3) of 50 mm diameter were prepared for conventional oedometer tests, aimed at analyzing the effect of change of the pore solution concentration on the soil mechanical behaviour. The main physical properties of these specimens are resumed in Table 3.3.

Table 3.3 Physical properties of oven-dried squeezed sodium bentonite specimens submitted to conventional oedometer tests, in equilibrium with NaCl 0.01 M and NaCl 0.05 concentrated solutions.

Sample	m_d [g]	w_0 [%]	e_0 [-]	e_{sat} [-]	w_{fin} [%]
SQ_NaB_2	9.0	-	1.60	5.17	107.8
SQ_NaB_3	9.2	-	1.54	6.02	205.2

The samples were both prepared by dusting the dry material inside the stainless steel ring in the plexiglass cell: the specimens reached an initial height, h_0 of 4.5 mm. Under a total axial stress of 12.3 kPa the sodium bentonite specimens were saturated with NaCl 0.01 M concentrated solutions. The dry material was allowed to swell for several days and later loading, unloading and reloading phases were performed.

For specimen SQ_NaB_2, after the initial swelling phase (A-B), step loading up to 49.0 kPa (B-C), unloading to 12.3 kPa (C-D), reloading up to 98.1 kPa (D-E), salt solution substitution at constant vertical stress (from NaCl 10 mM to NaCl 50 mM) (E-F), loading up to 196.1 kPa (F-G), unloading to 12.3 kPa (G-H), reloading up to 784.4 kPa (H-I), and finally unloading to 12.3 kPa (I-J) were conducted.

For specimen SQ_NaB_4 after the initial swelling phase (A-B), step loading up to 49.0 kPa (B-C), unloading to 12.3 kPa (C-D), reloading up to 98.1 kPa (D-E), salt solution substitution at constant vertical stress (from NaCl 10 mM to NaCl 50 mM) (E-F), loading up to 196.1 kPa (F-G), unloading to 12.3 kPa (G-H), reloading up to 392.3 kPa (H-I), salt solution substitution at constant vertical stress (from NaCl 50 mM to NaCl 10 mM) (I-J), loading up to 784.4 kPa (J-K), and finally unloading to 12.3 kPa (K-L) were conducted.

Graphs of Figure 3.11 (i.e. (a) SQ_NaB_2, and (b) SQ_NaB_3) represent the axial displacement, referred to the initial height, h_0, of the specimens and measured by LVDT transducer, as a function of time. From the graphs it is possible to observe that, even in these cases, each load was sustained long enough to reach the end of the consolidation phase.

The compression curves of the two specimens, are shown in Figure 3.12 (i.e. (a) SQ_NaB_2, and (b) SQ_NaB_3), in terms of void ratio, e, vs. total vertical stress, σ_v.

Under a total vertical stress of 12.3 kPa, sample SQ_NaB_2 swelled, during the saturation phase, from an initial void ratio e_0 = 1.60 (i.e. dry state), to e_{sat} = 5.17, reaching a height h_{sat} = 10.2 mm; on the contrary SQ_NaB_3 from e_0 = 1.54 to e_{sat} = 6.02, reaching h_{sat} = 12.4 mm. By referring the axial displacement of each phase to h_{sat}, it is possible to determine the volumetric strains, ε_v, induced by the loads and the salt solution substitutions, and to compare the compression curves, in terms of volumetric strains, ε_v, vs. total vertical stresses, σ_v, as represented in Figure 3.13.

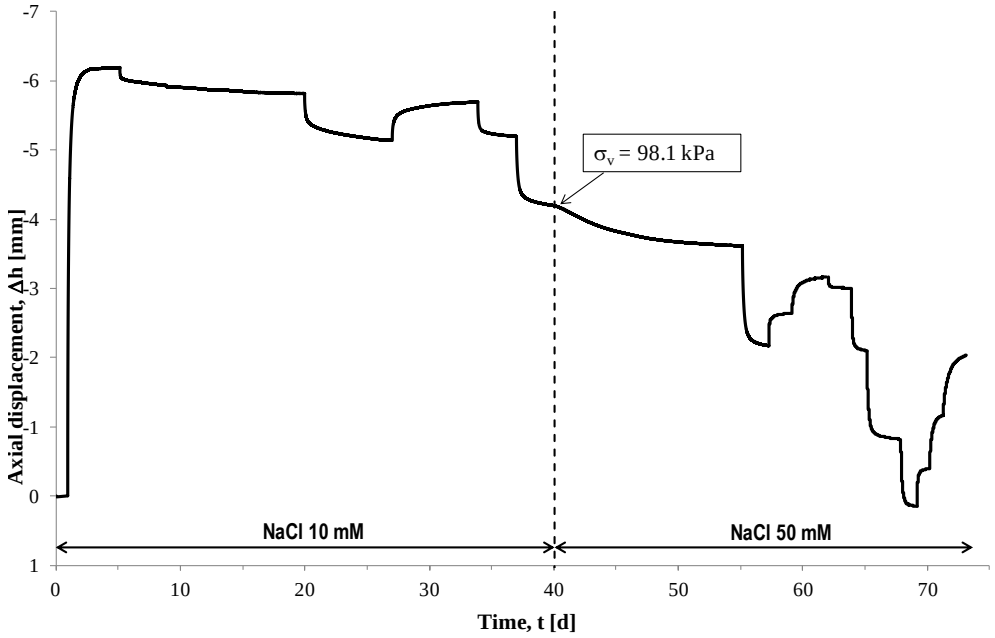

Figure 3.11 (a) Axial displacement measures of specimen SQ_NaB_2 as a function of time.

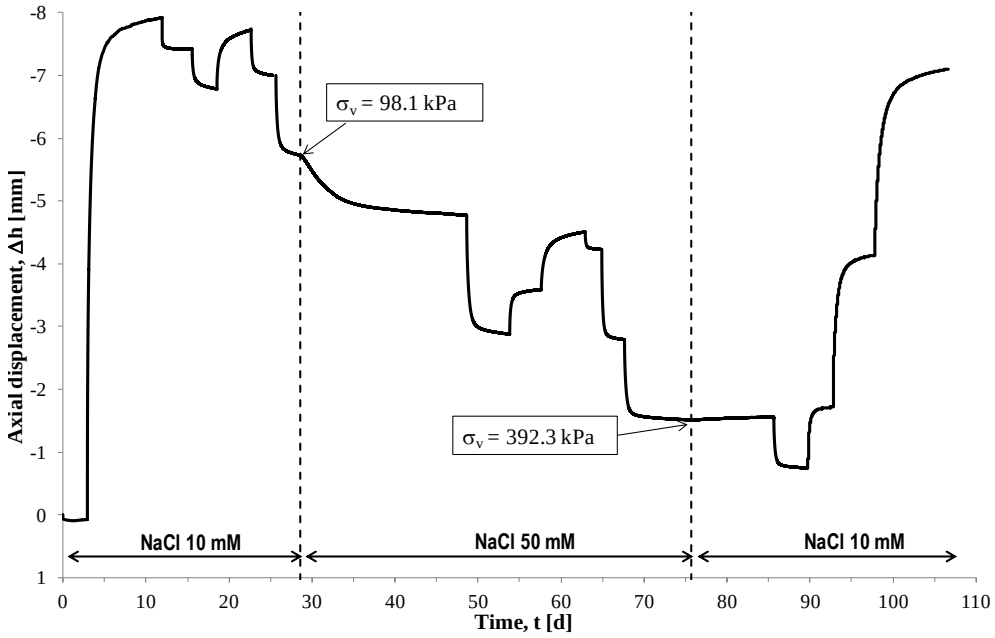

Figure 3.11 (b) Axial displacement measures of specimen SQ_NaB_3 as a function of time.

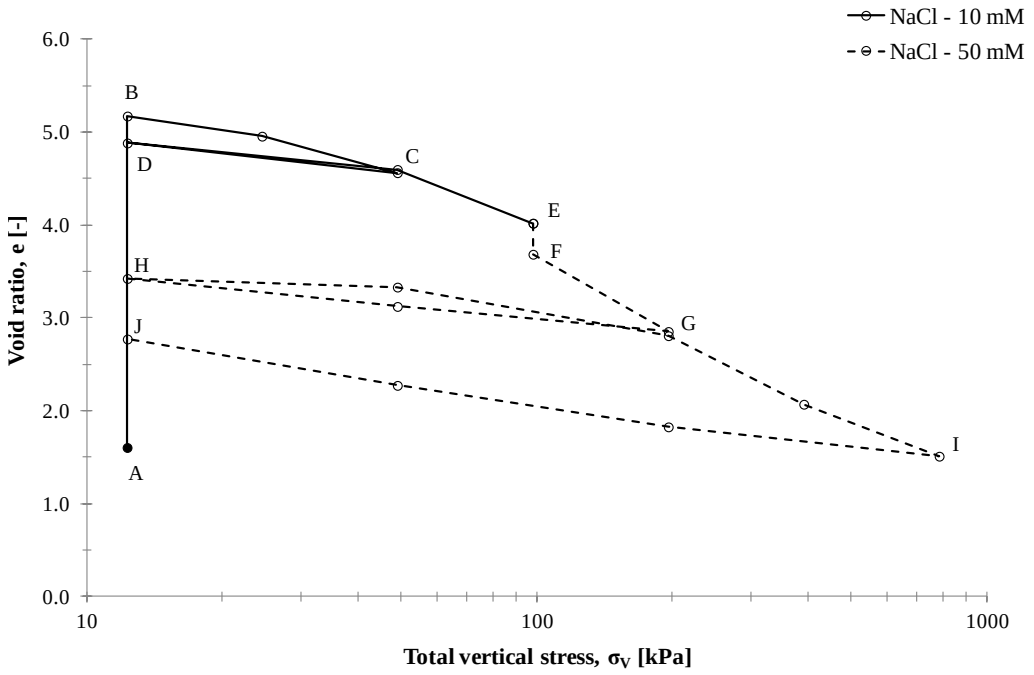

Figure 3.12 (a) Oedometer test on specimen SQ_NaB_2.

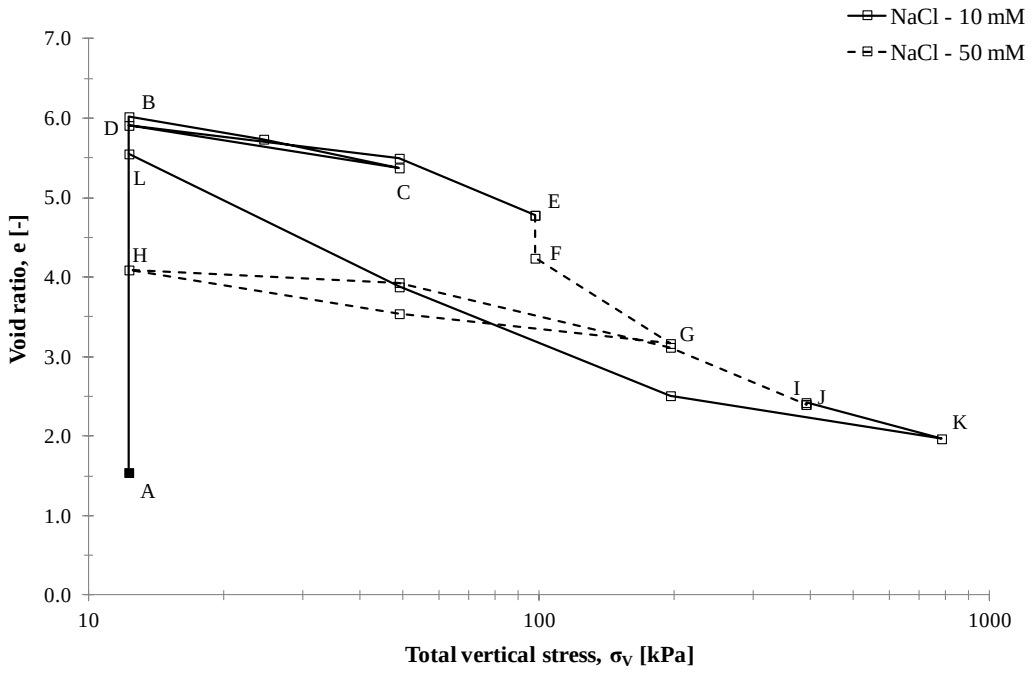

Figure 3.12 (b) Oedometer test on specimen SQ_NaB_3.

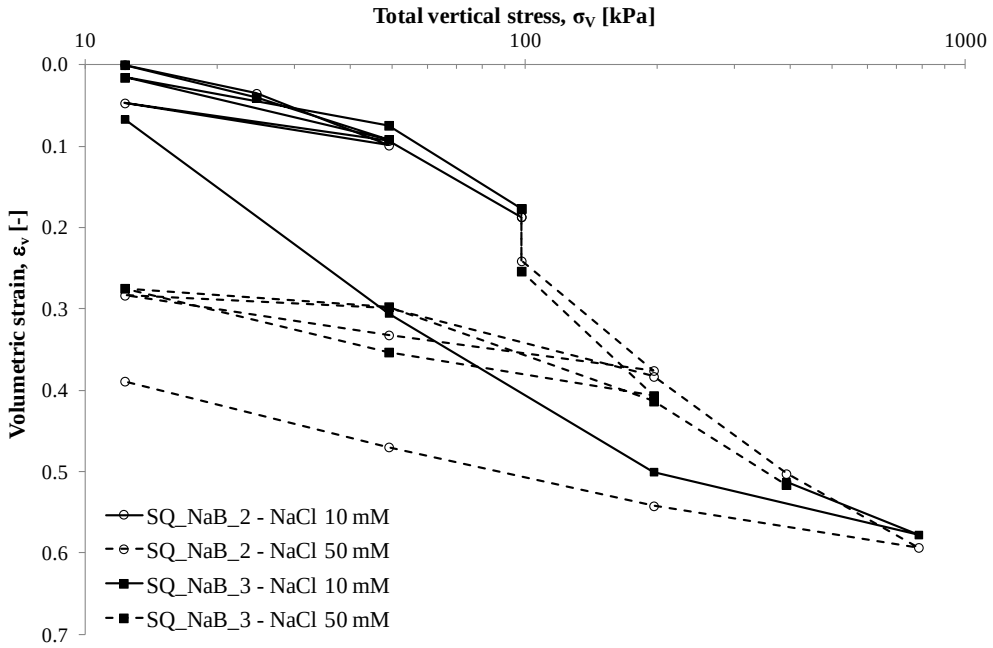

Figure 3.13 Comparison between oedometer tests on specimen SQ_NaB_2 (circles) and SQ_NaB_3 (squares) in equilibrium with NaCl 10 mM concentrated solutions (continuous lines) and with NaCl 50 mM concentrated solutions (dotted lines).

By observing the graphs reported in Figures 3.12 and 3.13, an appreciable volumetric strain, induced by the chemical effects of the salt solution substitution (i.e. from NaCl 10 mM to NaCl 50 mM), at a constant vertical stress of 98.1 kPa, is evident in both the tests. This result is in accordance with Gouy-Chapman double-layer theory: in fact an increase in the salt solution concentration causes a decrease in the double-layer thickness of clay particles, thus a consequently microstructure variation (i.e. compression) of sodium bentonite.

Conversely, the new substitution of the equilibrium solution (i.e. from NaCl 50 mM to NaCl 10 mM) of specimen SQ_NaB_3, did not produce a considerable expansive volumetric strain, at a constant vertical stress of 392.3 kPa, but a remarkable expansion upon unloading: in fact, by considering the specimen height in point B represented in Figure 3.12(a), bentonite sample was able to recover 90.91% of the volumetric strain induced in the 2nd and 3rd loading-unloading cycles. Thus, the coupling of reduction of the pore solution concentration and decrease of the stress unloading produced an increase in bentonite lamellae repulsion with subsequent

microstructure variation. It follows that, everything else being equal, the sample expansion induced by stress unloading can be negligible or very remarkable by considering the concentration of the pore solution in equilibrium with the material.

3.7.2 **Effect of salt solution on swelling behaviour of bentonite**

The effect of the concentration of equilibrium sodium chloride solutions was evaluated through nine swelling tests on squeezed oven-dried sodium bentonite specimens under oedometric conditions. Experimental results of such tests are reported in paragraph 1.4. In the present paragraph, on the basis of the proposed theoretical approach described above, a simple evaluation of effective stresses and swelling pressures acting on sodium bentonite specimens has been carried out, by using Eqs. (3.3) and (3.4).

A preliminary assumption on specimen SQ_NaB_HS1 was considered: since its final void ratio (i.e. 5.70) resulted to be higher than 5, in this case it may be assumed that there are no contacts between the solid particles, therefore the effective stresses can be considered null. Then, from Eq. (3.3) it follows that the swelling pressure is equal to the apparent effective stress (i.e. 12.3 kPa). On the basis of such hypothesis, it is possible to derive the moles of solid skeleton electric charge per volume of solid, $\overline{c}_{sk,0}$ through the following expression:

$$\overline{c}_{sk,0} = 2ec_s\sqrt{\left(\frac{u_{sw}}{2RTc_s}+1\right)^2-1} \tag{3.6}$$

A value of $\overline{c}_{sk,0}$ = 85 mM, associated to the void ratio which specimen SQ_NaB_HS1 reached under oedometric conditions, under an apparent effective stress of 12.3 kPa, in equilibrium with a 0.01 M concentrated NaCl solution, was obtained. It is interesting to observe that such a value of $\overline{c}_{sk,0}$ is similar to the previous results which were obtained for specimens submitted to the conventional oedometer tests and to the swelling pressure tests described above.

Even if $\overline{c}_{sk,0}$ can assume different values as a function of void ratio and, in particular, of salt concentration, due to the bentonite fabric changes, for the other eight specimens a constant value of $\overline{c}_{sk,0}$ = 85 mM was considered in order to derive swelling pressure values by means of Eq. (3.4): these data are resumed, together with the effective stresses obtained through Eq. (3.3), in Table 3.4; the theoretical trends of swelling pressure of bentonite are plotted as a function of void ratio in Figure 3.14. Effective stress values were interpolated by three different linear regression lines (see Figure 3.15), since three different NaCl equilibrium solutions were adopted.

Table 3.4 Initial and final physical properties of oven-dried squeezed sodium bentonite specimens submitted to swelling tests, under oedometric conditions, in equilibrium with different NaCl solutions

SPECIMEN	**σ_v (kPa)**	**c_s (mM)**	**e_0 (-)**	**e_f (-)**	**$\overline{c}_{sk,0}$ (mM)**	**u_{sw} (kPa)**	**σ'_v (kPa)**
SQ_NaB_HS1	**12.3**	10	1.59	5.70	85	12.3	0
SQ_NaB_HS2		50	1.61	4.09	85	5.3	7.0
SQ_NaB_HS3		250	1.58	2.98	85	2.0	10.3
SQ_NaB_HS4	**24.5**	10	1.58	4.39	85	19.5	5.0
SQ_NaB_HS5		50	1.61	3.63	85	6.7	18.8
SQ_NaB_HS6		250	1.57	2.64	85	2.6	21.9
SQ_NaB_HS7	**49.0**	10	1.60	3.45	85	29.1	19.9
SQ_NaB_HS8		50	1.60	2.83	85	11.0	38.0
SQ_NaB_HS9		250	1.58	2.31	85	3.4	45.6

As expected, swelling pressure tends to decrease, and, as a consequence, effective stress to increase, when the concentration of the NaCl equilibrium solution and an void ratio increase. This aspects follow from the microscopic phenomena which

occur in the bentonite microstructure: in accordance with the Gouy-Chapman DDL theory, swelling behaviour is inhibited as the concentration of salt solution increases, since thinner double layers surrounding clay particles have formed.

By considering both the theoretical expressions for swelling pressure and the linear regressions for effective stress, it is possible to obtain three trends of total vertical stresses as a function of void ratio, for different concentrations of NaCl equilibrium solution, as represented in Figure 3.16.

Actually, for each swelling test, the moles of solid skeleton electric charge per volume of solid, $\overline{c}_{sk,0}$ is lower or equal to 85 mM (i.e. the maximum void ratio which sodium bentonite may reach in equilibrium with a NaCl 10 mM concentrated solution). It follows that, in the other 8 cases, swelling pressure values result to be lower or equal to the swelling pressure analytically found. In such a way, the effective stresses acting between sodium bentonite lamellae are higher or equal to the values which were obtained on the basis of the analysis described above.

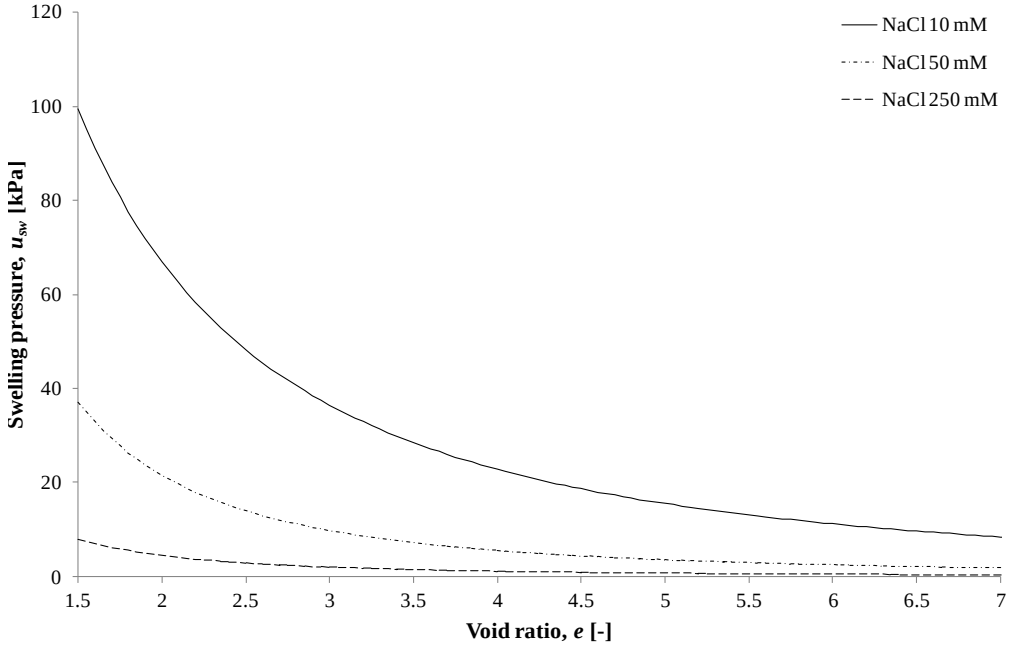

Figure 3.14 Theoretical trends of swelling pressure as a function of void ratio, for different concentrations of NaCl equilibrium solution, obtained for $\overline{c}_{sk,0}$ = 85 mM in Eq. (3.4)

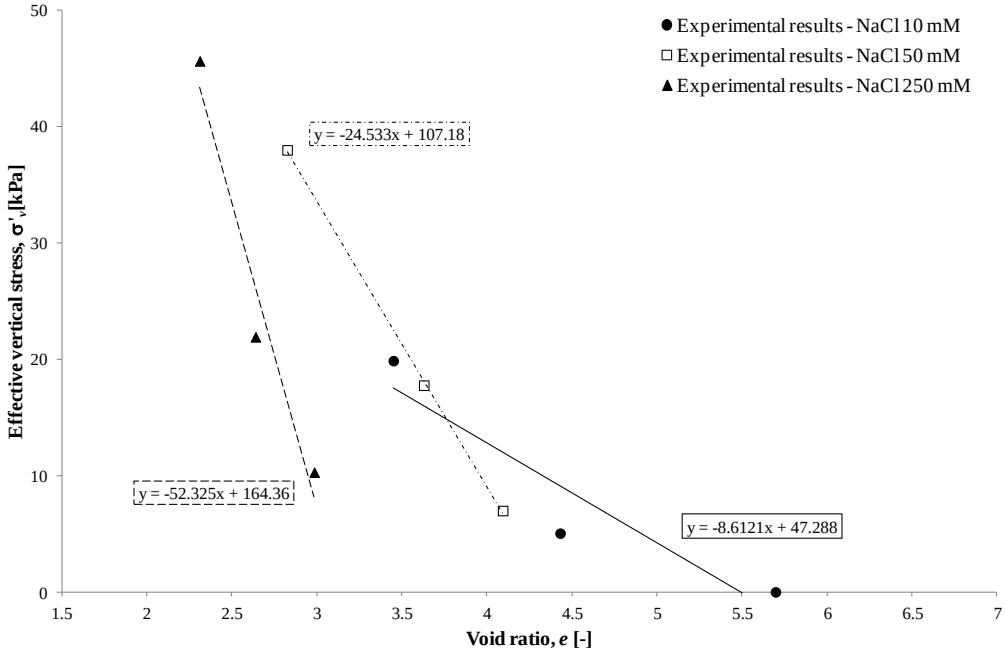

Figure 3.15 Effective vertical stress as a function of void ratio for different concentrations of NaCl equilibrium solution

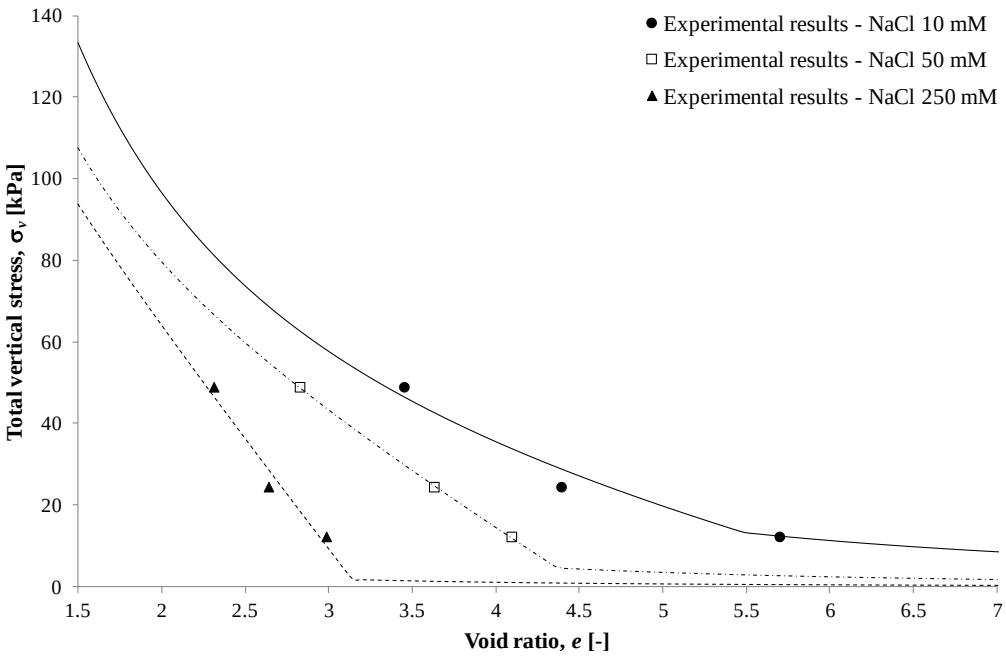

Figure 3.16 Total vertical stress as a function of void ratio for different concentrations of NaCl equilibrium solution

In Figure 3.17 swelling pressure values over total vertical stress values were plotted as a function of the final void ratio reached by each bentonite specimen: three different trends were obtained referred to the different molar concentrations of the equilibrium NaCl solutions. It is interesting to note that, for the same concentration, swelling pressure increases, referred to total vertical stress, as void ratio increases.

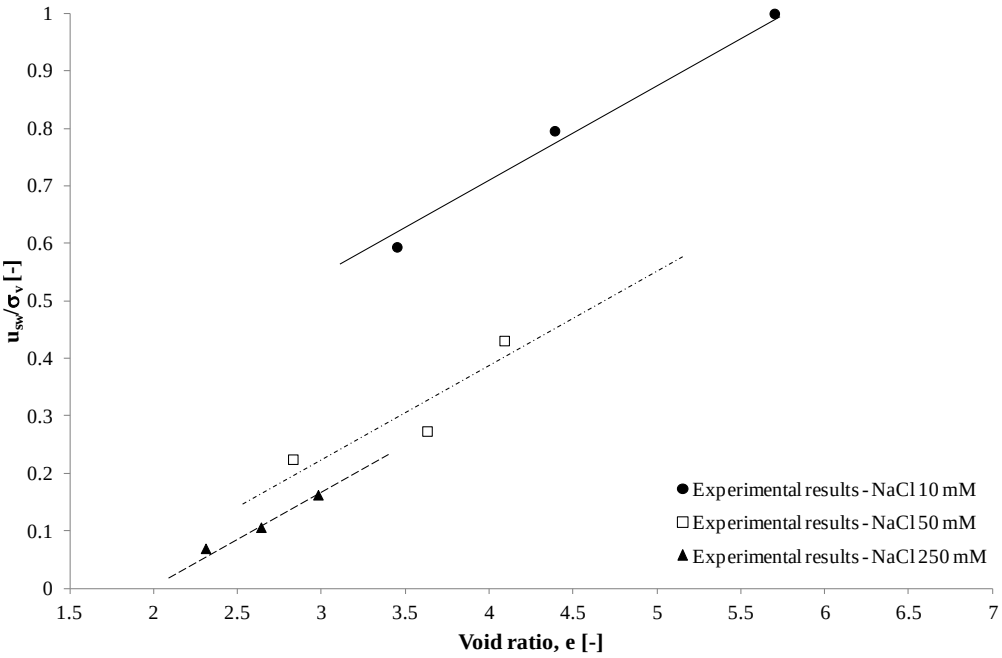

Figure 3.17 Swelling pressure over total vertical stress as a function of void ratio for different concentrations of NaCl equilibrium solution

4. CHEMICO-OSMOTIC BEHAVIOUR OF BENTONITES

This chapter reports the contents of the SUBMITTED Paper:

Boffa, G., Dominijanni, A., Manassero, M., Marangon, M., Zaninetta, L. (2016). Influence of specimen porosity and of sodium chloride pore solution concentration on chemico-osmotic behaviour of sodium bentonites. *Soils and Foundations*.

In the last paragraph, some other experimental results of a multiple stage chemico-osmotic test, performed in a new testing device, are presented.

Influence of specimen porosity and sodium chloride pore solution concentration on chemico-osmotic behaviour of sodium bentonites

Giacomo Boffa[a] (corresponding author), Andrea Dominijanni[b], Mario Manassero[c], Manuel Marangon[d], Luciano Zaninetta[e]

[a] Ph.D. Candidate, Politecnico di Torino, c.so Duca degli Abruzzi 24, 10129 - Torino, Italy, tel. number +390110907705, fax number +390110904899, e-mail address giacomo.boffa@polito.it

[b] Research Fellow, Politecnico di Torino, c.so Duca degli Abruzzi 24, 10129 - Torino, Italy, tel. number +390110907705, fax number +390110904899, e-mail address andrea.dominijanni@polito.it

[c] Professor, Politecnico di Torino, c.so Duca degli Abruzzi 24, 10129 - Torino, Italy, tel. number +390110904820, fax number +390110904899, e-mail address mario.manassero@polito.it

[d] Engineer, Syndial S.p.A. (ENI Group), Piazza Marcello Boldrini 1, 20097 - San Donato Milanese, MI, Italy, e-mail address Manuel.Marangon@syndial.it

[e] Engineer, Syndial S.p.A. (ENI Group), Piazza Marcello Boldrini 1, 20097 - San Donato Milanese, MI, Italy, e-mail address Luciano.Zaninetta@syndial.it

Keywords: sodium bentonites; chemico-osmotic tests; osmotic behaviour; clay microstructure; interpretative model

Abstract

Membrane behaviour represents a potential benefit in engineered clay-based barriers for geoenvironmental applications, especially if such barriers are comprised of sodium bentonite, a particular clay soil with a high content of montmorillonite, a smectitic mineral characterized by a high specific surface and a permanent negative electric charge. As a result of these characteristics, the electric interaction between montmorillonite particles and the ions in pore solution determines macroscopic phenomena which need to be supported by adequate theoretical modelling of transport properties. In the present paper, the effects of porosity on two natural sodium bentonite specimens submitted to multiple-stage chemico-osmotic tests were investigated. The chemico-osmotic reflection coefficient of specimens decreases and the osmotic effective diffusion coefficient increases with increasing porosity and increasing NaCl concentration. The experimental results were compared to literature data and interpreted on the basis of the proposed theoretical approach, under the hypothesis that the microscopic deviations of the state variables from their average values are negligible.

4.1 Introduction

Membrane behaviour in bentonite-based containment barriers consists in a coupled phenomen which results in solute restriction and chemico-osmosis; such a behaviour is particularly significant in engineered barriers, comprised of wholly or partly of sodium bentonite (e.g. Geosynthetic Clay Liners (GCLs), and Compacted Clay Liners (CCLs)) (Shackelford et al., 2003; Tang et al., 2014). GCLs consist of a thin layer of dry bentonite added to a layer or layers of geosynthetics, which can be either geotextiles or geomembranes (Bouazza, 2002), and in the last decades have been widely used in order to contain solid wastes and liquids (e.g. landfills, hydraulic and contaminant barriers) and, thus, to minimize the migration of contaminants into the surrounding environment.

The potential existence of membrane behaviour represents a beneficial aspect for geoenvironmental applications, since the containment function of engineered barriers can be significantly improved in the presence of such a behaviour. In this regard the evaluation of transport properties of bentonites under different boundary conditions have been the subject of significant theoretical and experimental research (Kemper and Rollins, 1966; Fritz, 1986; Shackelford and Daniel, 1991; Keijzer et al., 1999; Malusis, 2001; Malusis et al., 2001; Malusis and Shackelford, 2002a,b; Van Impe, 2002; Malusis et al., 2003; Manassero and Dominijanni, 2003; Shackelford et al., 2003; Shackelford and Lee, 2003; Dominijanni, 2005; Yeo et al., 2005; Dominijanni et al., 2006; Katsumi et al., 2008; Kang and Shackelford, 2009, 2010, 2011; Di Emidio, 2010; Dominijanni and Manassero, 2012a,b; Bohnhoff and Shackelford, 2013; Dominijanni et al., 2013; Malusis et al., 2012, 2013; Puma, 2013; Shackelford, 2013; Malusis and Daniyarov, 2014; Manassero et al., 2014; Meier et al., 2014; Tang et al., 2014).

Sodium bentonite is a clay soil which usually contains at least 70% of montmorillonite, a smectitic three layered (2:1) clay mineral consisting of an alumina octahedral sheet sandwiched between two silica tetrahedral sheets. The unit layer of montmorillonite has, on the faces, a permament negative lattice charge which derives from isomorphous substitutions of divalent cations (e.g. Mg^{2+} and Fe^{2+}) for trivalent aluminium (Al^{3+}) in the octahedral sheet and trivalent aluminium (Al^{3+}) for tetravalent silicon (Si^{4+}) in the tetrahedral sheet. The Cation Exchange Capacity (*CEC*, expressed in milliequivalents per 100 g of dry soil) measures the quantity of exchangeable cations which are preferentially adsorbed on the layer surfaces and neutralize their negative charge.

Montmorillonite crystals consist of parallel-aligned elementary alumino-silicate lamellae, which are approximately 10 Å thick and 1000-2000 Å wide, and this results in a very high specific surface ($\approx$ 760 m^2/g) (Dominijanni and Manassero, 2012a). It has been shown that bentonite may have a dispersed structure characterised by separated lamellae with high specific surfaces, or an aggregated structure which consists of packets of particles, the so-called tactoids, within which several lamellae are in a parallel array (Norrish, 1954); in the latter case, the specific

surface of tactoids depends on the number of lamellae per tactoid and is lower than specific surface of the dispersed structure.

The exchangeable cations are present at a certain distance from the surface of montmorillonite lamellae, which increases with decreasing valence of cations. Cations are attracted to the negatively charged surface through an electrical force, but they tend to diffuse away from this space with a high ion concentration as a consequence of their thermal energy: the balance of Coulomb electrical attraction and thermal diffusion leads to a diffuse double layer (DDL) of cations, with the concentration highest at the surface and gradually decreasing with distance from the surface (Yong and Warkentin, 1975). The Gouy-Chapman theory (Gouy, 1910; Chapman, 1913) is considered as the most successful for the description of the DDL. The interaction of DDLs of adjacent particles leads to chemico-osmotic behaviour of sodium bentonites: in fact restricted movement of ions in solution through the pores of bentonite is attributed to electrostatic repulsion of the ions by electric fields associated with the DDLs of adjacent bentonite particles (e.g. Fritz, 1986).

The electric interaction between montmorillonite particles and the ions in pore solution determines macroscopic phenomena which cannot be modelled on the basis of the classical theories of Soil Mechanics used to describe the movement of water and solutes through porous media (Mitchell, 1993). For instance, if a bentonite layer is interposed between two electrolyte solutions with different salt concentrations, a volumetric flux of water can be observed, even under a condition of null hydraulic gradient (i.e. membrane behaviour). The evaluation of bentonite performances requires an adequate theoretical approach which is able to model the simultaneous migration of water and solutes (Dominijanni and Manassero, 2012a,b).

Chemico-osmosis represents the movement of water from lower solute concentration to higher solute concentrations. Restricted passage of anions and cations occurs when the pore sizes of the porous medium (i.e. sodium bentonite) are sufficiently small such that electrostatic repulsion of the ions results from the interaction of electric fields associated with adjacent bentonite particles (e.g. Fritz, 1986). In this case, the overlapping negative electrical potentials resulting from the predominantly negative charges of the particle surfaces prevent anions from entering the pore, and

the cations within the electrolyte solution are similarly restricted from migration due to the requirement for electroneutrality in solution (Shackelford, 2011).

Membrane behaviour is quantified in terms of an efficiency coefficient representing the relative degree of solute restriction. In the science literature, this efficiency coefficient commonly is designated by the symbol, σ, and referred to as the "reflection coefficient". However, the symbol σ in the engineering literature typically is used to represent stress or electrical conductance (e.g., Mitchel and Soga, 2005). As a result, the symbol ω typically is preferred in the engineering literature to represent the "membrane efficiency coefficient". Since membrane behaviour also results in chemico-osmosis, ω often is referred to as the "chemico-osmotic efficiency coefficient", (Shackelford, 2011). In general, the value of ω ranges from zero ($\omega = 0$) in the case of absence of membrane behaviour, to unity ($\omega = 1$) in the case of an "ideal" membrane where all migrating solutes are restricted. The membrane efficiencies of natural bentonites that exhibit membrane behaviour generally range between zero and 100 percent (i.e., $0 < \omega < 1$), and such soils are referred to as "nonideal" or "semipermeable" membranes.

Membrane behaviour has been measured using both open (e.g. Kemper and Rollins, 1966) and closed (e.g. Malusis et al., 2001) hydraulic control systems (Shackelford & Lee, 2003; Shackelford, 2013). Control of the boundary conditions in open systems is far more difficult than control of boundary conditions in closed systems (Malusis et al., 2012). It is important to note that in membrane testing involving closed systems, liquid flow through the test specimen is prevented from occurring (e.g. Malusis et al., 2001; Malusis and Shackelford, 2002a,b; Yeo et al., 2005; Tang et al., 2014). As a consequence, a chemico-osmotic pressure difference develops across the specimen to counteract the tendency for chemico-osmotic flow, and the membrane efficiency is determined based on the measured magnitude of the pressure buildup and the salt concentrations at the boundaries (Kang and Shackelford, 2009).

Either rigid-wall (e.g. Malusis et al., 2001) or flexible-wall (e.g. Kang and Shackelford, 2009) cells can be used to measure membrane behaviour, although the vast majority of membrane testing has involved the use of rigid-wall cells, whereby

the volume of the specimen is maintained constant (Shackelford, 2013). The advantages of a flexible-wall cell include complete control over the state of stress existing within the test specimen and the ability to back-pressure, saturate and consolidate the specimen prior to membrane testing (Kang and Shackelford, 2009). In a closed system, membrane testing can start once chemical (source) solutions containing the same solute or solutes are circulated across both the top and bottom boundaries. The circulation rates are controlled to be the same via a flow-pump hydraulic system, and both the top and bottom circulation systems are closed loops, such that there is no volume change in either circulation system during circulation (Shackelford, 2013).

In general, semipermeable membrane behaviour in compressible clays, such as bentonites, is known to increase with decrease in the void ratio (i.e. porosity) of the material (Shackelford et al., 2003), with increase in content of high activity clay minerals, (i.e. smectitic minerals, in particular montmorillonite), with decrease in the concentration and/or valence of the principal cations in the pore water of the soil, and with decrease in bentonite hydraulic conductivity. It is important to note that the lower the valence of the exchangeable cations and the higher the specific surface of bentonite particles, the higher is bentonite membrane behaviour: monovalent exchangeable cations such as sodium determine a more appreciable semipermeable membrane behaviour than divalent calcium ions. Moreover, membrane behaviour can be enhanced with increasing consolidation effective stress (Kang and Shackelford, 2011).

In the present paper, the effects of the porosity of natural sodium bentonite specimens and different concentrations at the top boundary of the specimens on the membrane behaviour were investigated through multiple-stage chemico-osmotic tests, according to the procedure proposed by Malusis et al. (2001). Transport properties were measured for 2 different porosity values of specimens, and compared to experimental results which were found by Dominijanni et al. (2013) on the same material at a different porosity. All the results have been interpreted on the basis of the model proposed by Dominijanni and Manassero (2012b), with the aim of defining a simplified picture of the microstructure of the tested bentonite.

4.2 **Theoretical background**

The negative electric charge, per unit solid volume, of montmorillonite lamellae can be expressed as $F\cdot \bar{c}_{sk,0}$, where F is Faraday's constant (96,485 $\mathrm{C}\cdot\mathrm{mol}^{-1}$) and $\bar{c}_{sk,0}$ is the molar concentration per unit solid volume of the solid skeleton electric charge, which is assumed to have unit valence (i.e. z_{sk} = -1). Dominijanni and Manassero (2012b) have shown that $\bar{c}_{sk,0}$ is proportional to the effective specific surface of the solid particles, and decreases when the montmorillonite lamellae tend to aggregate to form the so-called tactoids, through the following expression:

$$\bar{c}_{sk,0} = \frac{(1 - f_{Stern})\sigma}{F}\rho_{sk} S' \qquad (4.1)$$

where F = Faraday's constant, σ is the surface charge of the single lamella (0.114 C m^{-2}), $f_{Stern} = \frac{\sigma_{Stern}}{\sigma}$ is the fraction of electric charge compensated by the cations specifically adsorbed in the Stern layer (typically ranging from 0.80 to 0.90 in the case for Na^+ ions), ρ_{sk} is the solid density of bentonite (assumed to be equal to 2.65 g cm^{-3}), and S' is the external specific surface of the tactoid, which corresponds to the total specific surface, S, of the single platelet (760 m^2 g^{-1}) over the number of lamellae per tactoid, N_l. $\bar{c}_{sk,0}$ is the only new macroscopic material parameter introduced into the model proposed by Dominijanni and Manassero (2012b), in order to account for the electro-chemical phenomena related to the microscopic surface forces.

The formation of tactoids reduces the surface area of the montmorillonite, which then behaves as a much larger particle with the diffuse double layer only fully manifesting itself on the outside surfaces of the tactoids (Dominijanni and Manassero, 2012b).

If the pore solution contains a single salt that is completely dissociated with the following stoichiometric reaction:

$$(\text{Cation})_{z_1}^{\nu_1}(\text{Anion})_{z_2}^{\nu_2} \rightarrow \nu_1(\text{Cation})^{z_1} + \nu_2(\text{Anion})^{z_2}$$

where z_1 and z_2 are the electrochemical valences of the cation and the anion, and ν_1 and ν_2 are the stoichiometric coefficients of the cation and the anion, respectively, the following condition has to be satisfied in order to preserve electroneutrality within a saturated porous medium (i.e. sodium bentonite), even in the presence of the solid skeleton electric charge:

$$z_1\overline{c}_1 + z_2\overline{c}_2 = \frac{\overline{c}_{sk,0}}{e} \tag{4.2}$$

where $\overline{c}_1$ and $\overline{c}_2$ are the molar concentrations of the cation and the anion, respectively, and e is the void ratio.

As a consequence, the solid skeleton electric charge influences the distribution of the ions contained in the pore solution. This phenomenon is known as the ion-partition effect and is expected to be more relevant for porous media characterized by higher solid skeleton charge concentrations as sodium bentonites (Dominijanni et al., 2013).

When an electrically charged porous medium is placed in contact with an external bulk solution which contains the same ions that are present in the pore solution, a thermodynamic equilibrium condition is reached, after a certain period of time, in which the water chemical potential and the ion electrochemical potentials between the two solutions are equal.

The equilibrium condition can be characterized by the following state variables of the external bulk solution: the absolute temperature, T, the hydraulic pressure (referenced to the atmospheric pressure, as is usual in soil mechanics), u, and the salt concentration, c_s. The state variables in the external bulk solution can be measured easily, whereas it is very difficult to determine the corresponding variables in the pore solution. The approximation by Donnan (1911), which neglects the microscopic deviations of the ion concentrations from their average values, that are induced by the electric potential distribution within the pores, can be considered acceptable (Dominijanni et al., 2013).

If a bentonite layer is interposed between two reservoirs with different hydraulic pressures or ion concentrations, a pore solution volumetric flux, q, and an ion mass flux, J_i, relative to the solid skeleton, are generated. The following flux equations can be derived from linear momentum balance equations of the fluid components, as described in details in Dominijanni et al. (2013):

$$q = -\frac{k}{\gamma_w}\left(\frac{\partial u}{\partial x} - \omega\frac{\partial \Pi}{\partial x}\right) \tag{4.3}$$

$$J_s = (1-\omega)qc_s - nD_\omega^*\frac{\partial c_s}{\partial x} \tag{4.4}$$

where

$$k = \frac{n\cdot\gamma_w}{\alpha\left[1+\dfrac{RT}{\alpha}\dfrac{(\Gamma_1-\Gamma_2)^2\nu_1\nu_2 c_s}{\nu_1\Gamma_2 D_2+\nu_2\Gamma_1 D_1}\right]} = \text{hydraulic conductivity;} \tag{4.5}$$

$$\omega = 1-\frac{\nu_1 D_2+\nu_2 D_1}{\nu_1\Gamma_2 D_2+\nu_2\Gamma_1 D_1}\Gamma_1\Gamma_2 = \text{reflection coefficient;} \tag{4.6}$$

$$J_s = \frac{J_1}{\nu_1} = \frac{J_2}{\nu_2} = \text{salt molar flux;} \tag{4.7}$$

$$D_\omega^* = (1-\omega)\cdot D_s = \text{osmotic effective diffusion coefficient;} \tag{4.8}$$

$$D_s = \frac{(\nu_1+\nu_2)D_1D_2}{\nu_1 D_2+\nu_2 D_1} = \text{macroscopic salt diffusion coefficient;} \tag{4.9}$$

$$\Gamma_2 = -\frac{\bar{c}_{sk,0}}{2\cdot e\cdot c_s}+\sqrt{\left(\frac{\bar{c}_{sk,0}}{2\cdot e\cdot c_s}\right)^2+1}$$

$$\Gamma_1 = \Gamma_2^{-1} = \frac{\bar{c}_{sk,0}}{2\cdot e\cdot c_s}+\sqrt{\left(\frac{\bar{c}_{sk,0}}{2\cdot e\cdot c_s}\right)^2+1} \quad = \text{partition factors;} \tag{4.10}$$

c_s = salt concentration of the external solution;

α = friction coefficient (Dominijanni et al., 2013);

n = soil porosity.

Eqs. (4.10) are valid in the case of both unitary ion electrochemical valences, such as for sodium chloride.

Under the hypothesis that the microscopic deviations of the variables from their average values are assumed to be negligible, the macroscopic ion diffusion coefficients, D_i, result to be equal to the ion effective diffusion coefficients, D_i^* (Dominijanni and Manassero, 2012b):

$$D_i = D_i^* = \tau_m D_{i,0} \qquad \text{i=1,2} \tag{4.11}$$

$$D_s = D_s^* = \frac{(\nu_1 + \nu_2) D_1^* D_2^*}{\nu_1 D_2^* + \nu_2 D_1^*} = \tau_m \frac{(\nu_1 + \nu_2) D_{1,0} D_{2,0}}{\nu_1 D_{2,0} + \nu_2 D_{1,0}} = \tau_m D_{s,0} \tag{4.12}$$

where τ_m is the dimensionless matrix tortuosity factor which accounts for the tortuous nature of the actual diffusive pathway through the porous medium (Malusis and Shackelford, 2002b), $D_{i,0}$ is the free (aqueous) solution diffusion coefficient of the *i-th* ion, D_s^* is the salt effective diffusion coefficient and $D_{s,0}$ is the free solution diffusion coefficient of the salt.

When the solid skeleton electric charge is equal to zero, the ion partition coefficients, Γ_i, are equal to 1 and Eqs. (4.3) and (4.4) reduce to the Darcy equation and the classical advective-diffusion equation, respectively.

The osmotic effective diffusion coefficient, D_ω^*, results to be related to the reflection coefficient, ω, through Eq. (4.8), so that D_ω^* = 0 when ω = 1. As a result, the condition ω = 1 implies a null salt flux through the porous medium, which, in this case, can be said to act as a "perfect" or "ideal" barrier.

If Eq. (4.8) is compared with the expression of D_ω^* proposed by Malusis and Shackelford (2002b) and Malusis et al. (2012):

$$D_\omega^* = \tau_r D_s^* \tag{4.13}$$

where τ_r is the restrictive tortuosity factor, which, as a consequence, results to be given by:

$$\tau_r = (1-\omega)\frac{D_s}{D_s^*}. \tag{4.14}$$

Moreover, under the hypotheses implied by Eq. (4.12), the expression of τ_r reduces to:

$$\tau_r = (1-\omega). \tag{4.15}$$

In laboratory, the coefficient *k* can be measured, under steady state conditions, using traditional permeameters, while ω and D_ω^* can be determined through the chemico-osmotic testing device developed by Malusis et al. (2001). This apparatus is able to impose the condition of no-volumetric flux (q = 0) through a soil sample in contact with two external solutions, maintained at constant salt concentrations, so that the global or averaged values of the coefficients can be measured. The global values of ω and D_ω^* are defined as follows (Auclair et al., 2002):

$$\omega_g = \frac{1}{\Delta c_s}\int_{c_b}^{c_t} \omega \cdot dc_s \tag{4.16}$$

$$D_{\omega g}^* = \frac{1}{\Delta c_s}\int_{c_b}^{c_t} D_\omega^* \cdot dc_s \tag{4.17}$$

where c_t and c_b represent the salt concentration at the top and the bottom boundaries of the bentonite sample, respectively, and $\Delta c_t = c_t - c_b$ is their difference. These coefficients can be determined by means of the following relations under steady state conditions:

$$\omega_g = \left(\frac{\Delta u}{\Delta \Pi} \right)_{q=0} \tag{4.18}$$

$$D^*_{\omega g} = \frac{L}{n} \left(\frac{J_s}{\Delta c_s} \right)_{q=0} \tag{4.19}$$

where $\Delta u = u_t - u_b$ and $\Delta \Pi = \Pi_t - \Pi_b$ represent the differences between the hydraulic pressure and the osmotic pressure at the boundaries of the bentonite sample, n is the sample porosity, and L is the sample thickness.

It is interesting to note that the relationship between D^*_ω and ω is also maintained between their corresponding global values: in fact, inserting Eq. (4.12) into Eq. (4.17) with $D_s = D^*_s$ leads to:

$$D^*_{\omega g} = (1 - \omega_g) \cdot D^*_s = (1 - \omega_g) \cdot \tau_m \cdot D_{s,0} \,. \tag{4.20}$$

In the case of a salt constituted by monovalent ions, inserting Eq. (4.6) into Eq. (4.16) and using Eqs. (4.10), the following expression of ω_g is obtained (Dominijanni and Manassero, 2012b):

$$\omega_g = 1 + \frac{\bar{c}_{sk,0}}{2 \cdot \Delta c_s \cdot e} \left[Z_2 - Z_1 - (2t_1 - 1) \cdot \ln \left(\frac{Z_2 + 2t_1 - 1}{Z_1 + 2t_1 - 1} \right) \right] \tag{4.21}$$

where

$$t_1 = \frac{D_{1,0}}{D_{1,0} + D_{2,0}} \text{ = cation transport number,} \tag{4.22}$$

$$Z_1 = \sqrt{1 + \left(\frac{2 \cdot c_t \cdot e}{\bar{c}_{sk,0}} \right)^2} \,, \tag{4.23}$$

$$Z_2 = \sqrt{1 + \left(\frac{2 \cdot c_b \cdot e}{\bar{c}_{sk,0}} \right)^2} \quad . \tag{4.24}$$

Further details on the theoretical background can be found in Dominijanni and Manassero (2012a,b) and in Dominijanni et al. (2013).

4.3 Materials and methods

4.3.1 Materials

The same Indian sodium bentonite tested by Dominijanni et al. (2013) was used for chemico-osmotic tests. Through the methylene blue adsorption method a cation exchange capacity of 105 meq/100 g was measured. The mineralogical composition of the material was evaluated through a X-ray diffraction analysis: the tested sodium bentonite presents primarily smectite, traces of calcite, quartz, mica and gypsum.
The bentonite is characterized by a liquid limit (*LL*) of 525 %, a plastic limit (*PL*) of 63%, and a hydraulic conductivity (k) of $8 \cdot 10^{-12}$ m/s, measured at a 27.5 kPa confining effective stress using de-ionized water as the permeant liquid. The specific gravity, G_s is assumed to be equal to 2.65 (Dominijanni et al., 2006).
The salt solutions were prepared with sodium chloride (ACS reagent, purity ≥ 99%) and de-ionized water (DW), at different molarity values in the range 10.82 - 52.78 mM, in order to evaluate the effect of the monovalent cations (i.e. Na^+) on the chemico-osmotic behaviour of the sodium bentonite at different void ratios. The DW (*pH* = 6.95; EC at 20 °C = 0.2 mS/m) consisted of tap water processed through a series of activated carbon filters, a reverse osmosis process and, finally, a UV lamp (Elix Water Purification system). Moreover, the DW was de-aerated prior to use, in order to limit the presence of air which could affect the experimental results. The electrical conductivity (*EC*) measured at 20 °C for the NaCl solutions ranged from 124.4 mS/m to 557.0 mS/m (see Figure 4.1).

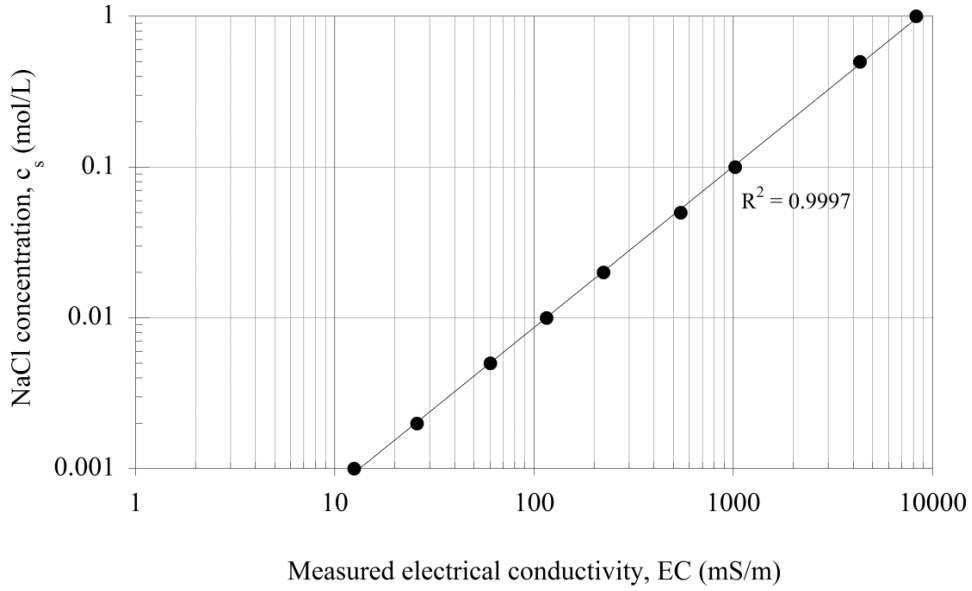

Figure 4.1 Calibration of sodium chloride (NaCl) concentration with electrical conductivity. R^2 is the coefficient of determination of the regression line

4.3.1 **Bentonite specimens preparation**

Prior to the chemico-osmotic testing phase, the sodium bentonite was submitted to the same 'squeezing' procedure described in Dominijanni et al. (2013), in order to remove the soluble salts, which are naturally present inside the powdered material, and, as a consequence, to prevent them from affecting the determination of the chemico-osmotic properties of the sodium bentonite.

In previous studies several authors (Malusis et al., 2001; Malusis and Shackelford, 2002a, 2002b; Shackelford and Lee, 2003; Yeo et al., 2005; Kang and Shackelford, 2009; Di Emidio, 2010; Kang and Shackelford, 2010, 2011) used a different process, called 'flushing' method, in order to remove soluble salts. It consists of an initial permeation phase, performed under back-pressure, which takes a long period of time (i.e. from months to a year), due to the low hydraulic conductivity of bentonite.

The 'squeezing' method, which consists of a series of consecutive phases of powder sodium bentonite hydration with DW, at a higher water content than the *LL*, and drained consolidation, by using a consolidometer, under a maximum load of 500 kPa

(instrumental limit), allows to reduce the salt removal time. During the consolidation phase, the drained solution was sampled daily, with the aim of controlling the *EC* and evaluating the soluble salt concentration in the bentonite pore-water (Figure 4.1). About 500 g of squeezed dry powder bentonite, characterized by an *EC* value lower than 50 mS/m, was produced in 60-70 days, using a 5 l consolidometer. The monitored *EC* results of the squeezing process are reported in Figure 4.2.
After this preliminary phase, the material was oven-dried at 105 °C and pulverized once again.

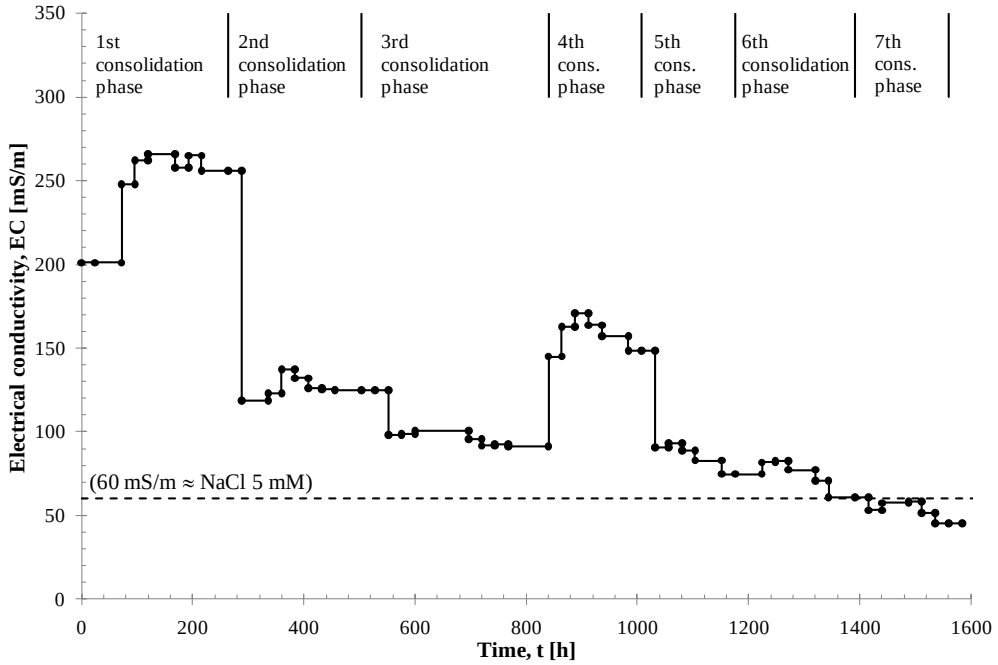

Figure 4.2 Electrical conductivity as a function of time during squeezing process

4.3.2 **Chemico-osmotic testing apparatus and procedures**

The main components of the chemico-osmotic testing device are shown in Figure 4.3 and Figure 4.4, and are the same as those used by Dominijanni et al. (2013) and described in detail in Malusis et al. (2001): they include an osmotic cell, a flow pump accumulator, a differential pressure transducer, which is necessary for

measuring the differential pressure which develops across the specimens during the tests, and a data acquisistion system.

The osmotic cell consists of a modified rigid-wall permeameter, in which the top piston and the bottom pedestal are endowed of three ports each: two enable the different solutions to circulate through the top (NaCl solution) and the bottom (DW) porous stones in order to establish a constant concentration gradient across the specimen. The third port is installed in both the top piston and the bottom pedestal with the aim of allowing for the differential pressure measurement across the specimen.

The flow-pump system consists of a dual-carriage syringe pump and two stainless steel accumulators (Model 33 - Twin syringe pump, produced by Harvard, Holliston, MA); it prevents the volumetric flux through the specimen by simultaneously injecting into and withdrawing from the porous stones the same volume of solution, as the syringes move at the same rate. The circulation rate should be sufficiently rapid to minimize changes in the boundary concentrations due to diffusion, but sufficiently slow to allow measurement of solute mass flux at the lower concentration boundary for evaluating the global osmotic effective diffusion coefficient (Malusis et al., 2001).

The test was carried out according to the procedure proposed by Malusis et al. (2001): a solution containing a known electrolyte concentration (NaCl) was circulated in the top porous stone, while DW was circulated in the bottom porous stone. The concentration difference across the specimen was maintained constant by continuously infusing the two liquids at the boundaries of the specimen.

Since the specimen was preliminary squeezed with DW to remove the soluble salts, the *EC* of the electrolyte solutions in the flux exiting from the porous stones at the steady state was induced solely by the contributions of Cl^- and Na^+ ions (Dominijanni et al., 2013). The *EC* of the withdrawn fluxes (i.e. from the top and bottom porous stones, respectively) was monitored by sampling the solution contained in the pistons, and the NaCl molar concentration was derived using the linear relation reported in Figure 4.1. Since the volumetric flux through the

specimen was hindered, the global reflection coefficient could be calculated using Eq. (4.18) (Groenevelt and Elrick, 1976; Malusis et al., 2001).

The diffusive solute flux through the specimen was calculated for the *n*-th sampling interval as follows

$$J_s^n = \frac{\sum_{m=1}^{n}\left(c_s^m \cdot \Delta V^m\right)}{A_S \cdot \Delta t^n} = \frac{\Delta Q^n}{\Delta t^n} \tag{4.25}$$

where c_s^m is the solute molar concentration measured by sampling the solution exiting from the bottom porous stone, ΔV^m is the volume of the solution circulating in the porous stones in the Δt^m interval, A_S is the cross-section of the specimen and ΔQ^n is the cumulative salt molar mass per unit area that passed through the specimen. The global osmotic effective diffusion coefficient, $D_{\omega g}^*$, is calculated at the steady state as follows:

$$D_{\omega g}^* = \frac{\Delta Q}{\Delta t} \cdot \frac{L}{n \cdot \left(c_{t,avg} - c_{b,avg}\right)} \tag{4.26}$$

where $c_{t,avg}$ and $c_{b,avg}$ are the average top and bottom salt concentrations, respectively.

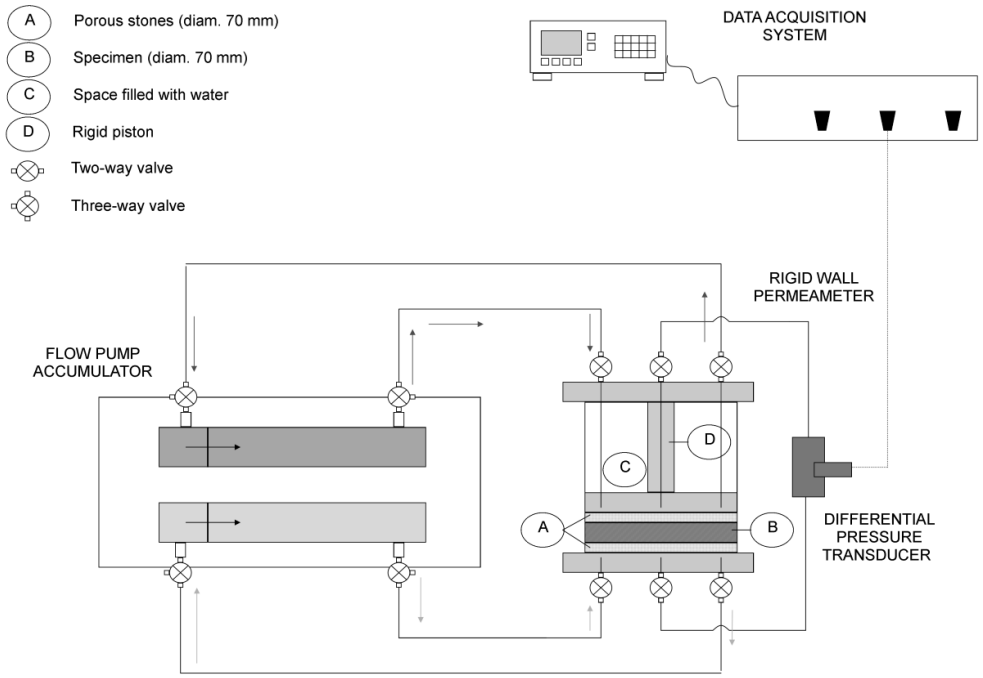

Figure 4.3 Schematic view of chemico-osmotic test apparatus (not to scale)

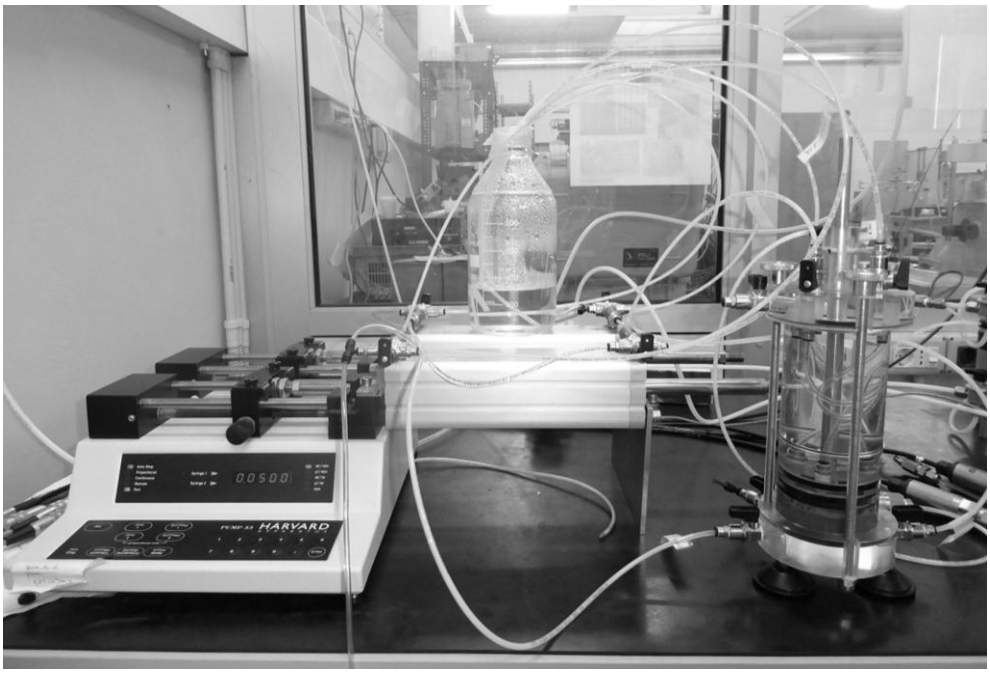

Figure 4.4 Pictorial view of chemico-osmotic test apparatus

4.4 Experimental results

Two oven-dried squeezed sodium bentonite specimens (i.e. SQ_NaB_COT1 and SQ_NaB_COT2) of 70 mm diameter and of 15 mm thickness were used for chemico-osmotic tests. In both cases, the specimens were prepared by prehydrating the squeezed bentonite in DW at a lower water content than the *LL* value, then by installing the slurry inside a drained compaction mould, and, finally, by statically compacting at a fixed porosity, i.e. respectively n = 0.86 (e = 6.26) for specimen SQ_NaB_COT1, and n = 0.91 (e = 10.37) for specimen SQ_NaB_COT2. After this preparation phase, each specimen was transferred to the modified rigid-wall permeameter in order to start the chemico-osmotic test.

After cell assemblage, DW was circulated through the top piston and the bottom pedestal for several days with the aim of establishing a steady baseline differential pressure, before the application of a concentration gradient across the specimen. A source concentration of NaCl then was injected into the top porous stone, while DW was continuously circulated in the bottom porous stone, as in Dominijanni et al. (2013).

Two multiple-stage chemico-osmotic tests were performed by sequential circulation of chemical solutions containing respectively 11.00, 19.77 and 51.22 mM NaCl concentrations for specimen SQ_NaB_COT1, and 10.82, 20.99 and 52.78 mM NaCl concentrations for specimen SQ_NaB_COT2, at a constant flow rate of 0.05 ml/min. The *EC* values of the salt mass fluxes withdrawn from the top and the bottom porous stones, measured during the testing stages, are shown respectively in Figure 4.5 for specimen SQ_NaB_COT1 and in Figure 4.6 for specimen SQ_NaB_COT2. These values depend on the NaCl concentrations imposed at the boundaries of the specimen: the *EC* values progressively increase during the test as the NaCl concentration of the injected solution in the top porous stone rises. The trends of the electrical conductivity of the flux withdrawn from the top porous stone, $EC_{t,exit}$, and the electrical conductivity of the flux withdrawn from the bottom porous stone, $EC_{b,exit}$, both show that a steady state has been reached for each stage.

Moreover, the difference between the *EC* values measured in the flux withdrawn from the top porous stone ($EC_{t,exit}$) and the *EC* values of the solutions injected into

the same stone ($EC_{t,ref}$) is due to the loss in NaCl mass induced by the diffusion through the bentonite from the top to the bottom boundary (Dominijanni et al., 2013).

In Figure 4.7 the experimental global reflection coefficient results, ω_g, are plotted as a function of time.

The ω_g values are determined using Eq. (4.18), on the basis of the differential pressure, Δu, measured during the test with a time step of 10 min, and the osmotic pressure, $\Delta\Pi$, calculated from the average of the top and bottom NaCl concentrations. For both tests, the steady state values of the variables are reported in Table 4.1 and Table 4.2 for each concentration stage. The NaCl concentrations were derived from the measured *EC* through the linear calibration reported in Figure 4.1. The steady state ω_g values tend to decrease as the salt concentration in the top porous stone increases.

The cumulative molar mass per unit area, *Q*, of the NaCl which migrated through the specimen during each stage of the test on specimen SQ_NaB_COT2 is reported in Figure 4.8; for specimen SQ_NaB_COT1 it was not possible to determine it. The values of the global osmotic effective diffusion coefficient, $D^*_{\omega g}$, which have been obtained from the *Q* measurements shown in Figure 4.8, are reported in Table 4.2.

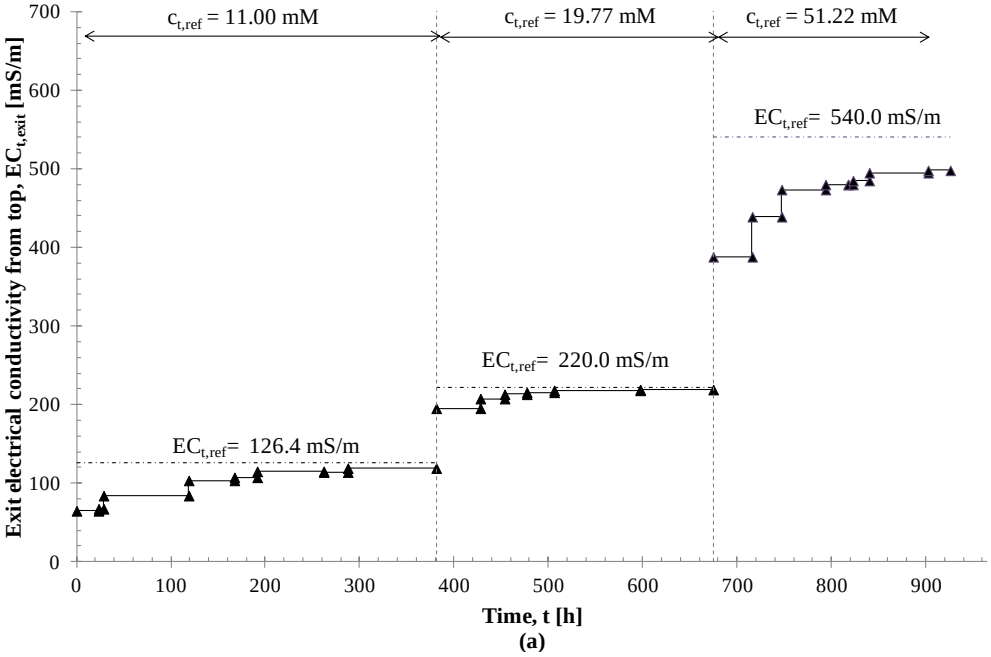

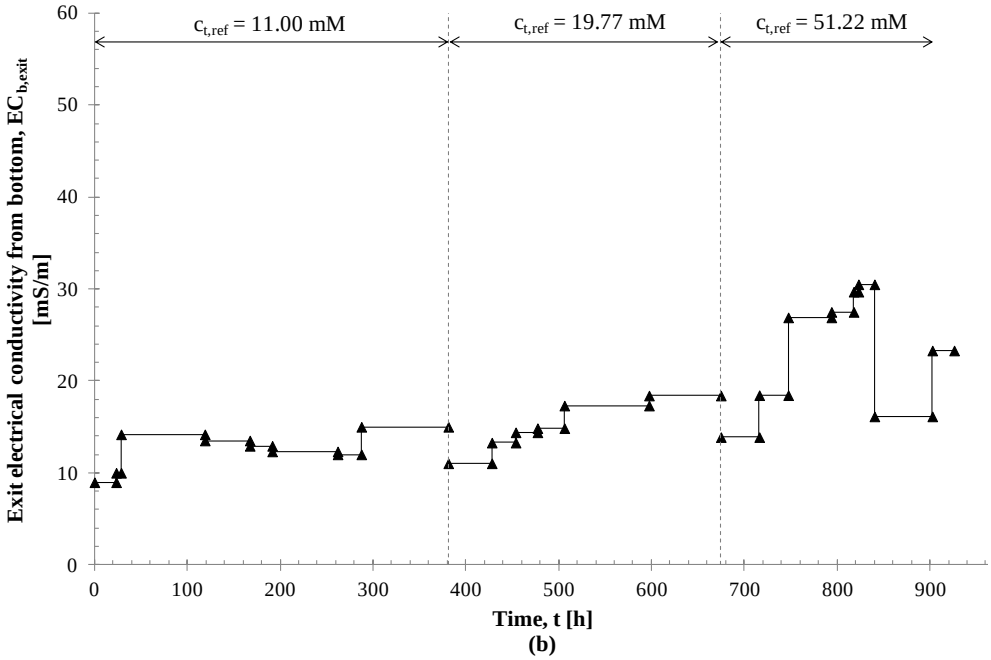

Figure 4.5 Electrical conductivity of salt flux withdrawn from (a) top porous stone and (b) bottom porous stone as a function of time during multiple-stage chemico-osmotic test on specimen SQ_NaB_COT1

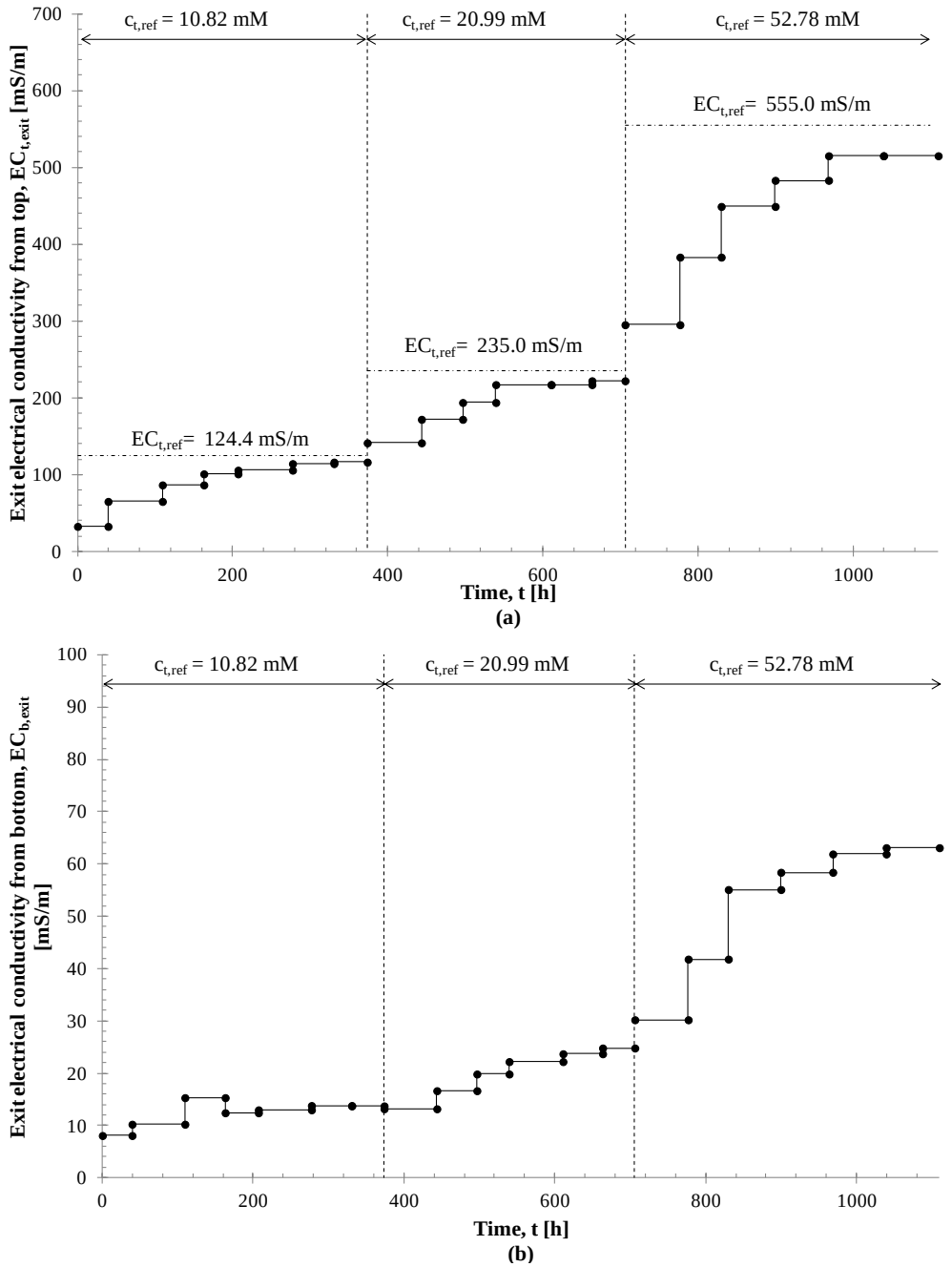

Figure 4.6 Electrical conductivity of salt flux withdrawn from (a) top porous stone and (b) bottom porous stone as a function of time during multiple-stage chemico-osmotic test on specimen SQ_NaB_COT2

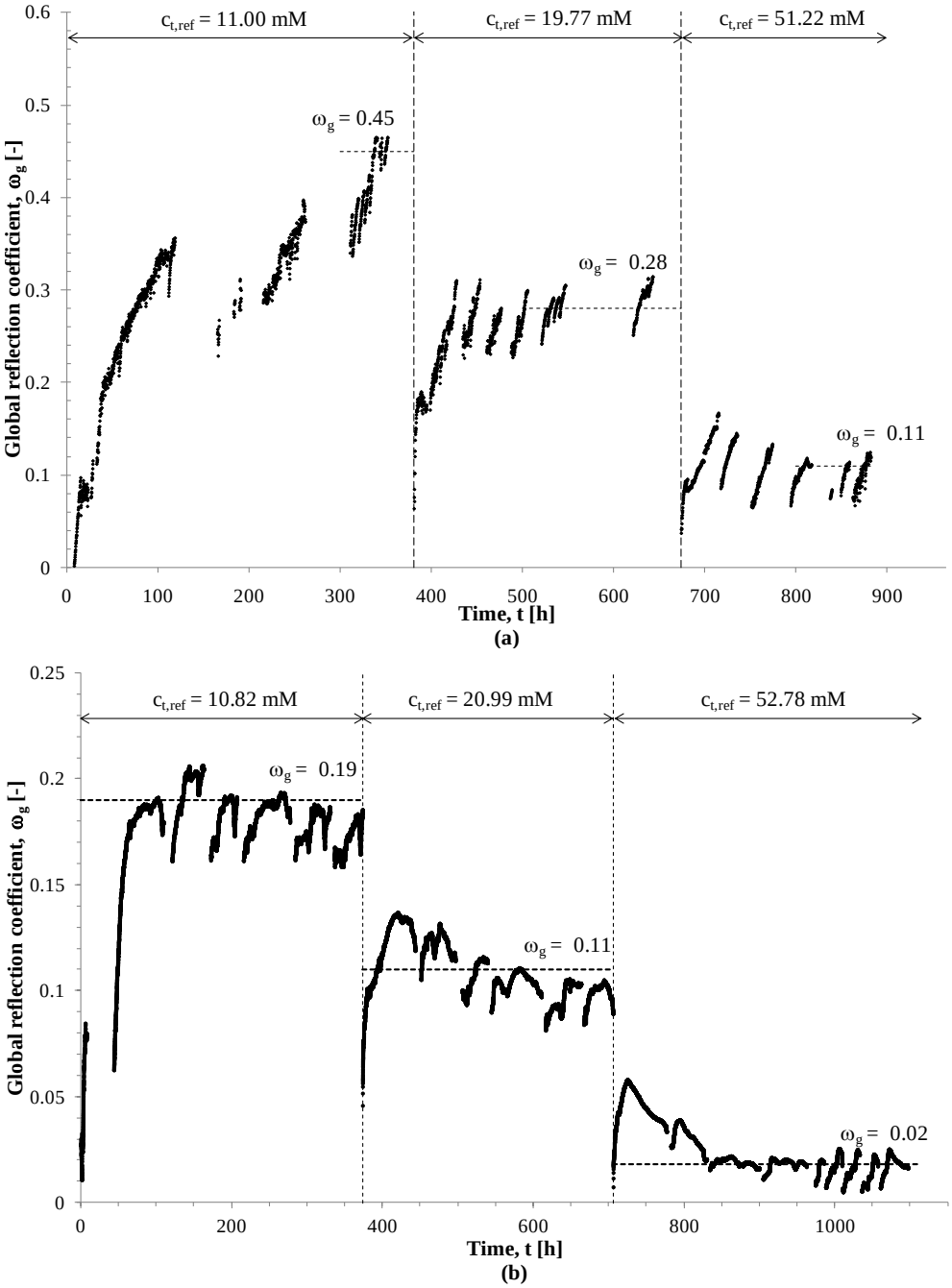

Figure 4.7 Global reflection coefficient as a function of time during multiple-stage chemico-osmotic tests: (a) specimen SQ_NaB_COT1, and (b) specimen SQ_NaB_COT2

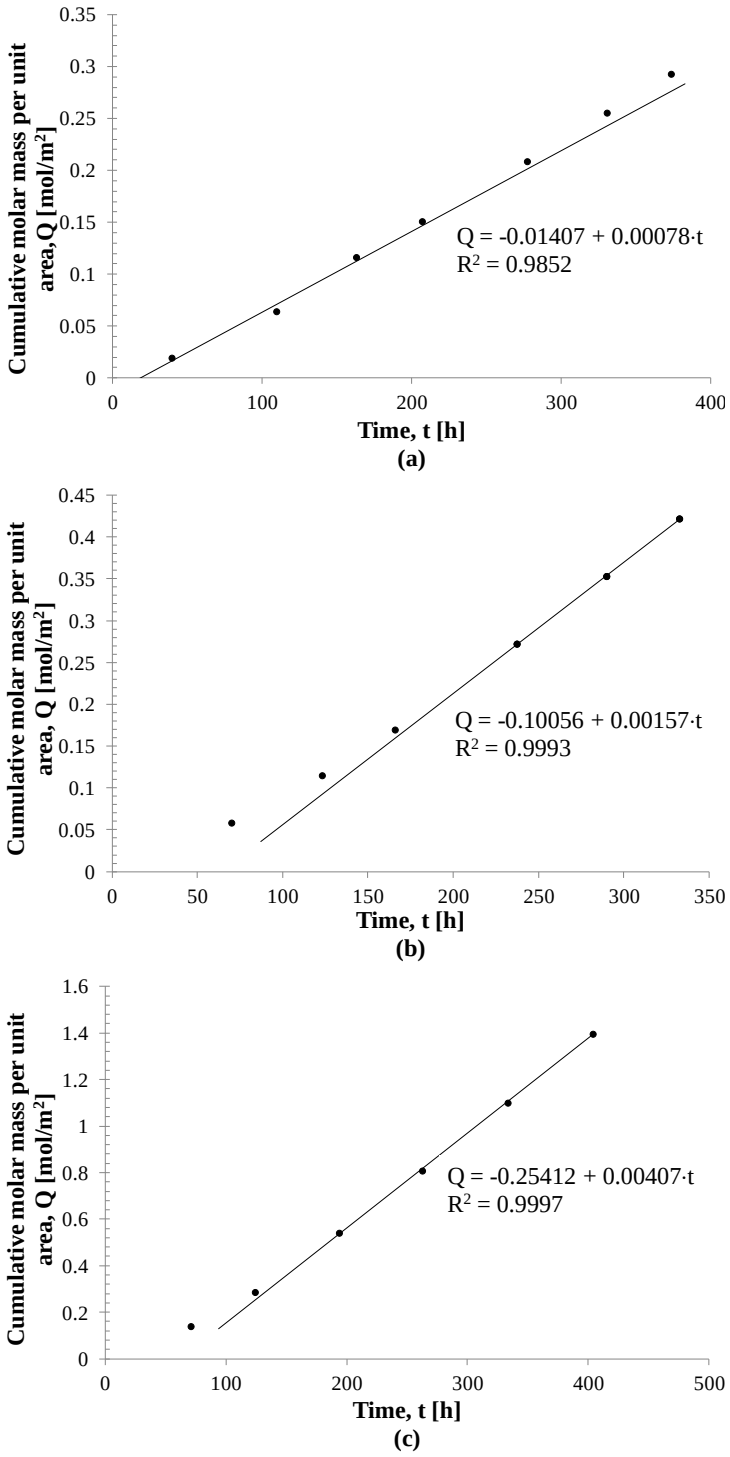

Figure 4.8 Cumulative molar mass of sodium chloride per unit area as a function of time during multiple-stage chemico-osmotic test on specimen SQ_NaB_COT2: (a) $c_{t,ref}$ = 10.82 mM; (b) $c_{t,ref}$ = 20.99 mM; (c) $c_{t,ref}$ = 52.78 mM

Table 4.1 Steady-state values of variables involved in multiple-stage chemico-osmotic tests on specimen SQ_NaB_COT1

$c_{t,ref}$ (mM)	$c_{t,exit}$ (mM)	$c_{b,exit}$ (mM)	$c_{t,avg}$ (mM)	$c_{b,avg}$ (mM)	Δu (kPa)	$\Delta\Pi$ (kPa)	ω_g (-)	$D^*_{\omega g}$ (10^{-10} m^2/s)
11.00	9.89	0.97	10.45	0.49	23.30	48.55	0.45	-
19.77	19.49	1.52	19.63	0.76	26.59	94.96	0.28	-
51.22	46.87	1.94	49.04	0.97	25.77	234.23	0.11	-

Table 4.2 Steady-state values of variables involved in multiple-stage chemico-osmotic tests on specimen SQ_NaB_COT2

$c_{t,ref}$ (mM)	$c_{t,exit}$ (mM)	$c_{b,exit}$ (mM)	$c_{t,avg}$ (mM)	$c_{b,avg}$ (mM)	Δu (kPa)	$\Delta\Pi$ (kPa)	ω_g (-)	$D^*_{\omega g}$ (10^{-10} m^2/s)
10.82	10.08	1.12	10.45	0.56	9.25	48.70	0.19	4.05
20.99	19.77	2.07	20.38	1.03	10.47	95.22	0.11	4.21
52.78	48.62	5.39	50.70	2.64	4.25	236.30	0.02	4.37

Table 4.3 Steady-state values of variables involved in multiple-stage chemico-osmotic tests on specimen tested by Dominijanni et al. (2013)

$c_{t,ref}$ (mM)	$c_{t,exit}$ (mM)	$c_{b,exit}$ (mM)	$c_{t,avg}$ (mM)	$c_{b,avg}$ (mM)	Δu (kPa)	$\Delta\Pi$ (kPa)	ω_g (-)	$D^*_{\omega g}$ (10^{-10} m^2/s)
5.16	5.12	0.83	5.14	0.42	15.65	23.02	0.68	-
10.27	9.61	0.85	9.94	0.43	26,87	46.33	0.58	2.54
20.24	18.93	1.45	19.58	0.72	30.32	91.89	0.33	3.52
51.94	47.39	4.39	49.67	2.19	32.38	231.30	0.14	4.19
109.31	97.18	9.78	103.24	4.89	23.96	479.21	0.05	4.60

4.5 Interpretation of test results and discussion

The experimental reflection coefficients obtained in this study were plotted in Figure 4.9 as a function of average concentration of bulk solution, $c_{avg} = (c_{t,avg} - c_{b,avg})/2$, together with laboratory results found by Kemper and Rollins (1966), Malusis and Shackelford (2002a), Dominijanni et al. (2013) and Tang et al. (2014). The obtained data result in a good agreement.

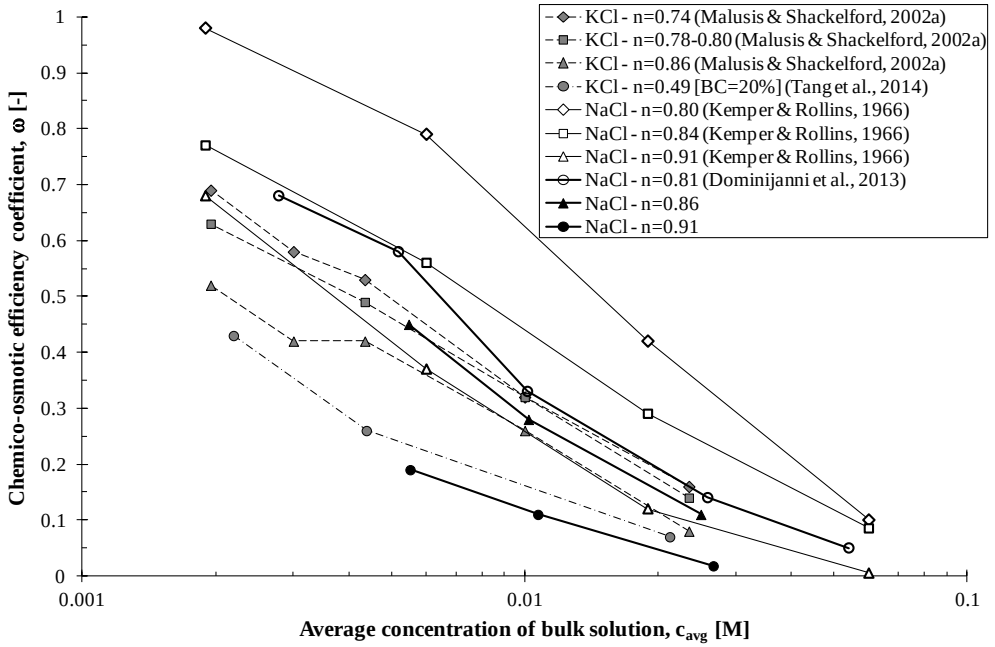

Figure 4.9 Chemico-osmotic efficiency coefficient, ω, as a function of average concentration of bulk solution, c_{avg}

Nevertheless, compared to results by Kemper and Rollins (1966), lower reflection coefficients were found for a porosity of $n = 0.91$: the cause of such differences can be attributed to the different testing device. Moreover, by comparing the obtained experimental data with those by Malusis and Shackelford (2002a), higher reflection coefficients were found for a porosity of $n = 0.86$: the explanation of this last issue can be attributed to the different specimen composition. The GCL is indeed a less homogeneous material than the consolidated sodium bentonite used in this study and, as a consequence, it presents lower chemico-osmotic performances even at the

same stress-strain conditions. Tang et al. (2014) performed chemico-osmotic tests on bentonite-amended compacted clays (e.g. Fukakusa clay mixed with bentonite at 20% content, characterized by a porosity value n ≅ 0.49) and found out lower chemico-osmotic efficient coefficients than all the others, excepted for specimen SQ_NaB_COT2 (i.e. n = 0.91). Thus, it is evident that bentonite content in clays influences membrane behaviour much more than clay porosity. Although these differences exist among the sets of data, the trends are similar, i.e. the reflection coefficient decreases with an increase in the average saline concentration across the specimen, and with an increase in the porosity. This behaviour is in accordance with the diffuse double-layer (Gouy – Chapman) theory, based on which the thickness of the diffuse double layers of adjacent bentonite lamellae and thus the extent of influence of the ion-restricting electric fields inside the soil pores decreases as the ion concentration in the pore water increases (Fritz, 1986).

According to the model proposed by Dominijanni and Manassero (2012b), it is possible to relate the experimental results of the two chemico-osmotic tests of this study to the physical and chemical properties of the tested bentonite specimens, by assuming that the microscopic deviations of the state variables from their average values are negligible. In such a case, on the basis of the proposed theoretical approach, the global reflection coefficient depends on the solid skeleton electric charge, $\overline{C}_{sk,0}$ through Eq. (4.21). Therefore, from the best-fitting of the theoretical curves with the experimental results, two different constant values of $\overline{C}_{sk,0}$ were found, respectively equal to 115 mM for specimen SQ_NaB_CTO1, and to 80 mM for specimen SQ_NaB_COT2, in accordance with the theoretical background. In fact, from Eq. (4.1), by assuming $\sigma = 0.114$ C m^{-2}, $f_{Stern} = 0.85$, $\rho_{sk} = 2.65$ g cm^{-3}, $S = 760$ m^2 g^{-1}, it follows that, in the case of $\overline{C}_{sk,0} = 115$ mM, the number of lamellae per tactoid, N_l is equal to 3, while in the case of $\overline{C}_{sk,0} = 80$ mM N_l is equal to 4, corresponding in both cases to aggregated structures. The interpretation of previous results is in accordance with the study carried out by Dominijanni et al. (2013), in which the authors obtained a similar value of $\overline{C}_{sk,0}$ (i.e. 90 mM), by interpreting

experimental results from a similar chemico-osmotic test on the same sodium bentonite, characterized by a different void ratio (i.e. e = 4.26), with NaCl solutions at different molar concentrations (i.e. 5.16, 10.27, 20.24, 51.94 and 109.31 mM). The 3 obtained theoretical curves are reported in Figure 4.10 with the experimental data. In order to determine ω_g, the salt concentration at the top boundary was taken equal to $c_{t,avg}$, while the salt concentration at the bottom boundary was considered equal to zero, i.e. $c_b \cong c_{b,avg} \cong 0$. The sodium transport number was calculated from the sodium and chloride free-solution diffusion coefficient values (Shackelford and Daniel, 1991): $D_{Na,0}$ = 13.3·10^{-10} m^2/s, $D_{Cl,0}$ = 20.3·10^{-10} m^2/s.

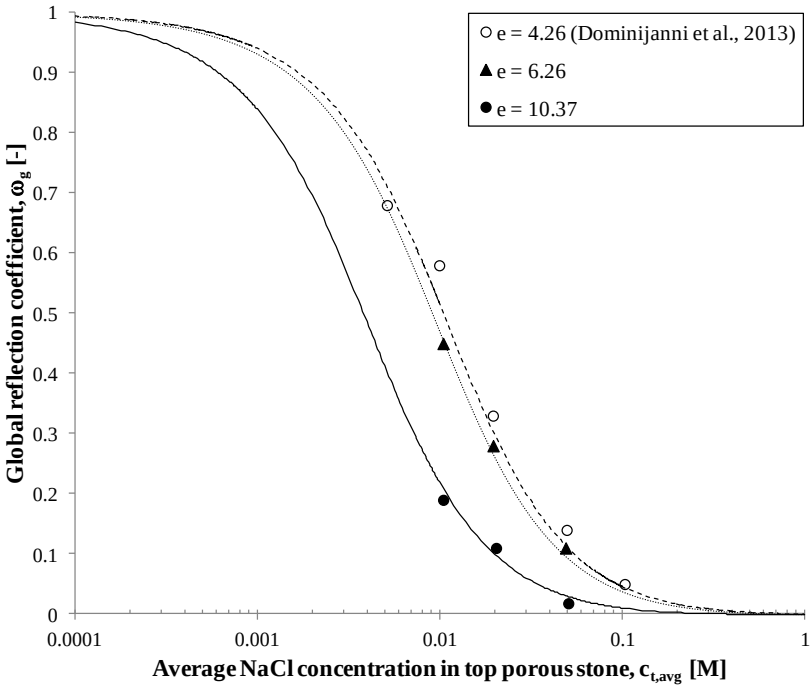

Figure 4.10 Global reflection coefficient, ω_g, as a function of average sodium chloride (NaCl) concentration at top boundary of bentonite specimen, with best-fitting theoretical curves, obtained respectively, for $\bar{c}_{sk,0}$ = 115 mM in equation (4.21) (micro-dotted line) for specimen SQ_NaB_COT1 (triangles), for $\bar{c}_{sk,0}$ = 80 mM (continuous line) for specimen SQ_NaB_COT2 (closed circles), and for $\bar{c}_{sk,0}$ = 90 mM (dotted line) for specimen tested by Dominijanni et al. (2013) (open circles)

In Figure 4.11, the experimental reflection coefficients were also fitted with the empirical semi-log linear curve proposed by Shackelford et al. (2003) and Malusis et al. (2003):

$$\omega_g = A + B \cdot \log\left(c_{t,avg}\right) \tag{4.27}$$

where A and B are the regression parameters. The value of the coefficient of determination, R^2 close to one confirms the ability of these empirical curves to fit the ω_g experimental data, as it was found by Malusis et al. (2003) for data obtained by Kemper and Rollins (1966) and Malusis and Shackelford (2002a). However, the regression parameters A and B should be intended as functions of the soil porosity (Malusis et al., 2003) and of the bottom boundary condition (i.e. $c_{b,avg}$). The advantage of interpreting the experimental data with the proposed theoretical model is that, when the single unknown parameter, $\overline{c}_{sk,0}$, has been calibrated on a restricted experimental data set, the global reflection coefficient values can be estimated for different soil porosities and boundary conditions through Eq. (4.21) (Dominijanni et al., 2013).

The tortuosity factor for specimen SQ_NaB_COT2 was determined by plotting the measured values of $D^*_{\omega g}$ as a function of the corresponding values of the complement to 1 of ω_g, i.e. 1 - ω_g and finding the intercept of the linear regression with the ordinate axis at 1 - ω_g = 1, i.e. ω_g = 0 (Figure 4.12). The tortuosity factor in Eq. (4.20) is in fact given by:

$$\tau_m = \left(\frac{D^*_{\omega g}}{D_{s,0}} \right)_{\omega_g = 0} \tag{4.28}$$

Where $D_{s,0}$ is the NaCl free solution diffusion coefficient, which is equal to $16 \cdot 10^{-10}$ m^2/s (Shackelford and Daniel, 1991).

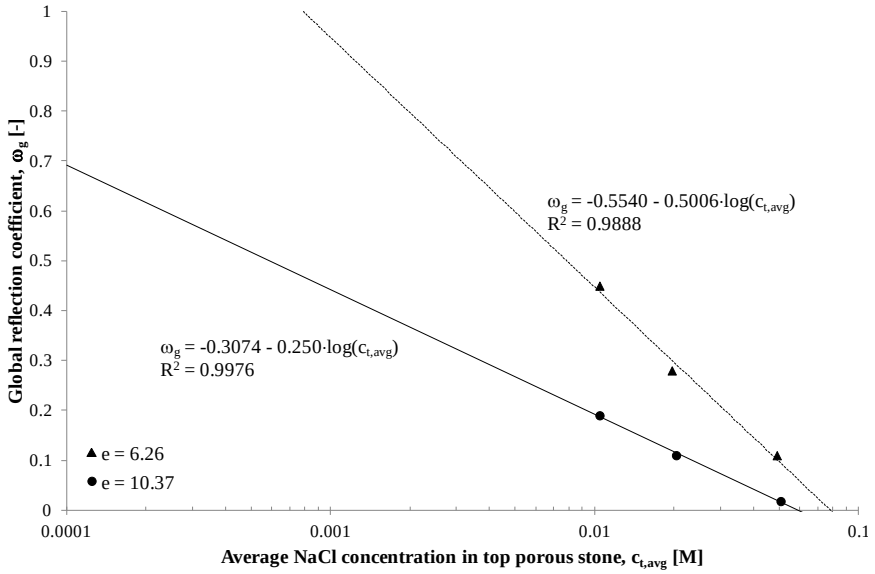

Figure 4.11 Semi-log regression of measured global reflection coefficients against average sodium chloride (NaCl) concentration at top boundary of bentonite specimens SQ_NaB_COT1 (triangles) and SQ_NaB_COT2 (circles)

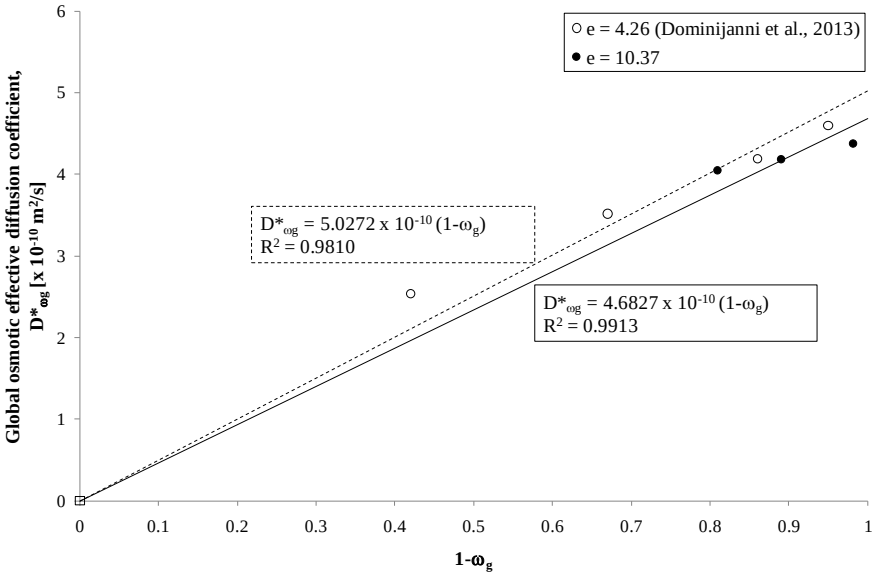

Figure 4.12 Global osmotic effective diffusion coefficient, $D^{*}_{\omega g}$, as a function of the complement to 1 of the global reflection coefficient, ω_g, with the theoretical linear relation given by equation (4.20) (continuous line for specimen SQ_NaB_COT2 and dotted line for specimen tested by Dominijanni et al., 2013)

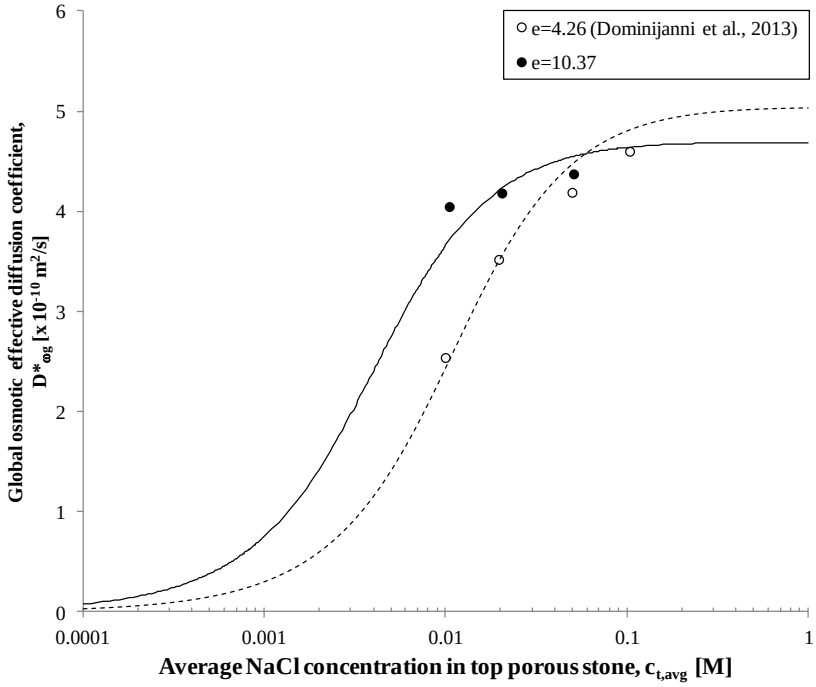

Figure 4.13 Global osmotic effective diffusion coefficient, $D^*_{\omega g}$, as a function of average sodium chloride (NaCl) concentration at top boundary of bentonite specimen, with best-fitting theoretical curves, obtained respectively, for $\bar{c}_{sk,0}$ = 80 mM and $\tau_m = 0.29$ in equations (4.20) and (4.21) (continuous line) for specimen SQ_NaB_COT2 (full circles), and for $\bar{c}_{sk,0}$ = 90 mM and $\tau_m = 0.31$ (dotted line) for specimen tested by Dominijanni et al. (2013) (void circles)

A value of τ_m equal to 0.29 was obtained for specimen SQ_NaB_COT2, while τ_m = 0.31 had been derived by Dominijanni et al. (2013) (Figure 4.12). The resulting theoretical curves of $D^*_{\omega g}$ are reported in Figure 4.13 as a function of the top boundary salt concentration.

The theoretical linear relationship between $D^*_{\omega g}$ and $1-\omega_g$ represented in Figure 4.12 under the hypothesis that the pore-scale variations in the state variables, i.e. hydraulic pressure, ion concentrations, and water velocity, within the soil are negligible, can be plotted again remembering relations (4.11)-(4.15): in such a way, it is possible to represent (Figure 4.14) the obtained results in terms of restrictive

tortuosity factor, τ_r, as a function of the chemico-osmotic efficiency coefficient, ω, together with a set of experimental data by Malusis & Shackelford (2002b), Malusis et al. (2013) and Dominijanni et al. (2013): the theoretical linear relation from Eq. (4.15) is in a very good agreement with the large number of experimental results (coefficient of determination, R^2 = 0.955). Therefore this can be considered an important indication of the ability of the proposed theoretical approach to properly simulate the bentonite systems behaviour referring in particular to the evaluation of their performances in terms of pollutant containment barriers (Manassero et al., 2014).

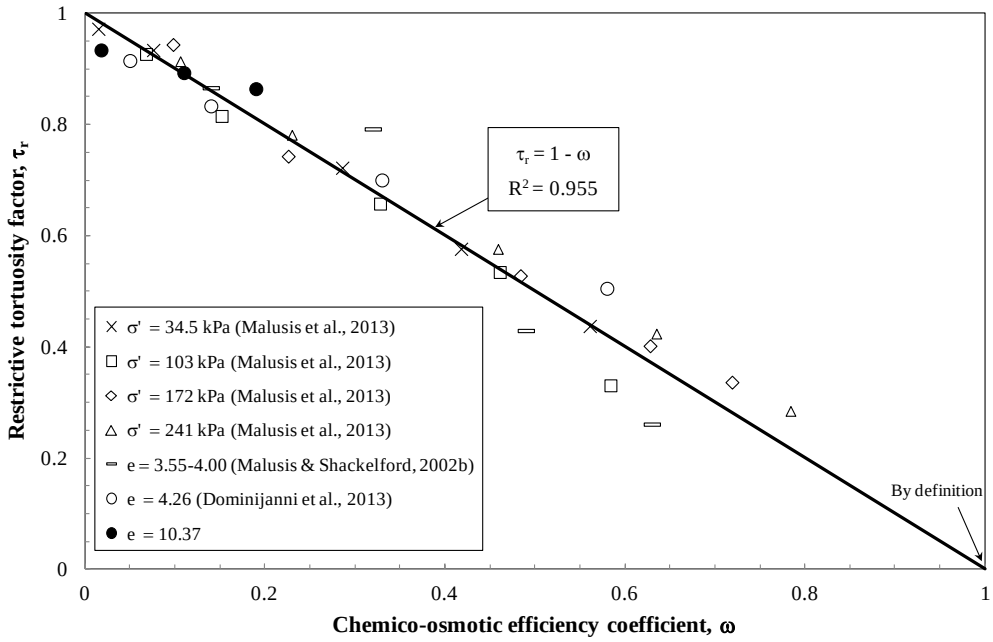

Figure 4.14 Restrictive tortuosity factor, τ_r, as a function of chemico-osmotic efficiency coefficient, ω, with the theoretical linear relation

Moreover, the possibility of fitting swelling pressure results (Dominijanni et al., 2013; Boffa et al., 2016), and transport properties (Dominijanni et al., 2013), with similar values of $\overline{C}_{sk,0}$ (Figure 4.15) may represent a significant evidence of the abitility of the theoretical model to describe the coupled chemical-hydraulic-mechanical behaviour of sodium bentonite.

Nevertheless, the results obtained for a single salt contained in the bentonite pore solution need to be extended to the more general problem of a solution containing an unspecified number of salts, in order to evaluate the performance of sodium bentonites which are used as contaminant barriers for real leachates (Dominijanni et al., 2013).

Finally, it is important to stress that the physical approach should not be mistaken for a microscopic modelling of soil behaviour, but it should be considered as a tool to use in order to understand why sodium bentonites behave in a given way at the macroscopic scale on the basis of a simplified picture of their microstructure (Dominijanni and Manassero, 2012b).

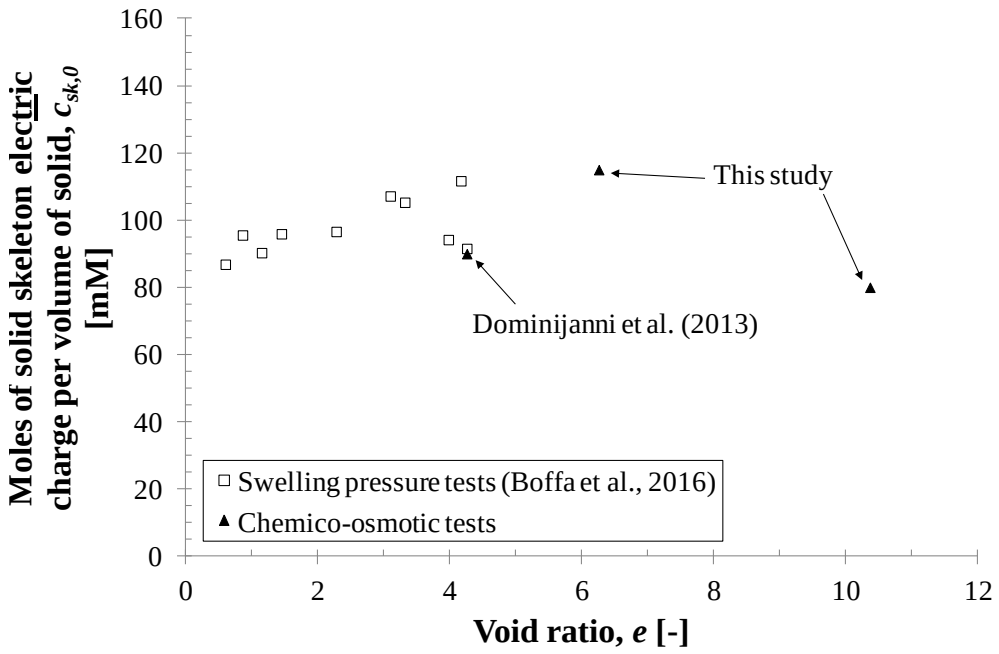

Figure 4.15 Moles of solid skeleton electric charge per volume of solid, $\overline{c}_{sk,0}$, obtained by theoretical interpretation of transport properties of sodium bentonite specimens and of swelling pressure data (Boffa et al., 2016), as a function of their void ratio

4.6 **Conclusions**

In this study the semipermeable membrane behaviour of sodium bentonites in contact with increasing NaCl concentration solutions was analysed by performing two chemico-osmotic tests on two bentonite specimens with different porosity. The experimental results were obtained by following testing procedures used by Dominijanni et al. (2013). The reflection coefficient was found to decrease with an increase in the average saline concentration across the specimen, and with an increase in the porosity, in agreement with previous literature values. The experimental data were interpreted on the basis of the theoretical approach proposed by Dominijanni and Manassero (2012b), and resulted to be in agreement with the trends given by the model, under the assumption that the microscopic deviations of the pore solution state variables from their average values are negligible. By accepting this hypothesis, from the experimental value of global reflection coefficient it was possible to derive two slightly different electric charge of the solid skeleton (per unit solid volume), $\overline{C}_{sk,0}$, indication of the same (i.e. aggregated) microstructure of the tested bentonite specimens. Similar values of this parameter were also found in other experimental tests aimed at evaluating the swelling and mechanical behaviour of sodium bentonites. The transport properties of sodium bentonite can be estimated from $\overline{C}_{sk,0}$, in order to evaluate its performance as a hydraulic and contaminant barrier in field applications. Nevertheless, further experimental results are needed in order to validate the theoretical approach under different boundary conditions.

References

1. Auclair, B., Nikonenko, V., Larchet, C., Métayer, M. & Dammak, L. (2002). Correlation between transport parameters of ion-exchange membranes. *Journal of Membrane Science* **195**, 89-102.
2. Boffa, G., Dominijanni, A., Manassero, M., Marangon, M., Zaninetta, L. (2016). Mechanical and swelling behaviour of sodium bentonites in equilibrium with low molarity NaCl solutions under oedometric conditions. *Acta Geotechnica* (submitted paper).
3. Bohnoff, G.L., Shackelford, C.D. (2013). Improving membrane performance via bentonite polymer nanocomposite. *Applied Clay Science* **86**, 83-98.
4. Bolt, G.H. (1956). Physico-chemical analysis of the compressibility of pure clays. *Géotechnique* **6**(2), 86-93.
5. Borgesson, L., Karnland, O., Johannesson, L.E. (1996). Modelling of the physical behaviour of clay barriers close to water saturation. *Engineering Geology* **41**, 127-144.
6. Bouazza, A. (2002). Geosynthetic clay liners. Review article. *Geotextiles and Geomembranes* **20**, 3-17.
7. Chapman, L. (1913). A contribution to the theory of electrocapillarity. *Philosophical Magazine* **25**, 475–481.
8. Di Emidio, G. (2010). *Hydraulic and chemico-osmotic performance of polymer treated clays*. Ph. D. Thesis, Ghent: Ghent University.
9. Dominijanni, A. (2005). Osmotic properties of clay soils. PhD Dissertation. Politecnico di Torino, Torino, Italy.
10. Dominijanni, A., Manassero, M., Vanni, D. (2006). Micro/macro modeling of electrolyte transport through semipermeable bentonite layers. In: Thomas, H.R. (Ed.), Proceedings of the 5th International Congress of Environmental Geotechnics, 26th-30th June, 2006, Cardiff, Wales, UK, vol. II. Thomas Telford, London, pp. 1123-1130.

11. Dominijanni, A. & Manassero, M. (2012a). Modelling the swelling and osmotic properties of clay soils. Part I: The phenomenological approach. *International Journal of Engineering Science* **51**, 32-50.
12. Dominijanni, A. & Manassero, M. (2012b). Modelling the swelling and osmotic properties of clay soils. Part II: The physical approach. *International Journal of Engineering Science* **51**, 51-73.
13. Dominijanni, A., Manassero, M., Puma, S. (2013). Coupled chemical-hydraulic-mechanical behaviour of bentonites. *Géotechnique* **63**(3), 191-205.
14. Donnan, F.G. (1911). Theorie der Membrangleichgewichte und Membranpotentiale bei Vorhandensein von nicht dialysierenden Elektrolyten. Ein Beitrag zur physikalisch-chemischen Physiologie [Theory of membrane equilibria and membrane potentials in the presence of non-dialysing electrolytes. A contribution to physical-chemical physiology], *Zeitschrift für Elektrochemie und angewandte physikalische Chemie* **17**, 572-581. English translation republished in *Journal of Membrane Science* **100** (1995), 45-55.
15. Fritz, S.J. (1986). Ideality of clay membranes in osmotic processes: a review. *Clays and Clay Minerals*, 34 (2), 214-223.
16. Gouy, G. (1910). Sur la constitution de la charge électrique à la surface d'un electrolyte. *Journal de Physique Théorique et Appliquée*, 9, 457–468.
17. Groenevelt, P.H., Elrick, D.E. (1976). Coupling phenomena in saturate homo-ionic montmorillonite. 2. Theoretical. Soil Sci. Soc. Am. J. **40**(6):820-823.
18. Kang, J.-B., Shackelford, C.D. (2009). Clay membrane testing using a flexible-wall cell under closed system boundary conditions. *Applied Clay Science* **44**(1-2), 43-58.
19. Kang, J.-B., Shackelford, C. D. (2010). Membrane behavior of compacted clay liners. *Journal of Geotechnical and Geoenvironmental Engineering* **136**(10), 1368-1382.

20. Kang, J.-B., Shackelford, C.D. (2011). Consolidation enhanced membrane behavior of a geosynthetic clay liner. *Geotextiles and Geomembranes* **29**(6): 544-556.
21. Katsumi, T., Ishimori, H., Onikata, M., Fukagawa, R. 2008. Long-term barrier performance of modified bentonite materials against sodium and calcium permeant solutions. *Geotextiles and Geomembranes* **26**, 14-30.
22. Keijzer, Th.J.S., Kleingeld, P.J., Loch, J.P.G. (1999). Chemical osmosis in compacted clayey material and the prediction of water transport. *Engineering Geology*, **53**(2): 151-159.
23. Kemper, W.D. & Rollins, J.B. (1966). Osmotic efficiency coefficients across compacted clays. *Soil Science Society of America, Proceedings* **30**, 529–534.
24. Malusis, M.A. & Shackelford, C.D. (2002a). Chemico-osmotic efficiency of a geosynthetic clay liner. *Journal of Geotechnical and Geoenvironmental Engineering* **128**, No. 2, 97–106.
25. Malusis, M.A. & Shackelford, C.D. (2002b). Coupling effects during steady-state solute diffusion through a semipermeable clay membrane. *Environmental Science and Technology* **36**, No. 6, 1312–1319.
26. Malusis, M.A. (2001). Membrane behaviour and coupled solute transport through a Geosynthetic Clay Liner. PhD Dissertation, Colorado State University, Fort Collins, Colorado, USA.
27. Malusis, M.A., Shackelford, C.D., Olsen, H.W. (2001). A laboratory apparatus to measure chemico-osmotic efficiency coefficients for clay soils. *Geotechnical Testing Journal* **24**, 229-242.
28. Malusis, M.A., Shackelford, C.D., Olsen, H.W. (2003). Flow and transport through clay membrane barriers. *Engineering Geology* **70**, 235–248.
29. Malusis, M.A., Shackelford, C.D., Maneval, J.E. (2012). Critical review of coupled flux formulations for clay membranes based on nonequilibrium thermodynamics. *Journal of Contaminant Hydrology* **138-139**, 40-59.
30. Malusis, M.A., Kang, J.-B., Shackelford, C.D. (2013). Influence of membrane behavior on solute diffusion through GCLs. Coupled Phenomena

in Environmental Geotechnics, M. Manassero, A. Dominijanni, S. Foti and G. Musso, Eds., July 1-3, 2013, Torino, Italy, CRC Press/Balkema, Taylor & Francis Group, London, 267-274.

31. Malusis, M.A., Daniyarov, A.S. (2014). Membrane efficiency of a dense, prehydrated GCL. 7th International Congress on Environmental Geotechnics, A. Bouazza, S. Yuen and B. Brown, Eds, November 10-14, 2014, Melbourne, Australia, 2014 Engineers Australia, 1166-1173.
32. Manassero, M. & Dominijanni, A. (2003). Modelling the osmosis effect on solute migration through porous media. *Géotechnique* **53**, No. 5, 481–492.
33. Manassero, M., Dominijanni, A., Musso, G., Puma, S. (2014). Coupled phenomena in contaminant transport. 7th International Congress on Environmental Geotechnics, A. Bouazza, S. Yuen and B. Brown, Eds, November 10-14, 2014, Melbourne, Australia, 2014 Engineers Australia, 144-169.
34. Meier, A., Sample-Lord, K. M., Castelbaum, D., Kallase, S., Moran, B., Ray, T., Shackelford, C.D. (2014). Persistence of semipermeable membrane behavior for a geosynthetic clay liner. 7th International Congress on Environmental Geotechnics, A. Bouazza, S. Yuen and B. Brown, Eds, November 10-14, 2014, Melbourne, Australia, 2014 Engineers Australia, 496-503.
35. Mitchell, J.K. (1993). *Fundamentals of soil behavior* (2nd ed.). New York: Wiley.
36. Mitchell, J.K., Soga, K. (2005). *Fundamentals of soil behaviour* (3rd ed.) New York: Wiley & Sons.
37. Norrish, K. (1954). The swelling of montmorillonite. Discussions of the Faraday Society, **18**, 120-134.
38. Puma, S. (2013). Chemico-mechanical improvement of bentonite barriers for pollutant containment. PhD Dissertation. Politecnico di Torino, Torino, Italy.
39. Shackelford, C.D. & Daniel, D.E. (1991). Diffusion in saturated soil: I. Background. *Journal of Geotechnical Engineering*, **117**, No. 3, 467–484.

40. Shackelford, C.D. & Lee, J.-M. (2003). The destructive role of diffusion on clay membrane behavior. *Clays and Clay Minerals* **51**, No. 2, 186–196.
41. Shackelford, C.D., Malusis, M.A. & Olsen, H.W. (2003). Clay membrane behavior for geoenvironmental containment. *Soil and Rock America Conference 2003* (Proceedings of the joint 12th Panamerican Conference on Soil Mechanics and Geotechnical Engineering and the 39th U. S. Rock Mechanics Symposium), Culligan, Einstein, and Whittle, Eds., Verlag Glückauf GMBH, Essen, Germany, Vol. 1, 767–774.
42. Shackelford, C.D. (2013). Membrane behavior in engineered bentonite-based containment barriers: State of the art. Coupled Phenomena in Environmental Geotechnics, M. Manassero, A. Dominijanni, S. Foti and G. Musso, Eds., July 1-3, 2013, Torino, Italy, CRC Press/Balkema, Taylor & Francis Group, London, 45-60.
43. Tang, Q., Katsumi, T., Inui, T., Li, Z. (2014). Membrane behavior of bentonite-amended compacted clay. *Soils and Foundations* **54**(3), 329-344.
44. Van Impe, P. O. (2002). Consolidation, contaminant transport and chemico-osmotic effects in liner materials. PhD Dissertation, Ancona University, Ancona, Italy.
45. Yeo, S.-S., Shackelford, C. D., Evans, J. C. (2005). Membrane behavior of model soil-bentonite backfills. *Journal of Geotechnical and Geoenvironmental Engineering* **131**(4), 418-429.
46. Yong, R.N., Warkentin B.P. (1975). Soil properties and behaviour. Developments in geotechnical engineering (vol. 5). Elsevier Scientific Publishing Company.

4.7 Further experimental results by means of a new testing cell

Two further chemico-osmotic tests, on the same type of sodium bentonite, were performed during the last part of the PhD research activity by means of a new osmotic cell (i.e. a stainless steel oedometer represented in Figure 4.16), which had been conceived under Puma's (2013) work.

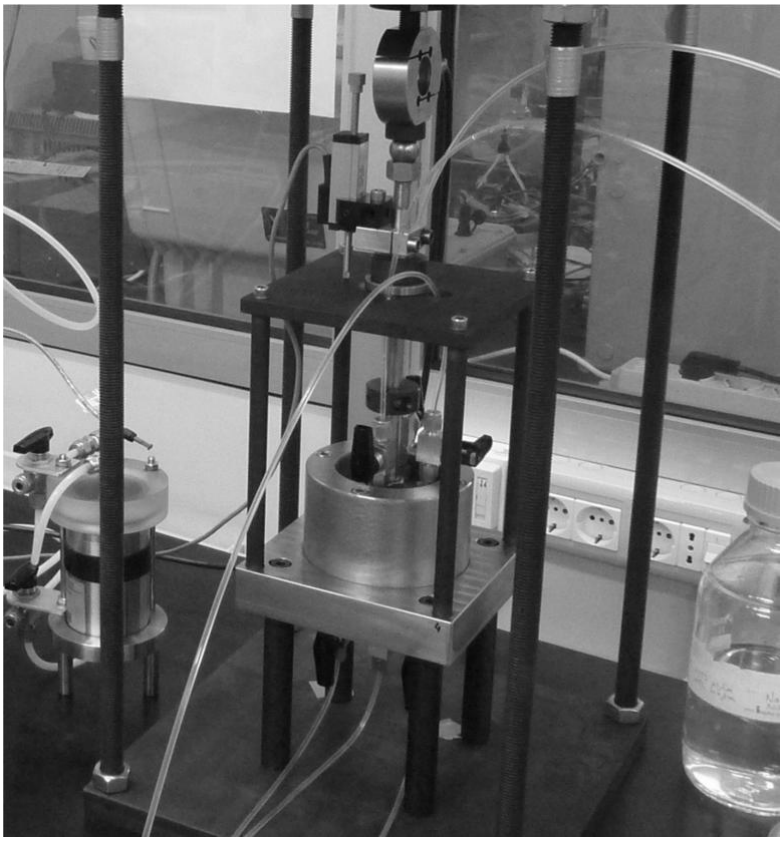

Figure 4.16 Detailed view of the new stainless steel oedometric cell

The main components of the device are shown in Figure 4.17 and Figure 4.18, and are partially the same as those used for the previous experimental activity. The new testing apparatus includes a stainless steel oedometer, a flow pump accumulator, two bladders, three pressure transducers, a displacement transducer (i.e. a Linear Variable Differential Transformer, LVDT), a load cell and a pneumatic piston.

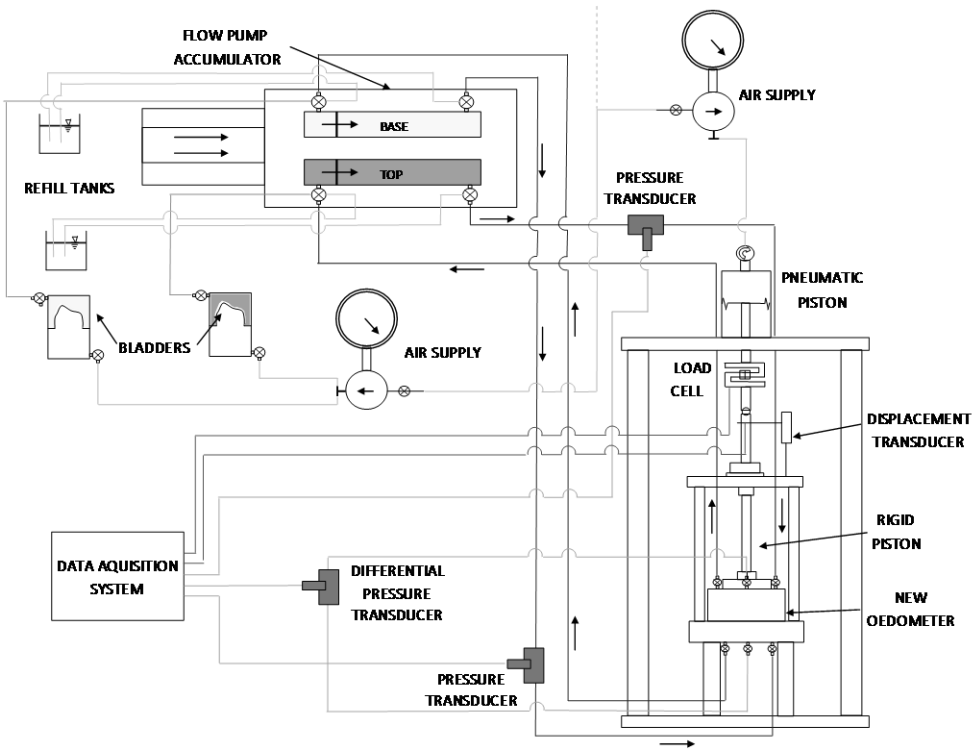

Figure 4.17 Schematic view of chemico-osmotic test apparatus with the new oedometer

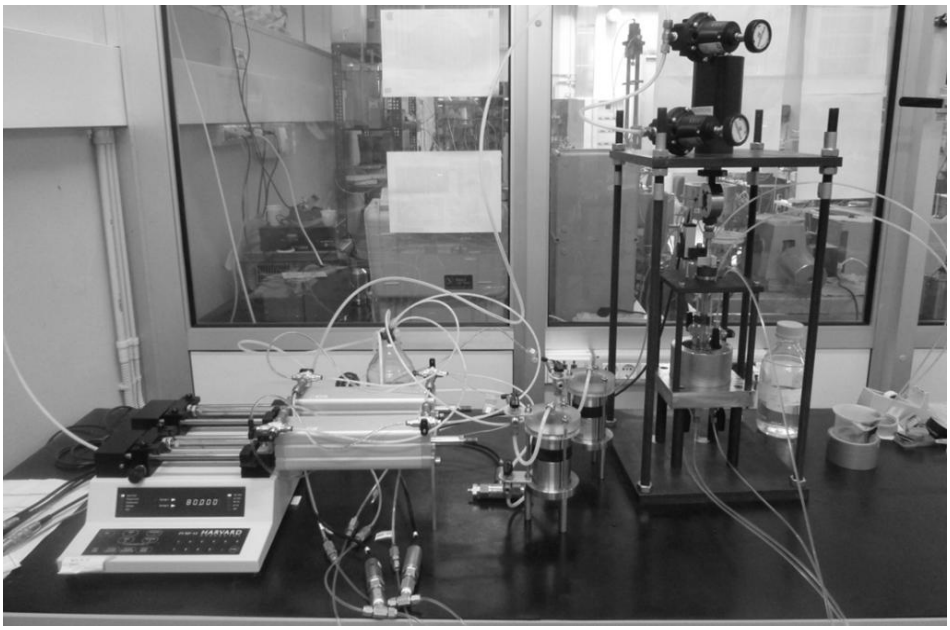

Figure 4.18 Pictorial view of chemico-osmotic test apparatus with the new oedometer

The stainless steel oedometer (diameter = 70 mm) represented in Figure 4.16 replaces the modified rigid-wall permeameter used for the previous chemico-osmotic tests. The oedometer matches with the need of containment of bentonite specimens characterized by very high swelling pressure without allowing loss of material. The top piston and the bottom pedestal of the oedometric cell are endowed of 3 drainage lines. As the previous rigid-wall permeameter, they allow for the circulation of the solutions in the porous stones (i.e. through the 2 peripheral lines), in order to maintain a constant pressure of solutions at the top and bottom boundaries of the specimen, and, moreover, to establish a constant concentration gradient across the bentonite specimen, and the simultaneous measurement of the differential pressure between the porous stones (i.e. through the central line with the differential pressure transducer). The other two pressure transducers allow for the control of the pressure in the lines during all the testing phases.

Bentonite specimens can be back-pressurized during the tests through two bladders, which are connected to the flow pump accumulator, in order to limit the presence of air in the system.

The displacement transducer lets the specimen height to be monitored, both during the preliminary phase (i.e. compaction/swelling stage), and during the effective testing phase, with the aim of controlling the porosity of the material.

The rigid piston of the oedometer is connected to the load cell, which allows for measurements of the pressure that has to be applied in order to hinder the axial strain of the specimen (i.e. swelling pressure). The maximum pressure which can be measured by the load cell is of 500 kPa.

Two oven-dried squeezed sodium bentonite specimens (i.e. SQ_NaB_COT3 and SQ_NaB_COT4) of 70 mm diameter were prepared for the new testing apparatus. A known amount of dry material was dusted inside the oedometer ring and DW and NaCl 0.01 M concentrated solution were respectively supplied to specimen SQ_NaB_COT3 and SQ_NaB_COT4 in order to saturate the material. The specimens were allowed to swell freely in the axial direction to a certain value of height, which corresponds to a fixed void ratio (i.e. respectively e = 3.93, corresponding to a porosity n = 0.80 for specimen SQ_NaB_COT3, and e = 3.32,

corresponding to a porosity n = 0.77 for specimen SQ_NaB_COT4). The piston was then blocked and the flushing stage could start: as described above, DW was circulated through the top piston and the bottom pedestal for several days with the aim of establishing a steady baseline differential pressure, before the application of a concentration gradient across specimen SQ_NaB_COT3, while NaCl 0.01 M solution was circulated through the porous stones for specimen SQ_NaB_COT4. Thus, it is to note that during the following stages of chemico-osmotic test, DW and NaCl 0.01 M solution were respectively circulated in the bottom porous stone of specimen SQ_NaB_COT3 and SQ_NaB_COT4.

Figure 4.19 Detailed view of displacement transducer and load cell

A source concentration of NaCl then was injected into the top porous stone: the chemico-osmotic test on specimen SQ_NaB_COT3 was carried out by sequential circulation of chemical solutions containing 20.99, 34.90 and 52.99 mM NaCl concentrations, while on specimen SQ_NaB_COT4 by sequential circulation of

NaCl 31.04 and 64.56 mM concentrated solutions; in both cases, the constant flow rate was 0.05 ml/min.

The *EC* values of the salt mass fluxes withdrawn from the top and the bottom porous stones, measured during the testing stages, are shown respectively in Figure 4.20 for specimen SQ_NaB_COT3 and in Figure 4.21 for specimen SQ_NaB_COT4. Even in this case, the trends of the electrical conductivity of the flux withdrawn from the top porous stone, $EC_{t,exit}$, and the electrical conductivity of the flux withdrawn from the bottom porous stone, $EC_{b,exit}$, both show that a steady state has been reached for each stage.

In Figure 4.22 the experimental global reflection coefficient results, ω_g for both specimens SQ_NaB_COT3,4 are plotted as a function of time. They were determined using Eq. (4.18), on the basis of the differential pressure, Δu, measured during the test with a time step of 10 min, and the osmotic pressure, $\Delta\Pi$, calculated from the average of the top and bottom NaCl concentrations. The steady state values of the variables are reported respectively in Table 4.4 for specimen SQ_NaB_COT3 and in Table 4.5 for specimen SQ_NaB_COT4 for each concentration stage. The NaCl concentrations were derived from the measured *EC* through the linear calibration reported in Figure 4.1. As expected, the steady state ω_g values tend to decrease as the salt concentration in the top porous stone increases.

The values of the global osmotic effective diffusion coefficient, $D^*_{\omega g}$, which have been obtained from the *Q* measurements shown respectively in Figure 4.23 for specimen SQ_NaB_COT3 and in Figure 4.24 for specimen SQ_NaB_COT4, are reported in Table 4.4 and Table 4.5.

In Figure 4.25 experimental values of the swelling pressure, u_{sw} for specimen SQ_NaB_COT4 are plotted as a function of time: they were measured of the test by means of the load cell connected to the rigid piston; at the steady state of each stage, the swelling pressure reached a stable value which can be associated to an average NaCl concentration, c_{avg}, which can be evaluated through average NaCl concentrations in top, $c_{t,avg}$, and bottom, $c_{b,avg}$, porous stones.

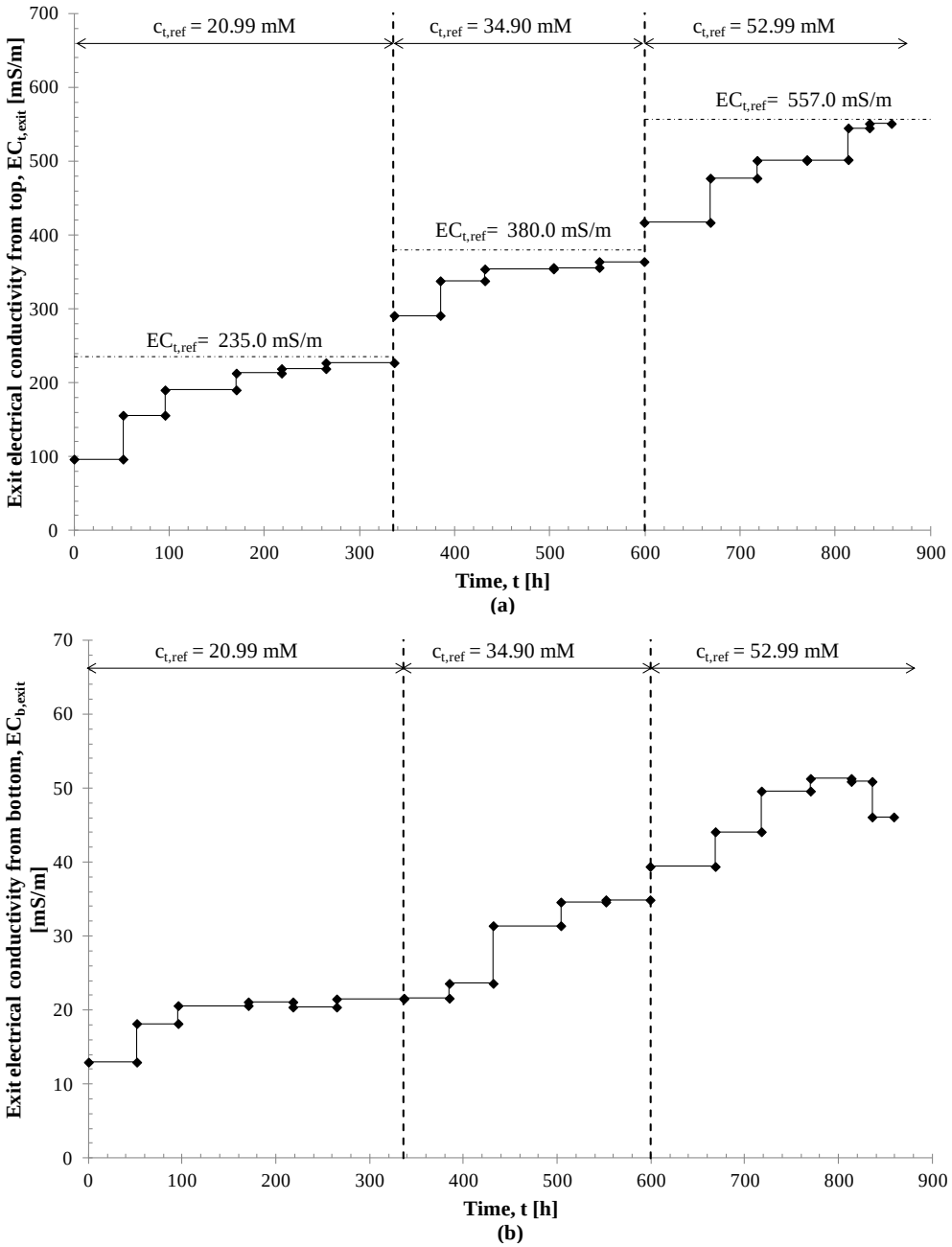

Figure 4.20 Electrical conductivity of salt flux withdrawn from (a) top porous stone and (b) bottom porous stone as a function of time during multiple-stage chemico-osmotic test on specimen SQ_NaB_COT3

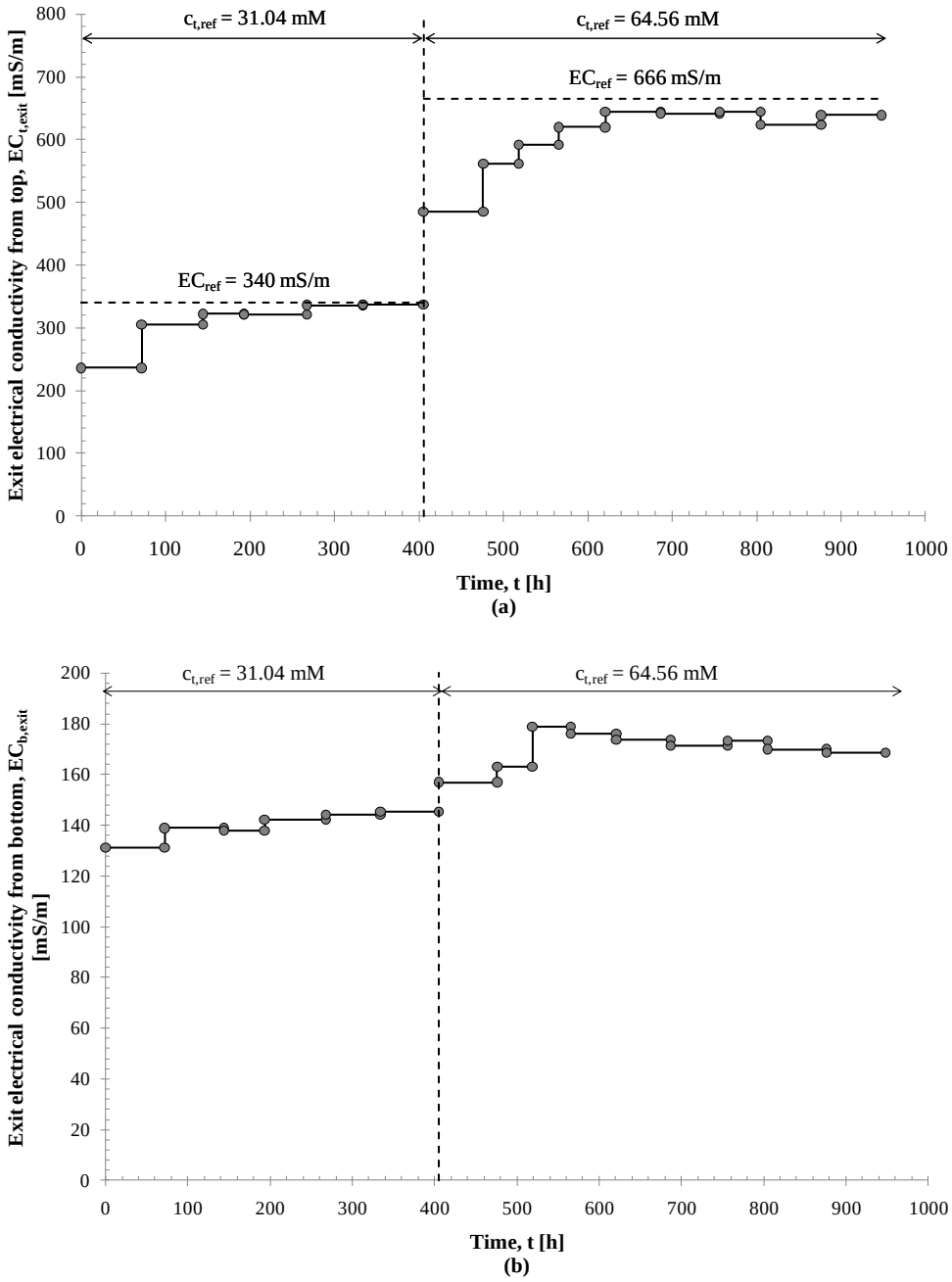

Figure 4.21 Electrical conductivity of salt flux withdrawn from (a) top porous stone and (b) bottom porous stone as a function of time during multiple-stage chemico-osmotic test on specimen SQ_NaB_COT4

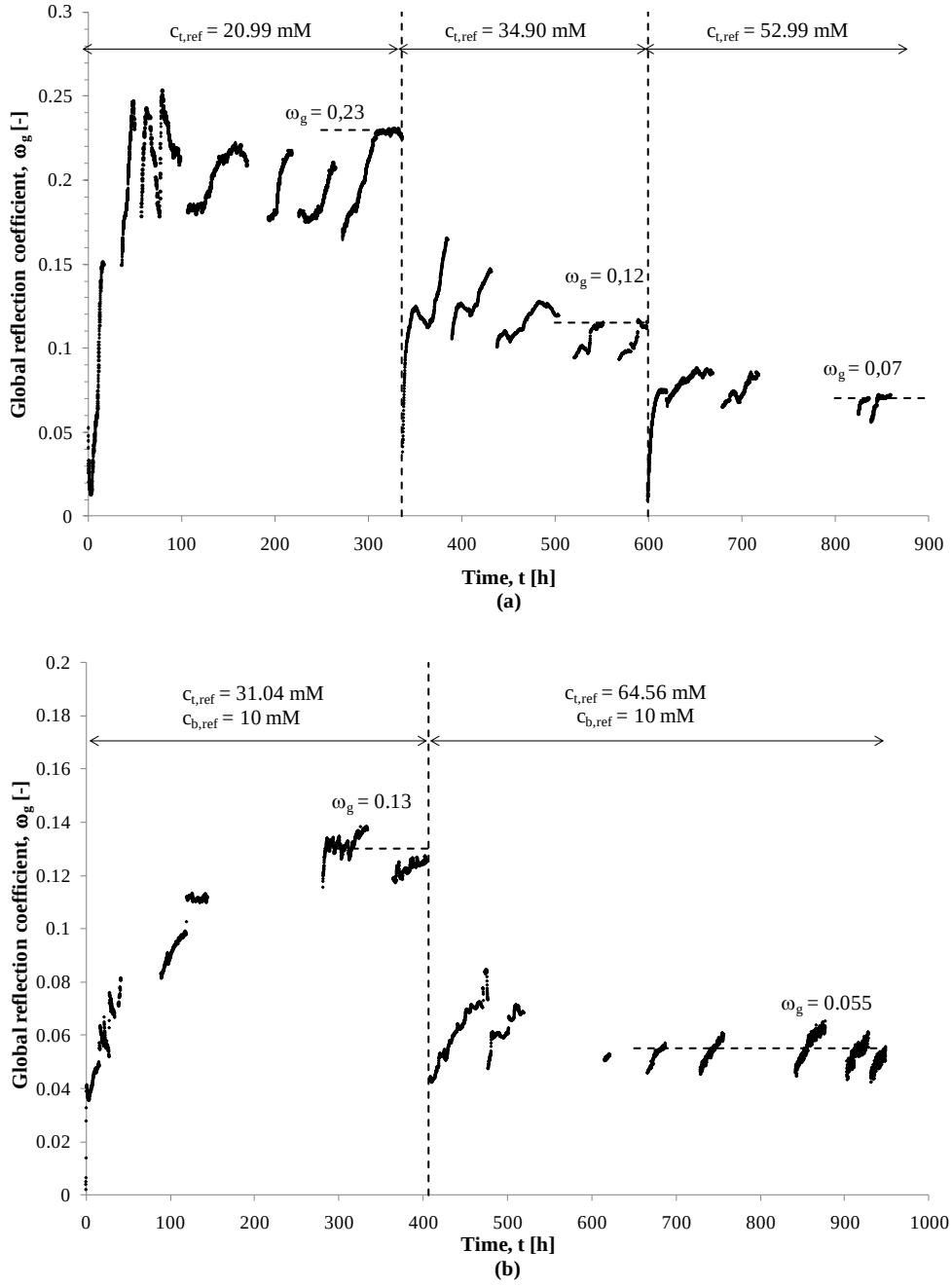

Figure 4.22 Global reflection coefficient as a function of time during multiple-stage chemico-osmotic tests, by means of the new stainless steel oedometer cell, on (a) specimen SQ_NaB_COT3 and (b) specimen SQ_NaB_COT4

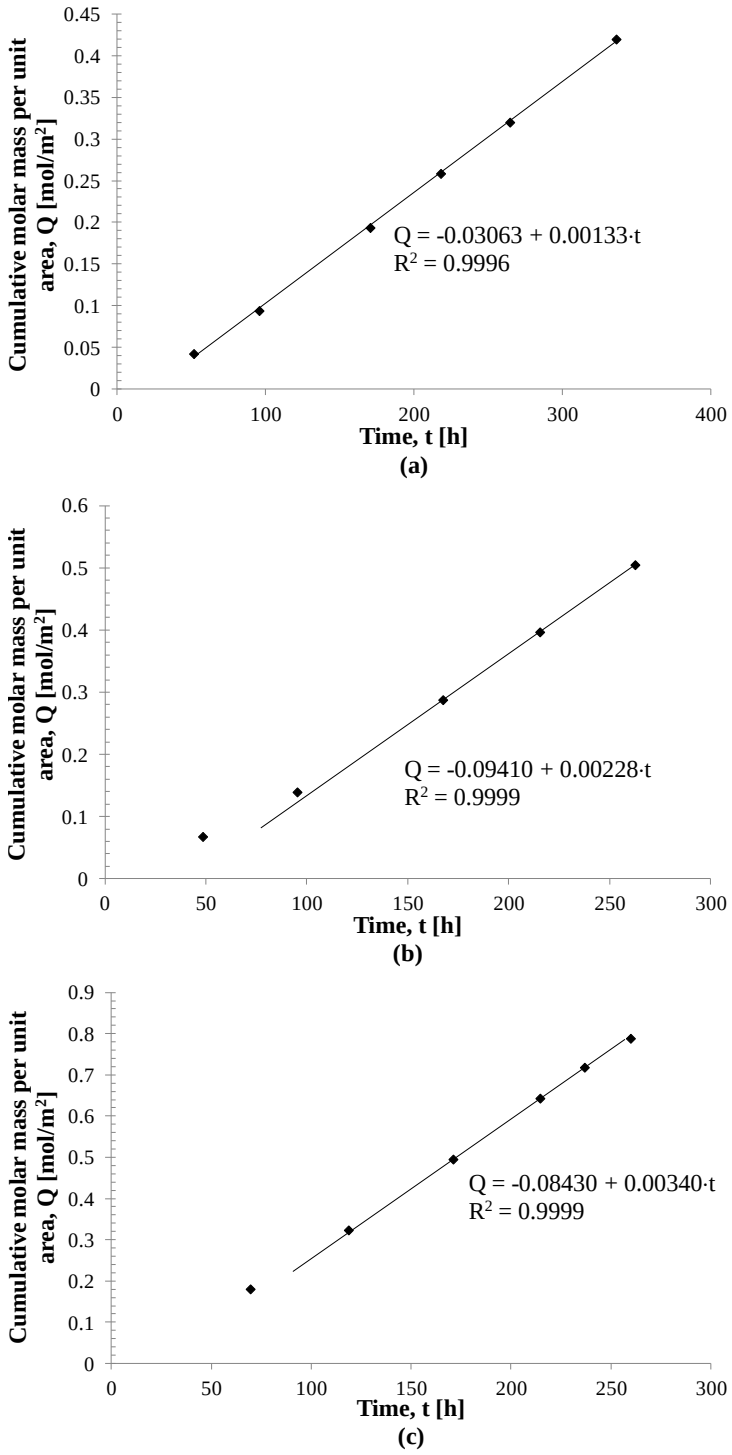

Figure 4.23 Cumulative molar mass of sodium chloride per unit area as a function of time during multiple-stage chemico-osmotic test on specimen SQ_NaB_COT3: (a) $c_{t,ref}$ = 20.99 mM; (b) $c_{t,ref}$ = 34.90 mM; (c) $c_{t,ref}$ = 52.99 mM

Table 4.4 Steady-state values of variables involved in multiple-stage chemico-osmotic test on specimen SQ_NaB_COT3.

$c_{t,ref}$ (mM)	$c_{t,exit}$ (mM)	$c_{b,exit}$ (mM)	$c_{t,avg}$ (mM)	$c_{b,avg}$ (mM)	Δu (kPa)	$\Delta\Pi$ (kPa)	ω_g (-)	$D^*_{\omega g}$ (10^{-10} m^2/s)
20.99	20.24	1.78	20.61	0.89	22.33	97.07	0.23	1.94
34.90	33.39	2.94	34.15	1.47	18.50	160.86	0.12	2.00
52.99	47.28	4.36	50.14	2.18	16.52	236.05	0.07	2.04

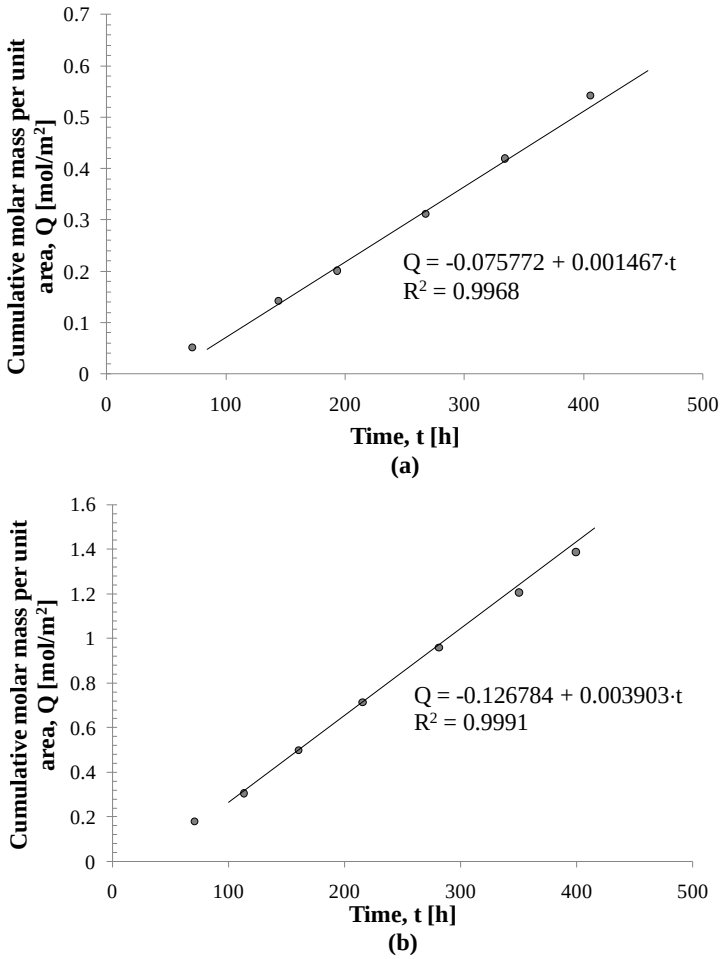

Figure 4.24 Cumulative molar mass of sodium chloride per unit area as a function of time during multiple-stage chemico-osmotic test on specimen SQ_NaB_COT4: (a) $c_{t,ref}$ = 31.04 mM; (b) $c_{t,ref}$ = 64.56 mM

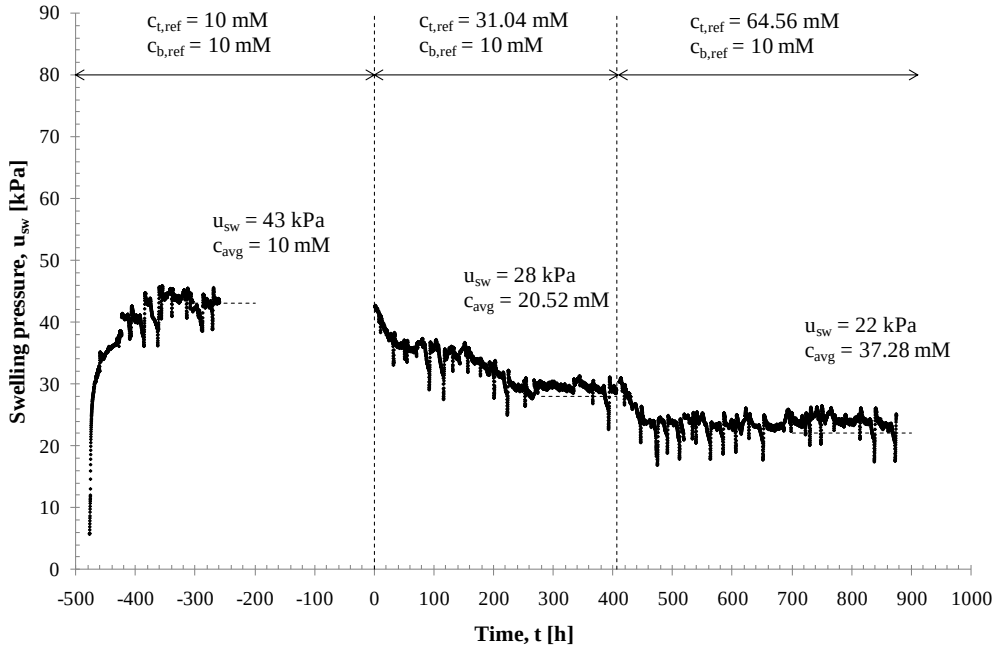

Figure 4.25 Swelling pressure as a function of time and of average NaCl concentration pore solution during multiple-stage chemico-osmotic test, by means of the new stainless steel oedometer cell, on specimen SQ_NaB_COT4

Table 4.5 Steady-state values of variables involved in multiple-stage chemico-osmotic test on specimen SQ_NaB_COT4 (in the bottom porous stone $c_{b,ref}$ = 10 mM during each stage).

$c_{t,ref}$ (mM)	$c_{t,exit}$ (mM)	$c_{b,exit}$ (mM)	$c_{t,avg}$ (mM)	$c_{b,avg}$ (mM)	Δu (kPa)	$\Delta\Pi$ (kPa)	ω_g (-)	$D^*_{\omega g}$ (10^{-10} m^2/s)
31.04	30.70	12.70	30.87	11.35	12.34	94.90	0.13	2.58
64.56	62.00	15.10	64.15	12.55	13.66	248.30	0.05	2.70

$c_{t,ref}$ (mM)	$c_{t,exit}$ (mM)	$c_{b,exit}$ (mM)	$c_{t,avg}$ (mM)	$c_{b,avg}$ (mM)	c_{avg} (mM)	u_{sw} (kPa)
10.00	-	-	-	-	10.00	43
31.04	30.70	12.70	30.87	11.35	20.52	28
64.56	62.00	15.10	64.15	12.55	37.28	22

It is interesting to plot all the experimental values of global reflection coefficient as a function of specimens' void ratio, by distinguishing the NaCl average concentration at the boundaries of bentonite (Figure 4.26): it is possible to note that the different way of specimens' preparation can affect transport properties of the material. In fact, as specimen SQ_NaB_COT3,4 were directly hydrated within the osmotic cell, they showed lower values of ω_g than specimens SQ_NaB_COT1,2 and that tested by Dominijanni et al. (2013), characterized by e = 4.26, which were prepared by prehydrating the squeezed bentonite in DW at a lower water content than the *LL* value, then by installing the slurry inside a drained compaction mould, and, finally, by statically compacting at a fixed void ratio. It seems that the prehydration phase can enhance the semipermeable membrane behaviour of bentonite.

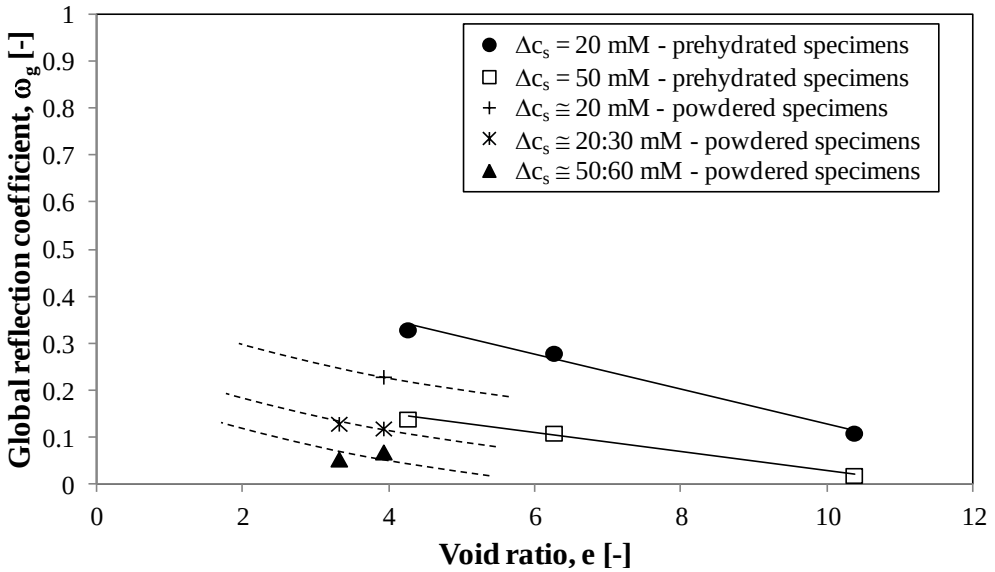

Figure 4.26 Experimental values of global reflection coefficient as a function of void ratio of bentonite specimens

Even in these cases, it was possible to relate the experimental results (i.e. transport properties and swelling pressure) to the physical and chemical properties of the bentonite specimens, by assuming that the microscopic deviations of the state variables from their average values are negligible (Dominijanni et al. 2013). On the

basis of the proposed theoretical framework, the global reflection and the swelling pressure coefficient depend on the solid skeleton electric charge, $\overline{c}_{sk,0}$ respectively through the following equations:

$$\omega_g = 1 + \frac{\overline{c}_{sk,0}}{2\cdot\left(c_t - c_b\right)\cdot e}\left[Z_2 - Z_1 - (2t_1 - 1)\cdot \ln\left(\frac{Z_2 + 2t_1 - 1}{Z_1 + 2t_1 - 1}\right)\right] \tag{4.29}$$

$$u_{sw} = 2RTc_{avg}\left[\sqrt{\left(\frac{\overline{c}_{sk,0}}{2ec_{avg}}\right)^2} + 1 - 1\right] \tag{4.30}$$

Therefore, from the best-fitting of the theoretical curve with the experimental results (Figure 4.27 and Figure 4.28), a constant value of $\overline{c}_{sk,0}$ = 65 mM was found in the case of specimen SQ_NaB_COT3, and of $\overline{c}_{sk,0}$ = 105 mM in the case of specimen SQ_NaB_COT4. These values of $\overline{c}_{sk,0}$ are in agreement with those found out from the other chemico-osmotic tests of the present chapter, as it can be observed in the graph of Figure 4.29, in which the effective fixed charge concentration of the solid skeleton, $\overline{c}_{sk,0}$ is represented as a function of void ratio, e of specimens.

In order to determine ω_g, the salt concentration at the top boundary was taken equal to $c_{t,avg}$, while the salt concentration at the bottom boundary was considered equal to zero, i.e. $c_b \cong c_{b,avg} \cong 0$ in the case of specimen SQ_NaB_COT3 and equal to $c_b \cong c_{b,avg} \cong$ 10 mM in the case of specimen SQ_NaB_COT4. Moreover, in order to determine u_{sw}, the average salt concentration, c_{avg}, in equilibrium with the bentonite was taken equal to a mean value between the average salt concentrations at the boundary of the specimen, i.e. $c_{t,avg}$ and $c_{b,avg}$. The sodium transport number was calculated from the sodium and chloride free-solution diffusion coefficient values (Shackelford and Daniel, 1991): $D_{Na,0}$ = 13.3·10^{-10} m^2/s, $D_{Cl,0}$ = 20.3·10^{-10} m^2/s. The resulting theoretical curves of $D^*_{\omega g}$ are reported respectively in Figure 4.30 as a function of the top boundary salt concentration.

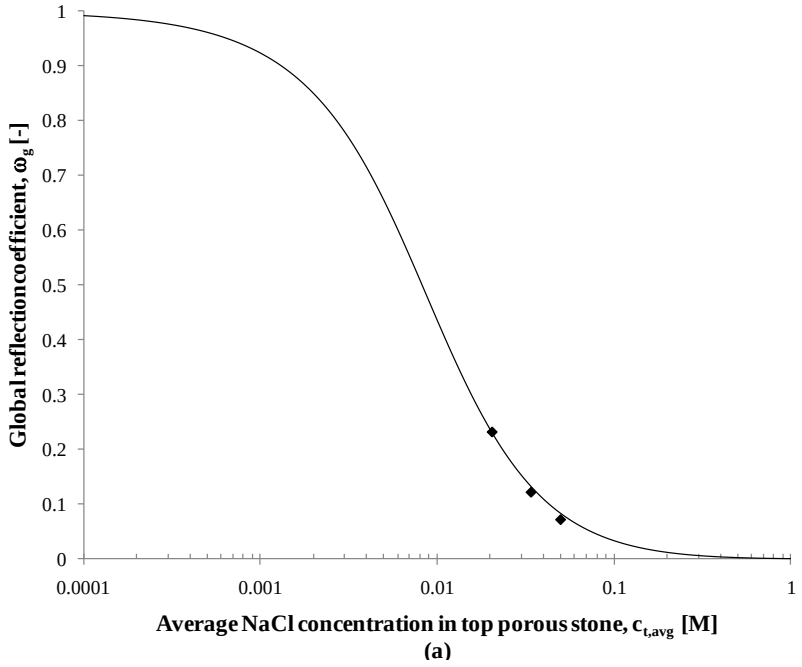

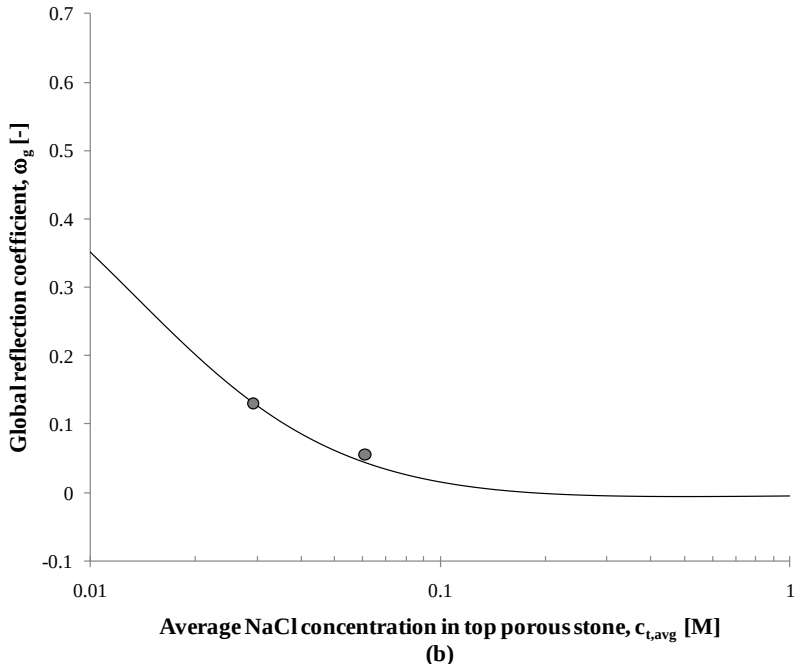

Figure 4.27 Global reflection coefficient, ω_g, as a function of average sodium chloride (NaCl) concentration at top boundary of bentonite specimen, with best-fitting theoretical curves, obtained respectively (a) for $\bar{c}_{sk,0}$ = 65 mM in equation (4.29) (continuous line) for specimen SQ_NaB_COT3, and (b) for $\bar{c}_{sk,0}$ = 105 mM in equation (4.29) (continuous line) for specimen SQ_NaB_COT4

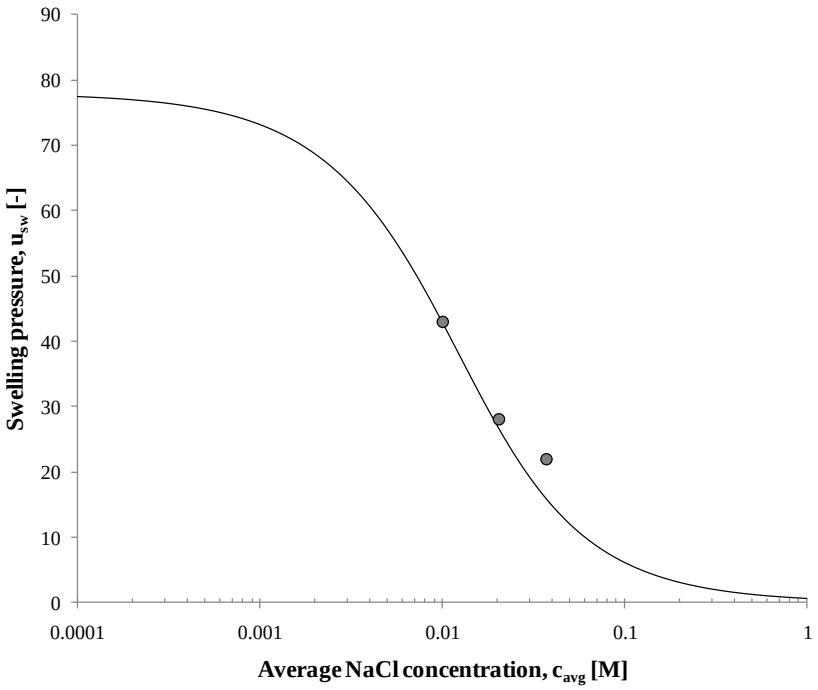

Figure 4.28 Swelling pressure, u_{sw}, as a function of average sodium chloride (NaCl) concentration, c_{avg}, with best-fitting theoretical curve, obtained respectively, for $\bar{c}_{sk,0}$ = 105 mM in equation (4.30) (continuous line) for specimen SQ_NaB_COT4

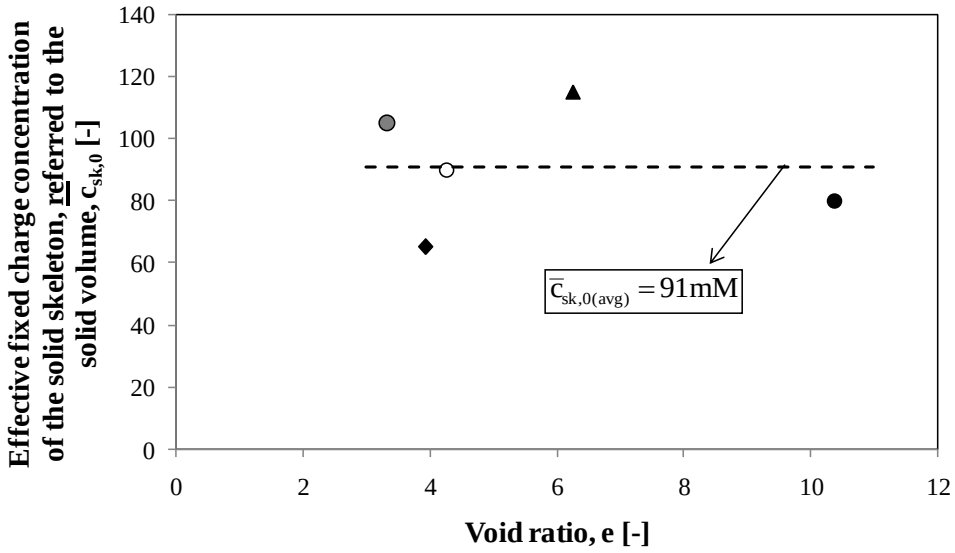

Figure 4.29 Values of the effective fixed charge concentration of the solid skeleton, $\bar{c}_{sk,0}$ as a function of void ratio, e, derived through the interpretation of global reflection coefficients, ω_g measured during chemico-osmotic tests on the same type of sodium bentonite.

The tortuosity factors for each specimen were determined by plotting the measured values of $D^{*}_{\omega g}$ as a function of the corresponding values of the complement to 1 of ω_g, i.e. 1 - ω_g, and finding the intercept of the linear regressions with the ordinate axis at 1 - ω_g = 1, i.e. ω_g = 0 (Figure 4.31). The tortuosity factor in Eq. (4.20) is in fact given by Eq. (4.28): a value of τ_m equal to 0.14 was obtained for specimen SQ_NaB_COT3, and equal to 0.18 for specimen SQ_NaB_COT4. These results are, as expected, lower than those obtained for bentonite specimens characterized by higher values of void ratio (i.e. for e = 4.26 and e = 10.37).

By plotting the results of the research activity in terms of restrictive tortuosity factor, τ_r, (i.e. the ratio between the osmotic effective diffusion coefficient and the effective salt diffusion coefficient) as a function of the chemico-osmotic efficiency coefficient, ω, together with experimental data by Malusis & Shackelford (2002b), Malusis et al. (2013) and Dominijanni et al. (2013), it is possible to find a very good agreement with the linear relationship predicted by the theoretical model (see Eq. (4.15)), as shown by the coefficient of determination, R^2 = 0.951 (Figure 4.32). Therefore this can be considered an important indication of the ability of the proposed theoretical model to properly simulate membrane behaviour of bentonite-based barriers.

Finally, it should be pointed out that the solid skeleton electric charge, $\overline{C}_{sk,0}$, can assume different values as a function of void ratio and, in particular, of salt concentration due to the bentonite fabric changes. Nevertheless, considering the high dilution of the salt solutions used during chemico-osmotic tests, the obtained data can be interpreted, in a first approximation, with constant values of $\overline{C}_{sk,0}$: despite these approximations, experimental results are quite well fitted by the theoretical curves. The possibility of fitting swelling pressure results (Dominijanni et al., 2013; Boffa et al., 2016), and transport properties (Dominijanni et al., 2013), with similar values of $\overline{C}_{sk,0}$ (average value of 95 mM) may represent a significant evidence of the abitility of the theoretical model to describe the coupled chemical-hydraulic-mechanical behaviour of sodium bentonite (Figure 4.33).

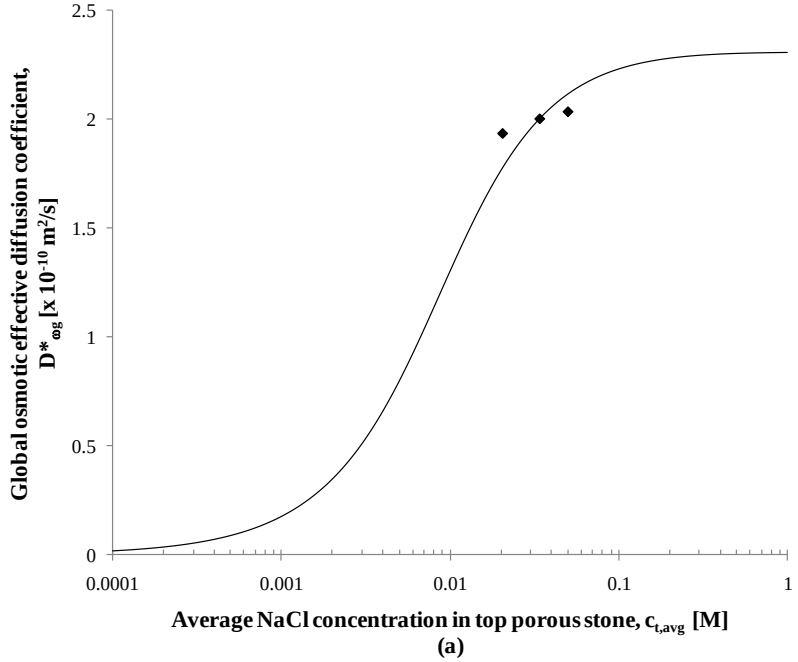

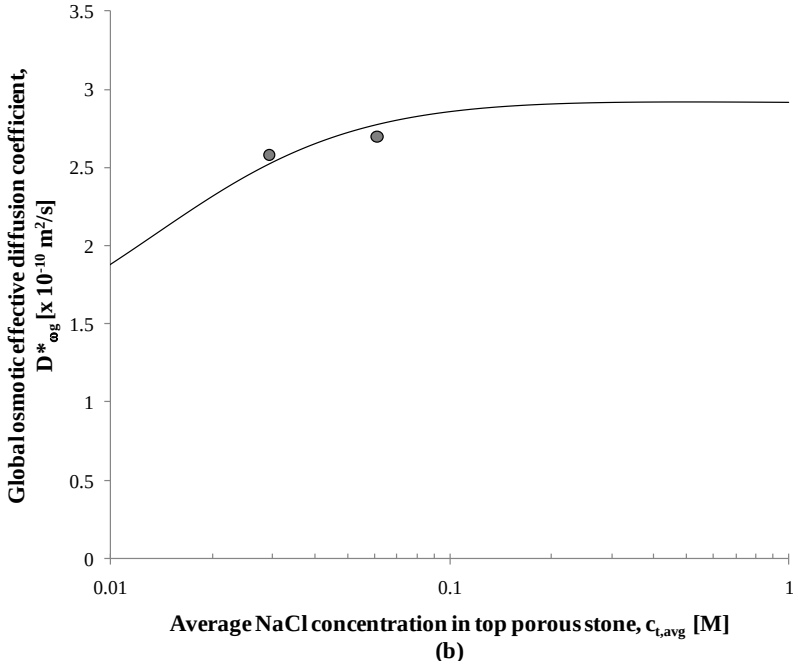

Figure 4.30 Global osmotic effective diffusion coefficient, $D^*_{\omega g}$, as a function of average sodium chloride (NaCl) concentration at top boundary of specimens, with best-fitting theoretical curve, obtained respectively (a) for $\overline{c}_{sk,0} = 65\,\text{mM}$ and $\tau_m = 0.14$ in equations (4.20) and (4.29) for specimen SQ_NaB_COT3, and (b) for $\overline{c}_{sk,0} = 105\,\text{mM}$ and $\tau_m = 0.18$ in equations (4.20) and (4.29) for specimen SQ_NaB_COT4

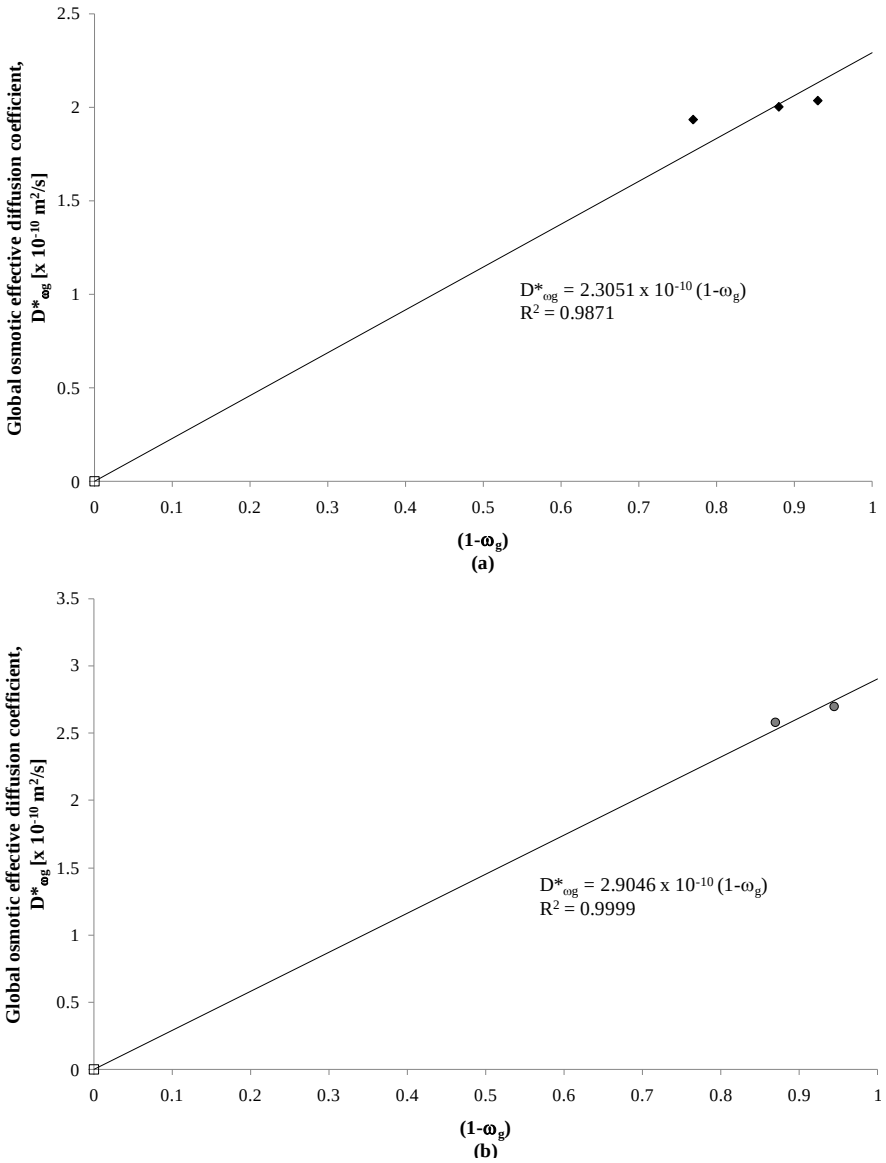

Figure 4.31 Global osmotic effective diffusion coefficient, $D^*_{\omega g}$, as a function of the complement to 1 of the global reflection coefficient, ω_g, with the theoretical linear relation given by equation (4.20) (continuous line) for (a) specimen SQ_NaB_COT3, and (b) specimen SQ_NaB_COT4

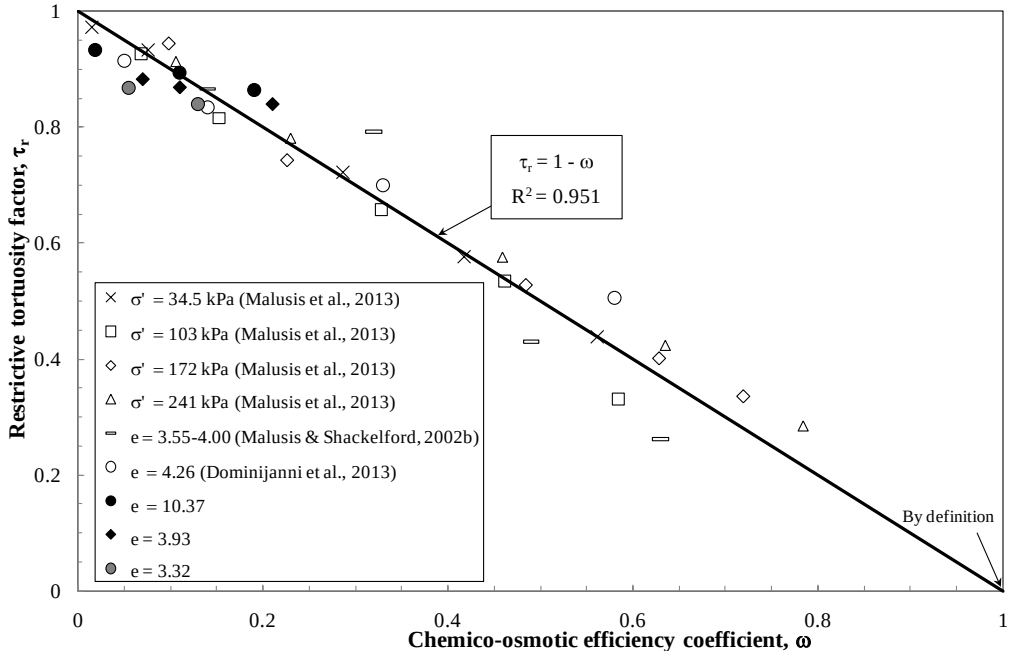

Figure 4.32 Restrictive tortuosity factor, τ_r, as a function of chemico-osmotic efficiency coefficient, ω, with the theoretical linear relation

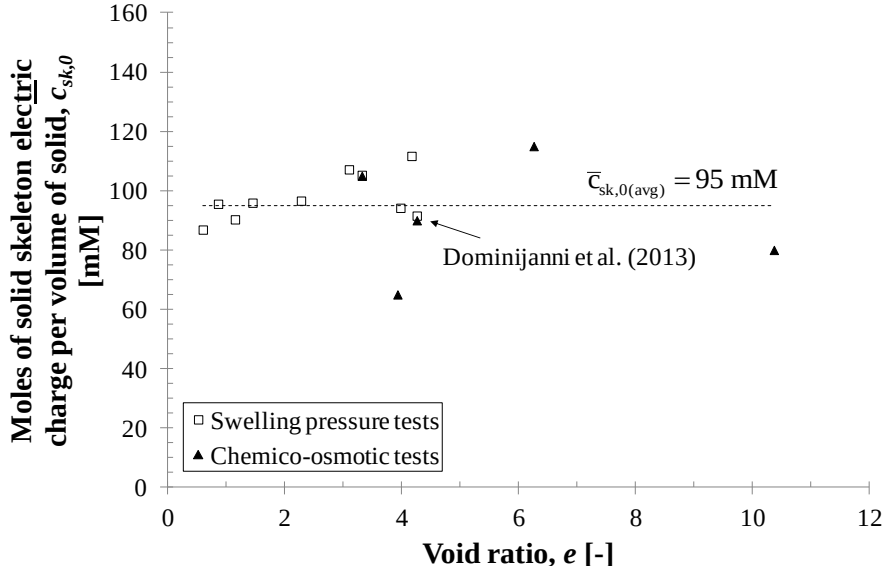

Figure 4.33 Moles of solid skeleton electric charge per volume of solid, $\overline{c}_{sk,0}$, obtained by theoretical interpretation of transport properties and swelling pressures of sodium bentonite specimens, as a function of their void ratio

References

1. Boffa, G., Dominijanni, A., Manassero, M., Marangon, M., Zaninetta, L. (2016). Mechanical and swelling behaviour of sodium bentonites in equilibrium with low molarity NaCl solutions under oedometric conditions. *Acta Geotechnica* (submitted paper).
2. Dominijanni, A., Manassero, M., Puma, S. (2013). Coupled chemical-hydraulic-mechanical behaviour of bentonites. *Géotechnique* **63**(3), 191-205.
3. Malusis, M.A. & Shackelford, C.D. (2002b). Coupling effects during steady-state solute diffusion through a semipermeable clay membrane. *Environmental Science and Technology* **36**, No. 6, 1312–1319.
4. Malusis, M.A., Kang, J.-B., Shackelford, C.D. (2013). Influence of membrane behavior on solute diffusion through GCLs. Coupled Phenomena in Environmental Geotechnics, M. Manassero, A. Dominijanni, S. Foti and G. Musso, Eds., July 1-3, 2013, Torino, Italy, CRC Press/Balkema, Taylor & Francis Group, London, 267-274.
5. Puma, S. (2013). Chemico-mechanical improvement of bentonite barriers for pollutant containment. PhD Dissertation. Politecnico di Torino, Torino, Italy.
6. Shackelford, C.D. & Daniel, D.E. (1991). Diffusion in saturated soil: I. Background. *Journal of Geotechnical Engineering*, **117**, No. 3, 467–484.

FINAL CONCLUSIONS

During the PhD research activity a theoretical and experimental work was developed with the aim of studying the mechanical and chemico-osmotic behaviour of sodium bentonite, contained in the so-called Geosynthetic Clay Liners (GCLs), in contact with standard (i.e. de-ionized water) and non standard liquids (i.e. sodium chloride solutions). GCLs are manufactured hydraulic barriers, consisting of a thin layer of bentonite supported by geotextiles and/or geomembranes, which can be adopted for geoenvironmental applications, as replacement materials for the more traditional compacted clay liners, in cover systems or in bottom lining of urban waste landfills and hazardous or radioactive wastes final disposals.

In the first chapter of the PhD thesis, mineralogical, chemical and physical characteristics of sodium bentonites have been described, with particular attention to swelling and osmotic phenomena influencing sodium bentonite microstructure. Sodium bentonite is a particular clay soil, which usually contains at least 70% of the three layered (2:1) clay mineral montmorillonite, that, at the microscopic scale, is characterized by a very high specific surface and a permanent negative surface charge induced by isomorphous substitution. Such microscopic properties are very important, because they confer excellent macroscopic properties (i.e. high swelling pressure, low hydraulic conductivity and semipermeable membrane behaviour) to bentonite contained in GCLs. An experimental study on the difference in the swelling and mechanical behaviour of sodium bentonite in equilibrium with NaCl solutions at different concentrations is also presented in the first chapter: the results

highlight that the microscopic scale structure has a deep influence on the swelling and mechanical properties of bentonite, in particular the tests performed on sodium bentonite with NaCl more concentrated solutions showed a significant decrease in the swelling behaviour, as a consequence of the decrease in thickness of the double diffuse layers surrounding bentonite particles.

Since the interaction between electrically charged montmorillonite particles and the ions in pore solution determines macroscopic phenomena which cannot be modelled on the basis of the classical theories used to describe the movement of water and solutes through porous media, different theoretical approaches are needed: such reference frameworks, which can be adopted in order to model mechanical behaviour and transport properties of bentonite, are summarized in the second chapter. Particular attention is devoted to the electric charge of the solid skeleton (per unit solid volume), $\overline{C}_{sk,0}$ which is a macroscopic material parameter introduced into the model proposed by Dominijanni and Manassero (2012a,b), in order to account for the electro-chemical phenomena related to the microscopic surface forces: it is proportional to the effective specific surface of the solid particles, therefore it increases in the case of dispersed structures of separated lamellae (which can be associated with low concentrations of NaCl solutions), while it is expected to decrease in the case of aggregated structures formed by packets of lamellae united in a parallel face-to-face array (which can be associated with high concentrations of NaCl solutions). This parameter is very important, since it influences both the mechanical and semipermeable membrane behaviour of bentonites.

The mechanical and swelling behaviour of sodium bentonite was investigated in chapter 3, by interpreting several experimental swelling pressure data derived from two types of oedometer tests. Two different preparation methods of specimens were adopted: several oven-dried bentonite specimens were directly hydrated within the oedometer ring with sodium chloride 0.01 M concentrated solutions, while others were hydrated and then consolidated from a water content lower than liquid limit. It is to note that in a preliminary phase soluble salts, which are naturally present in sodium bentonite as a consequence of its marine origin, were removed through the so-called “squeezing” method, in order to prevent them from affecting experimental

results: it consists of a series of consecutive phases of powder bentonite hydration with deionized water and drained consolidation, performed in a consolidometer, and it has the advantage, in comparison with the so-called "flushing" method, of reducing soluble salts removing time. The experimental swelling pressure data from oedometer tests were interpreted on the basis of the theoretical approach by Dominijanni and Manassero (2012b) and they result in agreement with the trends given by the proposed framework, under the assumption that the microscopic deviations of the pore solution state variables from their average values are negligible (Donnan, 1911). From the experimental values of swelling pressure it was possible to obtain two different values of $\overline{C}_{sk,0}$, (i.e. respectively 305 and 95 mM) as an indication of the different (i.e. respectively dispersed and aggregated) microstructure of the tested bentonite specimens. It should be pointed out that the solid skeleton electric charge, $\overline{C}_{sk,0}$, can assume different values as a function of void ratio and, in particular, of salt concentration due to the bentonite fabric changes. Nevertheless, considering the constant concentration and high dilution of the salt solution, within the study of mechanical behaviour of bentonites, the obtained data have been interpreted, in a first approximation, with a constant value of $\overline{C}_{sk,0}$. Despite these approximations, experimental results are quite well fitted by the theoretical curves.

The semipermeable membrane behaviour of squeezed sodium bentonite was then studied in chapter 4, by means of some multistage chemico-osmotic tests on specimens characterized by different void ratio values (i.e. 3.32, 3.93, 6.26 and 10.37), in order to evaluate the influence of porosity, n (i.e. void ratio, e) on transport properties of bentonite. Two different testing devices were used, i.e. a modified rigid-wall permeameter, which had been usually employed by several authors in literature, and a new testing apparatus, characterized by a stainless steel oedometer cell equipped with strain and stress controlling device: in the first case, bentonite was externally hydrated to a lower water content than the Liquid Limit of the material, and then consolidated in a compaction mould to the desired void ratio, while, in the latter case, a known amount of dry material was dusted inside the

oedometer ring and de-ionized water or 0.01 M NaCl solution were supplied in order to saturate the material to a fixed void ratio. Two phenomenological parameters that affect transport properties of bentonite, i.e. the chemico-osmotic reflection coefficient and the osmotic effective diffusion coefficient, were measured. In particular, the chemico-osmotic reflection coefficient, which represents the osmotic efficiency of the material in response to a saline concentration gradient, was found to decrease with an increase in the average saline concentration across the specimen, and with an increase in the porosity, in agreement with previous literature values (Kemper and Rollins, 1966; Malusis and Shackelford, 2002a; Dominijanni et al., 2013; Tang et al., 2014). The theoretical framework proposed by Dominijanni and Manassero (2012b) was found to be able to interpret semipermeable membrane behaviour of tested sodium bentonite for the different testing conditions (in terms of void ratio and difference in salt concentration between the boundaries of specimens) used during the experimental activity, by assuming that the microscopic deviations of the pore solution state variables from their average values are negligible (Donnan, 1911). From the experimental values of global reflection coefficient it was possible to derive four slightly different values (i.e. respectively 105, 65, 115 and 80 mM) of electric charge of the solid skeleton (per unit solid volume), $\overline{C}_{sk,0}$, whose mean value (i.e. 91 mM) is rather the same as that obtained through oedometer tests on bentonite specimens hydrated within the oedometer ring. A rather constant value of $\overline{C}_{sk,0}$, within a narrow low concentration range, is a particular indication of the consistency of the theoretical model. In particular, the possibility of interpreting experimental mechanical and transport parameters with the same $\overline{C}_{sk,0}$ value, as it occurred in the case of specimen SQ_NaB_COT4, may be considered a significant evidence of the abitility of the theoretical framework to describe the coupled chemical-hydraulic-mechanical behaviour of sodium bentonite.

Nevertheless it should be pointed out that the present PhD thesis has dealt with mechanical and osmotic behaviour of bentonites in contact with single salt solutions, containing monovalent cations: for this reason, further experimental tests are recommended in order to verify the applicability of the theoretical model proposed

by Dominijanni and Manassero (2012a,b) under different boundary conditions and for different salts contained in the pore solution.

References

1. Dominijanni, A. & Manassero, M. (2012a). Modelling the swelling and osmotic properties of clay soils. Part I: *The phenomenological approach. International Journal of Engineering Science* **51**, 32-50.
2. Dominijanni, A. & Manassero, M. (2012b). Modelling the swelling and osmotic properties of clay soils. Part II: The physical approach. *International Journal of Engineering Science* **51**, 51-73.
3. Dominijanni, A., Manassero, M., Puma, S. (2013). Coupled chemical-hydraulic-mechanical behaviour of bentonites. *Géotechnique* **63**(3), 191-205.
4. Donnan, F.G. (1911). Theorie der Membrangleichgewichte und Membranpotentiale bei Vorhandensein von nicht dialysierenden Elektrolyten. Ein Beitrag zur physikalisch-chemischen Physiologie [Theory of membrane equilibria and membrane potentials in the presence of non-dialysing electrolytes. A contribution to physical-chemical physiology], *Zeitschrift für Elektrochemie und angewandte physikalische Chemie* **17**, 572-581. English translation republished in *Journal of Membrane Science* **100** (1995), 45-55.
5. Kemper, W.D. & Rollins, J.B. (1966). Osmotic efficiency coefficients across compacted clays. *Soil Science Society of America, Proceedings* **30**, 529–534.
6. Malusis, M.A. & Shackelford, C.D. (2002a). Chemico-osmotic efficiency of a geosynthetic clay liner. *Journal of Geotechnical and Geoenvironmental Engineering* **128**, No. 2, 97–106.
7. Tang, Q., Katsumi, T., Inui, T., Li, Z. (2014). Membrane behavior of bentonite-amended compacted clay. *Soils and Foundations* **54**(3), 329-344.

ACKNOWLEDGEMENTS

Al termine del mio dottorato di ricerca, ripercorrendo nella mia mente questi ultimi tre anni sento il bisogno di ringraziare quanti mi hanno permesso di portare a termine questo lavoro, di crescere molto da un punto di vista umano e tecnico-scientifico, e di raggiungere un traguardo così importante.

Desidero ringraziare i Proff. Mario Manassero e Guido Musso, innanzitutto per avermi trasmesso la passione per la Geotecnica, per avermi incoraggiato ad intraprendere un percorso così stimolante ed interessante, e per avermi seguito con grande entusiasmo durante questi anni.

Porgo un sentito ringraziamento agli Ingg. Andrea Dominijanni e Sara Puma, per la loro professionalità, la gentilezza e la costante disponibilità, indispensabili per lo svolgimento delle prove di laboratorio e per la stesura di questo elaborato.

Un grazie particolare va ai tecnici del DIPLAB, Ingg. Giovanni Bianchi e Oronzo Pallara, e a Giuseppe Angeloni di ISMGEO, per il loro aiuto in laboratorio nella preparazione delle prove, e per aver risolto innumerevoli situazioni critiche.

Desidero ringraziare inoltre i tesisti e gli studenti collaboratori part-time, senza i quali l'attività sperimentale sarebbe stata decisamente più complicata: Nicolò Guarena, Irene Gambino, Fabio Furno, Cristian Trevisan, Giuseppe Terramagra, Stefania Griva, Matteo Bocco, Mariangela Diano, Jacopo Cavalli, Chiara Elsa Denegri, Silvia Gambino e Andrea Borgognone.

Ringrazio i miei colleghi e compagni di avventura di questi ultimi tre anni, Carmine Terrioti, Luca Buffa, Emanuela Di Battista, Oscar Borla, Andrea Bassani, ed in

modo particolare Gianluca Bella ed Arash Azizi, dottorandi geotecnici, a cui devo molto, e con i quali ho condiviso svariate giornate in laboratorio e ai convegni a cui abbiamo partecipato insieme.

Grazie ai numerosi amici di Villa San Giuseppe, in particolare Wettu, Kate, Costa, Tyson, Jobby, Mago, Fra&Andre Monte, Vittozz1, Tools, Carlo, Paolino, per aver allietato i tanti momenti, di studio e di allegria, passati insieme nel corso di questi anni, e per avermi reso partecipe di una realtà extra-universitaria unica e straordinaria.

Grazie di cuore a mia Madre, a mio Padre, a mio Fratello Edoardo, ai quali dedico questa mia "fatica", e a tutte le persone care della mia famiglia, per l'impagabile fiducia che hanno riposto in me, per avermi costantemente incoraggiato e sostenuto ad andare avanti e a fare le mie scelte.

Infine un ringraziamento speciale va ad Isabella, che mi sopporta e supporta quotidianamente con amore incondizionato, per avermi aiutato a superare i vari problemi incontrati durante questo percorso.

Torino, 16 maggio 2016